

AD-A147 216

THE RELATIONSHIP BETWEEN RADIATION SENSITIVITY AND  
REDOX EQUILIBRIA(U) VANDERBILT UNIV NASHVILLE TN DEPT  
OF MECHANICAL AND MATERIALS. D L KINSEY SEP 84

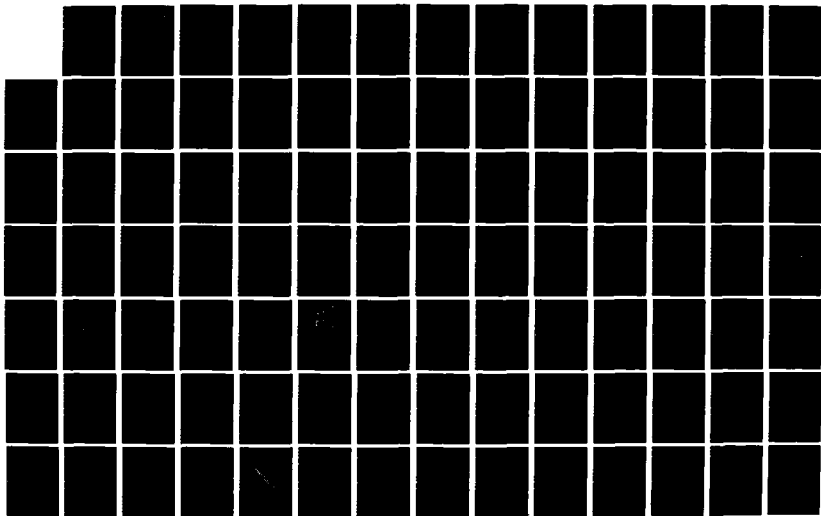
1/2

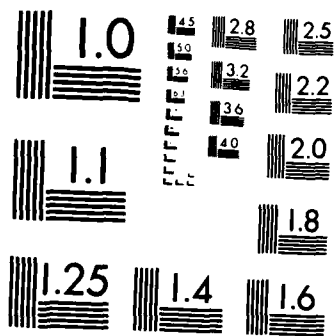
UNCLASSIFIED

ARO-17942. 8-M5 DRAG29-81-K-0118

F/G 11/2

NL





MICROCOPY RESOLUTION TEST CHART  
NATIONAL BUREAU OF STANDARDS-1963-A

ARO 17942.8-MS



AD-A147 216

THE RELATIONSHIP BETWEEN RADIATION SENSITIVITY  
AND REDOX EQUILIBRIA  
FINAL REPORT

SUBMITTED TO

U. S. ARMY RESEARCH OFFICE  
RESEARCH TRIANGLE PARK, NC 27709

Contract No. DAAG 29-81-K-0118

Period Covered:

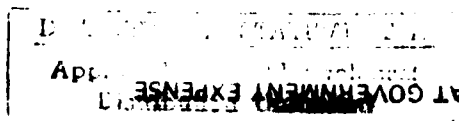
June 1, 1981 - July 31, 1984

Submitted by

D. L. Kinser  
Mechanical and Materials Engineering  
Vanderbilt University  
Nashville, TN 37235



DTIC FILE COPY



5 2 1 0 3 0 1 2 5

UNCLASSIFIED

SECURITY CLASSIFICATION OF THIS PAGE (When Data Entered)

MASTER COPY - FOR REPRODUCTION PURPOSES

REPORT DOCUMENTATION PAGE		READ INSTRUCTIONS BEFORE COMPLETING FORM
1. REPORT NUMBER <b>ARO 17942.8-MS</b>	2. GOVT ACCESSION NO. <b>AD-A47316</b> N/A	3. RECIPIENT'S CATALOG NUMBER <b>N/A</b>
4. TITLE (and Subtitle) <b>"The Relationship Between Radiation Sensitivity and Redox Equilibria"</b>		5. TYPE OF REPORT & PERIOD COVERED <b>Final Report</b> <b>6/1/81 - 7/31/84</b>
7. AUTHOR(s) <b>D. L. Kinser</b>		6. PERFORMING ORG. REPORT NUMBER
9. PERFORMING ORGANIZATION NAME AND ADDRESS <b>Vanderbilt University</b> <b>416 Kirkland Hall</b> <b>Nashville, TN 37240</b>		8. CONTRACT OR GRANT NUMBER(s) <b>DAAG 29-81-K-0118</b>
11. CONTROLLING OFFICE NAME AND ADDRESS <b>U. S. Army Research Office</b> <b>Post Office Box 12211</b> <b>Research Triangle Park, NC 27709</b>		10. PROGRAM ELEMENT, PROJECT, TASK AREA & WORK UNIT NUMBERS
14. MONITORING AGENCY NAME & ADDRESS (if different from Controlling Office)		12. REPORT DATE <b>September 1984</b>
		13. NUMBER OF PAGES
		15. SECURITY CLASS. (of this report) <b>Unclassified</b>
		15a. DECLASSIFICATION/DOWNGRADING SCHEDULE
16. DISTRIBUTION STATEMENT (of this Report)  <b>Approved for public release; distribution unlimited.</b>		
17. DISTRIBUTION STATEMENT (of the abstract entered in Block 20, if different from Report)  <b>NA</b>		
18. SUPPLEMENTARY NOTES  <b>The view, opinions, and/or findings contained in this report are those of the author(s) and should not be construed as an official Department of the Army position, policy, or decision, unless so designated by other documentation.</b>		
19. KEY WORDS (Continue on reverse side if necessary and identify by block number)  <b>Glasses, radiation effects, optical properties, electrical conductivity, electron paramagnetic resonance, GeO<sub>2</sub> glass, GeS<sub>2</sub> glass, radiation damage, glass processing, fiber optics, sol-gel glasses</b>		
20. ABSTRACT (Continue on reverse side if necessary and identify by block number)  <b>The objective of this research program is to achieve an understanding of the relationship of glass processing variables to radiation sensitivity of the glass. Glass processing variables include melting time, melting atmosphere, cooling rate and annealing time. The principle applications of the results of this program are in fiber optic communication systems and other glass applications in radiation environments. Results indicate that optical defects, paramagnetic defects and electrical properties are subject to influence by</b>		

DD FORM 1 JAN 73 1473

EDITION OF 1 NOV 65 IS OBSOLETE

UNCLASSIFIED

SECURITY CLASSIFICATION OF THIS PAGE (When Data Entered)

20. Abstract, continued.

glass processing variables. These processing effects also extend to the sensitivity of the properties to radiation damage.

Accession For	
NTIS GRA&I	<input checked="" type="checkbox"/>
DTIC TAB	<input type="checkbox"/>
Unannounced	<input type="checkbox"/>
Justification	
By _____	
Distribution/	
Availability Codes	
Dist	Avail and/or Special
A/1	



## TABLE OF CONTENTS

Abstract (DD Form #1473) . . . . .	i
Final Report	
Introduction . . . . .	1
Participating Scientific Personnel . . . . .	4

### Appendices:

#### I. Presentations (Abstracts only)

- a. "New Paramagnetic Resonance Spectra of GeO<sub>2</sub> Glasses and Their Correlation with Optical Bands", R. Weeks, D. Kinser, R. Magruder, and M. Wells
- b. "The Effect of Fusion Conditions on the Electrical Properties of GeO<sub>2</sub> Glasses", R. Magruder, D. Kinser, R. Weeks and G. Kordas
- c. "The Effects of Fusion Temperature upon Paramagnetic States of GeO<sub>2</sub> Glasses", G. Kordas, R. Weeks and D. Kinser
- d. "UV Optical Properties of GeO<sub>2</sub> Glasses as a Function of Fusion Conditions", J. Jackson, R. Quarles, M. Wells, and D. Kinser
- e. "Fusion Temperature Effects on DC Conductivity of GeO<sub>2</sub> Glasses", R. Magruder, R. Weeks, and D. Kinser

#### II. Publications

- a. "The Influence of Melting Conditions on the Radiation Sensitivity of GeO<sub>2</sub> Glass" R. Weeks, D. Kinser, G. Kordas, R. Magruder, and M. Wells
- b. "Effect of Gamma Radiation on the Direct-Current Resistivity of GeO<sub>2</sub>" R. Magruder, D. Kinser, and R. Weeks
- c. "The Effect of Fusion Conditions on the Intrinsic Paramagnetic States of GeO<sub>2</sub> Glasses", G. Kordas, R. Weeks, and D. Kinser
- d. "Paramagnetic Defects in Germanium Sulfur Glasses" G. Kordas, R. Weeks, D. Kinser, and R. Quarles

## II. Publications, Continued

- e. "The Influence of Fusion Temperature on the Defect Center Concentration of  $\text{GeO}_2$  Glass" G. Kordas, R. Weeks and D. Kinser
- f. "The Effect of Melt Temperature on the DC Conductivity of  $\text{GeO}_2$  Glasses" R. Magruder, D. Kinser, R. Weeks, and J. Jackson
- g. "Effects of Densification on the Defect Center Concentration in Germanium-Doped Silica Optical Fiber Preforms" G. Kordas, D. Kinser and R. Weeks (accepted for publication)
- h. "Paramagnetic Conduction Electrons in  $\text{GeS}_x$  Glasses" G. Kordas, R. Weeks, and D. Kinser (accepted for publication)
- i. "Electron Spin Resonance (ESR) Study of Sol-Gel Glasses" G. Kordas and R. Weeks (accepted for publication)
- j. "Fusion Temperature Effects on the Annealing Behavior of  $\text{GeO}_2$  Glasses as Measured by the DC Resistivity" R. Magruder, D. Kinser, and R. Weeks (accepted for publication)
- k. "The Effects of Thermal History and Irradiation on the DC Conductivity of High Purity  $\text{GeO}_2$  Glasses" R. Magruder (Ph.D. Dissertation)

"The Relationship Between Radiation Sensitivity and Redox Equilibria"

Introduction

The objective of this research program is to achieve an understanding of the relationship of glass processing variables and radiation sensitivity of the glass. Processing variables examined in the course of our work include melting time, melting temperature, melting atmosphere, cooling rate and annealing time.

The principle application of the results of this work is for use in fiber optic communication systems where radiation hardening is desirable. The glass systems of interest are predominantly  $\text{SiO}_2$  based fibers with various dopants including  $\text{B}_2\text{O}_3$  and  $\text{GeO}_2$ . The processing temperatures in  $\text{SiO}_2$  systems are very high; thus, we have focused upon an analogue system  $\text{GeO}_2$  which can be processed at more easily attainable temperatures. We have also examined  $\text{GeS}_2$  glasses because of its utility in the IR region and because it is amenable to stoichiometry modification.

Results of EPR studies indicate that two paramagnetic defect types are present in the  $\text{GeO}_2$  glasses. The functional dependence of the concentration of each defect upon the temperature at which the glass was equilibrated and fused ( $T_\phi$ ) is not Arrhenius. It is clear that the defect concentration is a function of  $T_\phi$  and this is a previously unreported observation. EPR studies have also been conducted upon  $\text{GeO}_2$  glasses subjected to  $^{60}\text{Co}$  gamma irradiation. These studies indicate that the growth of radiation-induced defects is a function of the  $T_\phi$  used in preparing the glass. Thus, we have demonstrated

the effect of glass "processing" variables upon the growth of paramagnetic defects.

We have also employed DC conductivity techniques to examine the role of processing and radiation upon the mobility of trace levels of sodium ions in  $\text{GeO}_2$  glasses. These results indicate that glasses fused at higher temperatures have lower mobilities than those fused at lower temperatures. We have interpreted these results to indicate that the sodium ion probe is encountering more defects in the glass fused at the higher temperature. We have also examined the influence of radiation upon sodium ion mobility in a suite of glasses fused over a range of temperatures. These results indicate that radiation-induced defects interact with the sodium ion in a fashion so as to reduce mobility.

The results of optical measurements in the UV region on  $\text{GeO}_2$  glasses indicate that the magnitude of the UV absorption depends upon the  $T_\phi$  employed in preparing the glass. The intensity of the UV absorption behaves in an Arrhenius fashion with  $T_\phi$  with an activation of 2.3 eV. This indicates that the activation energy for the formation of the defect responsible for the optical absorption is 2.3 eV. A limited study of the role of oxygen partial pressure during fusion indicates that the intensity of the UV absorption falls with increasing oxygen partial pressure for the two fusion temperatures examined. Theory predicts that the concentration of defects should be proportional to  $p^{-1/n}$  where  $n$  depends upon the mechanism of generation of the defect. The data presently available indicate that the magnitude of  $n$  is greater than 5 and less than 16.

Some studies have been conducted on  $\text{GeS}_2$  glasses of varying stoichiometry and  $T_\phi$ . These results indicate that our observations on  $\text{GeO}_2$  glasses can be generalized although some of the details of the defects present are different.

A recent conference entitled "Effects of Modes of Formation on the Structure of Glass" was organized and held at Vanderbilt. This conference brought together approximately 100 glass scientists from throughout the world to exchange current research results and ideas in the area of the present contract. The proceedings of this conference containing approximately fifty papers will be published in the Journal of Non-Crystalline Solids in the Spring of 1985.

PARTICIPATING SCIENTIFIC PERSONNEL

D. L. Kinser, Professor of Materials Science

R. A. Weeks, Research Professor of Materials Science

G. Kordas, Research Assistant Professor of Materials Science

R. Magruder, III, Graduate Student

M. Wells, Graduate Student

R. Quarles, Graduate Student

J. Montgomery, Undergraduate Student

K. Wilder, Undergraduate Student

APPENDIX I.a.

NEW PARAMAGNETIC RESONANCE SPECTRA OF  $\text{GeO}_2$  GLASSES

AND THEIR CORRELATION WITH OPTICAL BANDS

R. A. Weeks, Oak Ridge National Laboratory  
Oak Ridge, Tennessee

D. Kinser, R. Magruder, M. Wells, Vanderbilt University  
Nashville, Tennessee

Paramagnetic resonance spectra of  $\text{GeO}_2$  glasses were measured at 9 and 35 GHz and temperatures from 100 to 300 K. Glasses were fused in air and at  $\sim 3 \times 10^{-6}$  atm  $\text{P}_{\text{O}_2}$  at temperatures of 1650, 1550, and 1450 C. Quenching rates from the fusion temperature ranged from  $10^6$  C/sec to  $50$  C/sec. The concentration of the  $E'_1$  center, measured in the virgin glasses were least in the 1450 C glass and approximately the same in the 1550 and 1650 C glasses and largest in the sample cooled at  $10^6$  C/sec. Annealing the samples at 405 C for one hour reduced the intensity by more than an order of magnitude. Two additional components were detected. One at  $g=2.35$  and width  $\Delta H$  1100 gauss and an approximately symmetric shape, and the second at  $g=1.99$  with a shape approximately that expected for axial symmetry. The intensity of these components were dependent upon fusion temperatures and had the least intensity in glass fused at 1450 C and  $3 \times 10^{-6}$  atm  $\text{P}_{\text{O}_2}$ . Correlations between ESR and optical spectra will be discussed as will tentative models for the additional EPR components.

Presented at The Physics of  
Non-Crystalline Solids Conference,  
Montpellier, France, July 1982

APPENDIX I.b.

THE EFFECT OF FUSION CONDITIONS ON THE ELECTRICAL  
PROPERTIES OF  $\text{GeO}_2$  GLASSES

R. Magruder, D. Kinser, R. Weeks, & G. Kordas  
Department of Mechanical & Materials Engineering  
Vanderbilt University  
Nashville, Tennessee

The dc electrical properties of a series of high purity  $\text{GeO}_2$  glasses melted in air between  $1200^\circ$  and  $1700^\circ\text{C}$  were measured. The observed changes are not correlated with neutron activation analysis of impurities or IR measurements of OH. The resistivity of the glasses increases with increasing fusion temperatures. The resistivity of samples fused at the same temperature increase with decrease in cooling rate of the glass from fusion. The activation energy of the conduction process was calculated to be  $\sim 1.0$  eV. Irradiation with  $\text{Co}^{60}$  produced an increase in the resistivity which increased with increasing dose. The activation energy of the conduction process was calculated to be approximately 1.1eV in the irradiated glasses. We suggest that the irradiation changes the electronic configuration of the potential wells in which the charge carriers are localized.

We suggest that the absence of a change in activation energy for samples cooled at different rate is due to a densification of the glasses and does not affect the activation energy within the cooling rate examined. The correlation with the  $\text{E}'$  center concentration will be discussed.

APPENDIX I.c.

# The American Ceramic Society

## PRESENTATION ABSTRACT DATA FORM

For Office Use Only

Date: \_\_\_\_\_  
Paper #: \_\_\_\_\_  
Room: \_\_\_\_\_  
Hotel: \_\_\_\_\_  
Time on Program: \_\_\_\_\_  
 Paper  Poster

**TITLE:** The Effects of Fusion Temperature upon Paramagnetic States of GeO<sub>2</sub> Glasses

(use * to denote presenting author(s))	Author	Author	Author
Author(s):	G. Kordas *	R. A. Weeks	D. L. Kinser
Company:	Vanderbilt University	Vanderbilt University	Vanderbilt University
Mailing Address:	P.O. Box 24-B	P.O. Box 1678-B	P.O. Box 1689-B
State/Zip:	Nashville, TN 37235	Nashville, TN 37235	Nashville, TN 37235
Phone Number:	(615) 322-3965	(615) 322-3537	(615) 322-3965
Member Number:			MR063656

### Abstract Only

Type abstract **50 words maximum**, double space in this block. Excess after the first 50 words will be deleted.

A new oxygen related defect center was observed in  $\gamma$ -ray irradiated (1.05 by 10<sup>5</sup>R) GeO<sub>2</sub> glasses fused at temperatures between 1200° and 1650°C. The new center has maximum concentration in glasses fused at 1450°C. Fusion temperature dependence of the concentration of this center differs from the H<sub>0</sub> center and is similar to the E<sub>1</sub> center.

Author please complete this section

Time Required for Presentation 15 minutes

Projection Equipment Supplied upon Request by ACeS at no charge:  35 mm slide  
 16 mm film  Overhead  None is requested.

All other projection equipment must be supplied by the speaker.

Poster session: ACeS will supply 4 x 4 Poster Boards on Table Top.

### INSTRUCTIONS

Presented at Annual Meeting of  
American Ceramic Society,  
Pittsburgh, PA, Spring 1984

Please read and follow all directions, and fill in all information.

Do not use all capital letters.

Make 2 photocopies of this form and return all 3 copies to your program chairman.

Program chairman will return one copy to you, including date, time, and place of your presentation.

Give complete mailing address, and phone numbers for all authors so information on meetings can be sent directly to them.

Be sure to indicate what audio-visual equipment you will need.

THIS FORM MAY BE REPRODUCED AS NEEDED

APPENDIX I.d.

# The American Ceramic Society

## PRESENTATION ABSTRACT DATA FORM

For Office Use Only

Date: \_\_\_\_\_

Paper # \_\_\_\_\_

Room: \_\_\_\_\_

Hotel: \_\_\_\_\_

Time on Program: \_\_\_\_\_

Paper  Poster

**TITLE:** UV Optical Properties of GeO<sub>2</sub> Glasses as a Function of  
Fusion Conditions

(use \* to denote  
presenting author(s))

	Author	Author	Authors
Author(s):	John Jackson *	R. Quarles	M. Wells, D. Kinser, R. Weeks
Company:	Vanderbilt Univ.	Vanderbilt Univ.	Vanderbilt Univ.
Mailing Address:	P.O. Box 1689B	P.O. Box 1689 B	P.O. Box 1689B
State/Zip:	Nashville, TN 37235	Nashville, TN 37235	Nashville, TN 37235
Phone No: ( ) _____	( ) _____	( ) _____	
Member Number			MR063656 (Kinser)

### Abstract Only

Type abstract **50 words maximum**, double space in this block. Excess after the first 50 words will be deleted.

The behavior of a 2450 Å absorption peak as a function of fusion temperature and oxygen partial pressure has been studied. The fusion temperature studies suggest that an oxygen deficiency is responsible for the absorption but the partial pressure dependence disagrees. This apparent anomaly is discussed and rationalized upon the basis of multiple defect centers.

Author please complete this section **15** minutes  
Time Required for Presentation \_\_\_\_\_ minutes

Projection Equipment Supplied upon Request by ACerS at no charge:  35 mm slide

16 mm film  Overhead  None is requested.

All other projection equipment must be supplied by the speaker

Power Session: ACerS will supply 4' x 4' Poster Boards on Table Top

### INSTRUCTIONS

Presented at Annual Meeting of  
American Ceramic Society,  
Pittsburgh, PA Spring 1984

- Please read and follow all directions, and fill in all information
- Do not use all capital letters
- Make 2 photocopies of this form and return all 3 copies to your program chairman.
- Program chairman will return one copy to you, including date, time, and place of your presentation
- Give complete mailing address, and phone numbers for all authors so information on meetings can be sent directly to them
- Be sure to indicate what audio-visual equipment you will need.

THIS FORM MAY BE REPRODUCED AS NEEDED

APPENDIX I.e.

# The American Ceramic Society

## PRESENTATION ABSTRACT DATA FORM

For Office Use Only

Date: \_\_\_\_\_  
Paper #: \_\_\_\_\_  
Room: \_\_\_\_\_  
Hotel: \_\_\_\_\_  
Time on Program: \_\_\_\_\_  
     Paper    Poster

**TITLE:** Fusion Temperature Effects on DC Conductivity of GeO<sub>2</sub> Glasses

(use * to denote presenting author(s))	Author	Author	Author
Author(s):	<u>R. H. Magruder, III *</u>	<u>R. A. Weeks</u>	<u>D. L. Kinser</u>
Company:	<u>Vanderbilt University</u>	<u>Vanderbilt University</u>	<u>Vanderbilt University</u>
Mailing Address:	<u>P.O. Box 1689B</u>	<u>P.O. Box 1678B</u>	<u>P.O. Box 1689B</u>
State/Zip:	<u>Nashville, TN 37235</u>	<u>Nashville, TN 37235</u>	<u>Nashville, TN 37235</u>
Phone No.:	<u>(615) 322-3537</u>	<u>(615) 322-3965</u>	<u>(615) 322-3537</u>
Member Number:			<u>MR063656</u>

### Abstract Only

Type abstract **50 words maximum**, double space in this block. Excess after the first 50 words will be deleted.

The DC conductivity of a series of high purity GeO<sub>2</sub> glasses melted and equilibrated in air between 1350° and 1690° C were measured. The resistivity of these glasses increased with increasing fusion temperature. These results are rationalized using arguments which conclude that the structure of the glasses change with fusion temperature.

Author please complete this section

Time Required for Presentation 15 minutes.

Projection Equipment Supplied upon Request by ACeS at no charge:  35 mm slide  
 16 mm film     Overhead     None is requested.

All other projection equipment must be supplied by the speaker.

Poster Session: ACeS will supply 4' x 4' Poster Boards on Table Top.

### INSTRUCTIONS

Presented at Annual Meeting of  
American Ceramic Society,  
Pittsburgh, PA Spring 1984

- Please read and follow all directions, and fill in all information
- Do not use all capital letters.
- Make 2 photocopies of this form and return all 3 copies to your program chairman.
- Program chairman will return one copy to you, including date, time, and place of your presentation.
- Give complete mailing address and phone numbers for all authors so information on meetings can be sent directly to them.
- Be sure to indicate what audio-visual equipment you will need.

THIS FORM MAY BE REPRODUCED AS NEEDED

APPENDIX II.a.

# The Influence of Melting Condition on the Radiation Sensitivity of GeO<sub>2</sub> Glass

R.A. Weeks, D.L. Kinser, G. Kordas, R. Magruder, and M. Wells

Vanderbilt University, Nashville, Tennessee 37235 U.S.A.

A major fraction of optical waveguides are currently fabricated from silica germania glasses. Absorption losses in the 800 to 1500 nm range due to cation impurities have been well identified. On the other hand, there are few reports on the affect of fusion temperature, cooling rate and redox equilibria on absorption losses from 200 to 3000 nm. It has been reported (1) that heating GeO<sub>2</sub> glass in vacuum alters the production rate of the E'<sub>1</sub> centers by irradiation.

We report here preliminary results on some of the effects of variations in fusion temperatures and cooling rates on some properties of GeO<sub>2</sub> glasses. Glasses of electronic grade GeO<sub>2</sub> were fused at 1450, 1550, 1650 and 1690 for three hours in air. All glasses were cooled at approximately 5°C/sec. Fragments of one of the glasses were subsequently melted and splat cooled. Cooling rates (2) were approximately 10<sup>6</sup> C/sec. The results of neutron activation analysis for impurities (3) in μgm/gm were Na(18), Al(15), Cr(13), Zn(15), and Cl(1400). The concentration of OH measured by IR absorption was 230 ppm.

An EPR spectrum characteristic of all our glasses is shown in Figure 1A for measurements at 9 GHz. The component 1A is assymmetric and has a width between the maximum and minimum of the first derivative curve ΔH ~600 G. Band C components are indicated in Figure 1B. The C component has approximately axial symmetry with g<sub>⊥</sub> = 1.94 and g<sub>∥</sub> = 1.9. The B component, on the low field side of the E' center is possibly an oxygen related center.

The variation of the intensity of the E'<sub>1</sub> center as a function of fusion temperature and after <sup>60</sup>Co irradiation is shown in Figure 2. All of the samples cooled at 5°C/sec have E' center concentrations that vary slightly with fusion temperature but are approximately 1.5 x 10<sup>15</sup>/gm. The splat cooled sample (10<sup>6</sup>C/sec) has a concentration 1.5 x 10<sup>16</sup>/gm. The increase in E'<sub>1</sub> concentration after <sup>60</sup>Co irradiation is approximately linear with dose for samples fused at 1550, 1650, and 1690C. In the splat cooled sample, the increase is almost zero although the initial concentration is approximately 10 times greater than for the other fusion and cooling conditions.

The A component, Figure 1A, is also shown in Figure 3a and b as a function of atmosphere in which the sample was measured. It is evident from these data that the A component can be eliminated if a GeO<sub>2</sub> sample is placed in a vacuum (~10<sup>-5</sup> μm pressure) prior to measurement. Figure 3B shows that upon re-exposure to ambient atmosphere the A component has not reappeared after 3 hours. Because the intensity of the B and C components were much less than that of the E'<sub>1</sub> center, the variation of their intensities as a function of fusion temperature were not measured.

Optical absorption spectra of the various glasses, as fused and after  $^{60}\text{Co}$  irradiations up to  $7.7 \times 10^5$  R, have been measured from 200 to 2,000 nm. At wavelengths greater than 350 nm, no absorption bands were detected in as fused samples whose thickness were  $\leq 0.1$  cm. The single resolved absorption band shown in Figure 4 has been discussed in prior research<sup>(2)</sup>. Because of the relatively high absorptivity at  $\lambda < 300$  nm, thin samples ( $d=0.03\text{cm}$ ) were necessary. Reflectivity losses were eliminated by placing a sample in the reference beam and a thicker sample in the sample beam of the spectrometer. The position of the only peak detected shifts from 257 nm to 270 nm and the intensity increases with increasing fusion temperature. Any changes in intensity of this band with irradiation up to  $7.7 \times 10^5$  R were less than the error of measurements. After irradiation, no new bands were detected.

#### CONCLUSIONS:

Since a 3 hour fusion time is insufficient for diffusion to establish thermodynamic equilibria at 1450 C, discussions of the data on the glass fused at this temperature will not be included in the following. Although there are differences in  $E_1'$  center concentrations in the as-fused glasses fused at 1550, 1650, and 1690 C, these differences are small. Thus, we conclude that fusion temperatures in this range have only small effects on the  $E_1'$  center concentration. However, the increase in  $E_1'$  center concentration with irradiation is least in the 1690 glass and highest in the 1550 glass. Hence, the fusion temperature does affect the concentration of the precursor  $E_1'$  sites. Because the differences in  $E_1'$  center concentrations between the 1550, 1650, and 1690 C fusions are small, we tentatively ascribe the order of magnitude differences between the splat cooled samples and the other fusions to the difference in cooling rates. A second difference between the splat cooled samples and others is the rate of increase in  $E_1'$  center concentration with radiation dose. In the splat cooled sample, the rate is almost zero whilst in the other samples it is almost linear (see Figure 2A). Again, we tentatively ascribe this difference in rates to the difference in cooling rates.

Since the mobilities of electrons and holes are high, we argue that the equilibrium distribution of these are maintained during cooling. Conversely, ion mobility is orders of magnitude slower and, consequently, the concentration of ions displaced from their proper two-fold and four-fold concentrations at fusion temperatures is determined by fusion temperature and cooling rates. Thus, the splat cooled glass has a concentration of such displaced ions that is much higher than in the slowly cooled glasses. One consequence of this difference is that the  $E_1'$  center concentration in the splat cooled glasses is higher than in the slowly cooled glasses. A second consequence is a much lower concentration of the  $E_1'$  center precursor sites in the splat cooled glass. Since strain in the splat cooled glass is much higher than in the slowly cooled glasses, it

appears that the "strained bonds" hypothesized<sup>(4)</sup> for precursor sites for E<sub>1</sub> centers is not valid for GeO<sub>2</sub> glass. A slow cooling rate not only decreases the E<sub>1</sub> center concentration in the as-fused glasses but increases many fold the concentration of the precursor E<sub>1</sub> sites. This concentration in 1550 C and 1650 C glasses after a dose  $7.7 \times 10^5$  R exceeds the E<sub>1</sub> center concentration in the splat cooled glass.

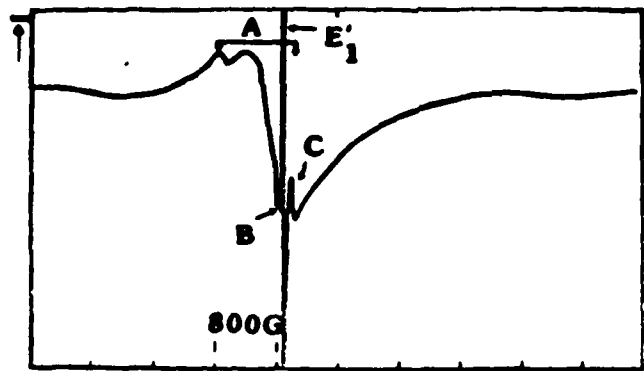
Since the intensity of the A component decreased when a sample was placed in vacuum and did not increase with addition of Fe, it cannot be assigned to ferrimagnetic impurities. The decrease in vacuum indicates that it is due to surface and near-surface paramagnetic species and results from an interaction of the sample surface with normal atmosphere. A plausible possibility is a hydration reaction. Since the ratio of the 35 GHz line width to the 9 GHz line width is 1.7, we attribute the line width to magnetic interactions between the spin states.

We have shown that the fusion temperature and cooling rate affect the concentration of the E<sub>1</sub> centers and its precursor state in GeO<sub>2</sub> glasses. At least three additional paramagnetic components have been observed but their source has not been conclusively identified. One of these, the A component, is due surface and near-surface paramagnetic species that are generated by a reaction with normal atmosphere, probably a hydration reaction.

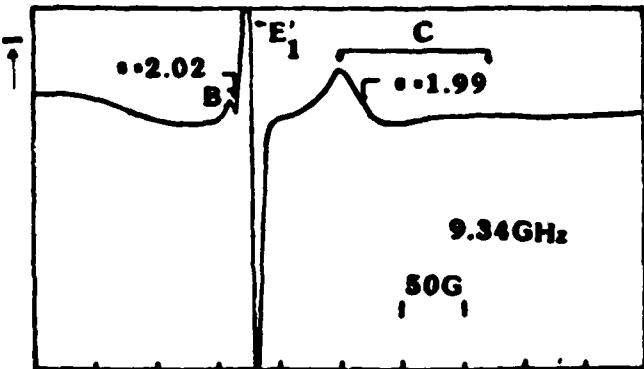
We wish to acknowledge the support of the Army Research Development Office, Contract #DAAG29-81-K-0118.

#### References:

1. T. Purcell and R. A. Weeks, Physics and Chemistry of Glasses, 10(1969), 5, pp.198.
2. P. Vergano and D. R. Uhlmann, Physics and Chemistry of Glasses, 11(1970), 2, p.39.
3. A. E. Owen, Electronic and Structural Properties of Amorphous Semiconductors, Edited by P.G. le Comber and J. Mort, Academic Press, London, 1973, pp.161
4. Neutron activation analyses were made at Oak Ridge National Laboratories by John Bate.
5. J. Friebele and D. L. Griscomb, Treatise on Materials Science and Technology, edited by M. Tomozawa and R. H. Doremus, Academic Press, New York, Volume 17, Glass II, 1979, pp.257.



1A. 4030



1B. 3425 → H(kG)

Fig. 1. EPR spectra characteristic of GeO<sub>2</sub> glasses fused at several temperatures.

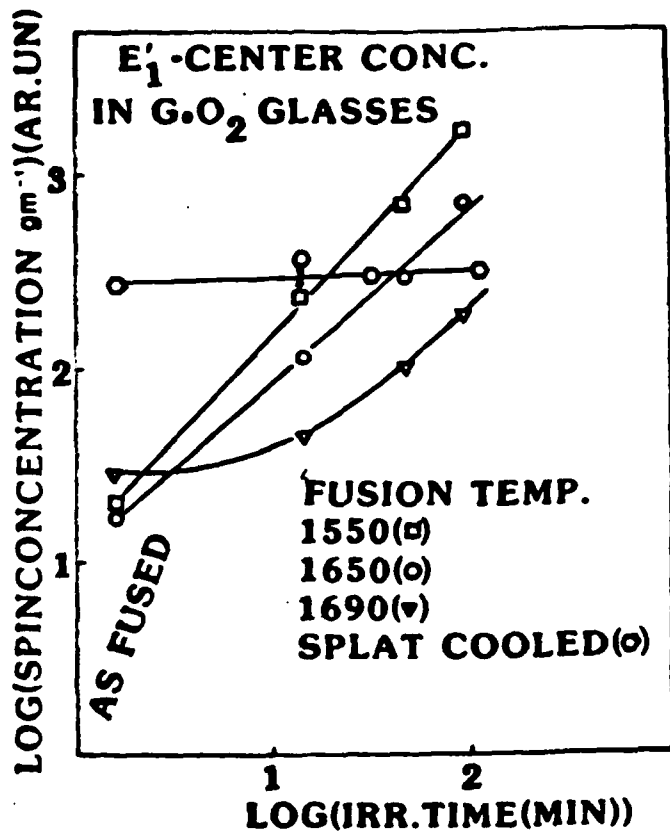


Fig. 2. The intensity of the E'<sub>1</sub> center as a function of fusion temperature and <sup>60</sup>Co γ-ray irradiation. The curve is that expected for a rate of one E'<sub>1</sub> center/photon.

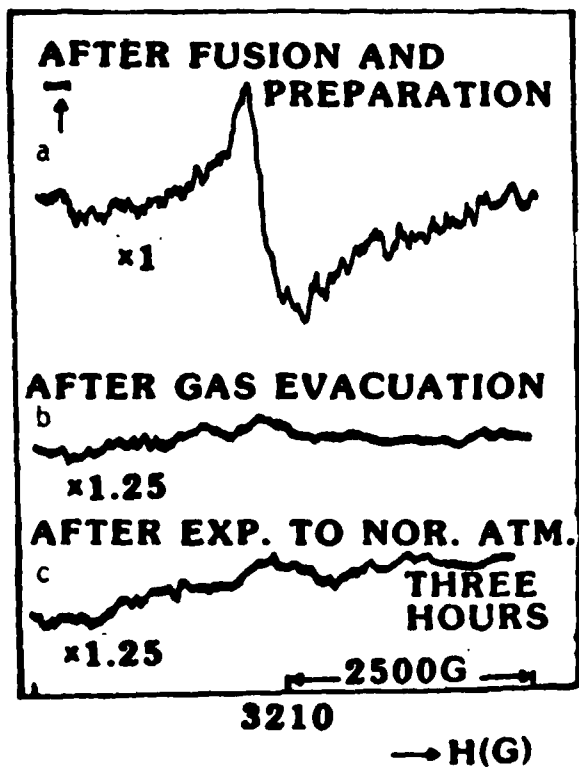


Fig. 3. The intensity of the A component as a function of three treatments.

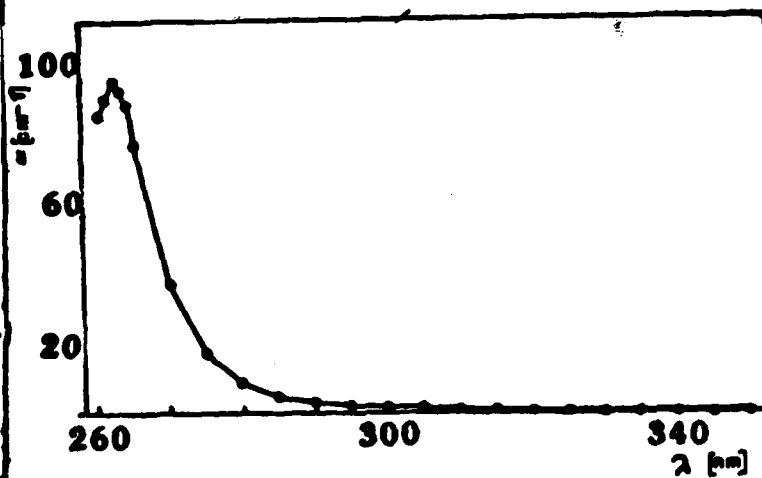


Fig. 4. Optical absorption coefficient versus wavelength of GeO<sub>2</sub> glass.

APPENDIX II.b.

# **Effect of Gamma Radiation on the Direct-Current Resistivity of GeO<sub>2</sub>**

**ROBERT H. MAGRUDER III, DONALD L. KINSER, and ROBERT A. WEEKS**

Reprinted from the Journal of the American Ceramic Society, Vol. 66, No. 4, April 1983  
Copyright 1983 by The American Ceramic Society

## Effect of Gamma Radiation on the Direct-Current Resistivity of $\text{GeO}_2$

ROBERT H. MAGRUDER III,\* DONALD L. KINSER,\* AND ROBERT A. WEEKS\*

College of Engineering, Vanderbilt University, Nashville, Tennessee 37235

*Results of dc resistivity measurements on high-purity  $\text{GeO}_2$  glasses before and after radiation with  $^{60}\text{Co}$  are reported. For these glasses, the dc resistivity is increased by irradiation in a stable and reproducible fashion. This effect is attributed to the interaction of radiation-induced defects with the sodium-ion charge carriers.*

IT IS known that gamma irradiation decreases resistivity of silicate,<sup>1</sup>  $\text{As}_2\text{S}_3$ - $\text{As}_2\text{Se}_3$ ,<sup>2</sup> and iron-phosphate glasses.<sup>3</sup> The general observation is that the induced change decays with time at room temperature. Mike *et al.*<sup>4</sup> attempted to document permanent effects of dc resistivity using electron irradiation in sodium silicate glasses. Their results indicate no statistically significant irreversible effect on resistivity after decay of transient effects.

Numerous studies<sup>5-7</sup> of fused silica and several of  $\text{GeO}_2$ <sup>8,9</sup> document the formation of stable defects as a consequence of gamma irradiation. The present work reports results

of gamma irradiation of  $\text{GeO}_2$  glasses which show stable increases in the dc resistivity and are stable for long periods after irradiation.

Samples were prepared by fusing electronic-grade  $\text{GeO}_2$ \* in platinum crucibles in an electric furnace at 1650°C for 3 h. The crucible and melt were removed and the samples air-cooled to room temperature at an average rate of 5°C/s from 1650° to 400°C. The samples were then removed from the crucible with a core drill and cut into wafers  $\approx 1$  mm thick from the resulting 22-mm diameter cylinder. These wafers were polished to 400 grit, and gold electrodes in a guard ring configuration were evaporated on the wafers. Sample currents were measured using a high-speed picoammeter.<sup>†</sup> Trace-element analyses of

the samples were obtained by neutron activation,<sup>‡</sup> and the OH content was estimated using the 2.7- $\mu\text{m}$  ir band with the extinction coefficient,<sup>10</sup> as reported for  $\text{SiO}_2$  glasses (Table I).

Several recent studies<sup>11,12</sup> have concluded that the charge carrier in glasses similar to the present glasses is a consequence of sodium ion motion. They have observed that glasses with sodium contents from 39 to 1130 ppm display classical Arrhenius behavior with activation energies independent of sodium content over the range examined. Measurements of the present glass as well as those from the literature are plotted in Fig. 1. The samples from Ref. 11 and Ref. 12 display differences in intercept which are opposite those which would be predicted from the sodium content; we attribute these differences to thermal-history variances. With a sodium level of 20 ppm, present results fall between the two previously noted. The activation energy for the two previous works and for the present measurements is 96.6 kJ/mol ( $1.00 \pm .02$  eV) and are indistinguishable within the experimental error. Thus, we are in agreement with Kelly *et al.*<sup>11</sup> and Cordaro<sup>12</sup> that the charge carrier is the sodium ion.

The results of irradiation with  $^{60}\text{Co}$  gamma rays on the present glass are shown in Fig. 2 which also includes the results of a glass measurement after annealing for 1 h at 415°C. This annealing treatment was conducted at 20°C below the observed

CONTRIBUTING EDITOR—R. K. MACCRONE

Received November 22, 1982; approved December 13, 1982.

Supported by the Army Research Office—Durham under Contract No. DAAG-29-81-K-0118.

\*Member, the American Ceramic Society.

†Eagle-Picher, Quapaw, OK.

‡Keithley Instruments Inc., Cleveland, OH.

‡Performed at Oak Ridge National Laboratories.

Table I. Trace Elements in GeO<sub>2</sub> Glasses from Neutron Activation and Infrared Analysis

Element	Level (ppmw)
Na	18.4 ± 0.3
Cl	1376 ± 16
Al	14.1 ± 1.3
Fe	<15
Cr	13.1 ± 2.0
K	<70
Mg	<60
Ca	<31
Ti	<70
Sr	<50
Mo	30.4 ± 4.8
Ni	<19
OH*	200
Others	<15

\*OH was determined by measuring the 2.7- $\mu$ m absorption. In the absence of an extinction coefficient for OH in GeO<sub>2</sub> glasses, it is assumed that the extinction coefficient for OH in SiO<sub>2</sub> (Ref. 10) is approximately correct.

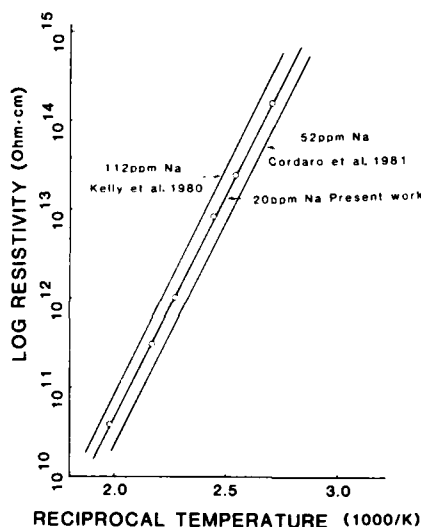


Fig. 1. Log of dc resistivity as a function of reciprocal temperature for two low-sodium glasses from literature and one glass from the present work.

Littleton softening point of 435°C. Note that annealing the as-cooled sample resulted in a modest increase in the resistivity without any change in the activation energy. The influence of gamma is to increase the resistivity and the activation energy. The activation energies for each of the treatments are summarized in Table II. These results are repeatable from sample to sample to within  $\pm 1.9$  kJ/mol for samples irradiated to  $<10^9$  rad. The sample irradiated to  $1 \times 10^9$  rad exhibited a hysteresis with temperature indicating annealing of the irradiation effect above  $\approx 190^\circ\text{C}$ . This effect was not observed for samples subjected to higher temperatures and lower doses. The higher temperature data for the sample irradiated at  $1 \times 10^9$  are substantially identical to those of the unirradiated sample; indeed after annealing, the resistivity of the sample follows the curve for the annealed sample.

Data in Fig. 1 exhibit a variation of

resistivity with Na content that is not proportional to Na content. If, as has been suggested, the charge carriers are Na ions, proportionality would be expected. The authors attribute the nonproportionality to differences in thermal histories of the samples (Fig. 2).

The present results thus indicate that for the low-alkali glasses under study, the dc resistivity is increased in a stable (at room temperature and higher) and reproducible fashion by gamma irradiation.

An increase of activation energy with radiation dose over a limited dose range is thus established by the present data. Note that this effect has not been previously observed in high-alkali glasses.

The model chosen to reinforce the present results is a simple refinement of the model<sup>13</sup> accepted for the motion of alkali ions in silicate, germanate, phosphate, and borate glasses. The model proposes that the alkali ion is thermally activated in its motion through the glassy network. A hypothetical plot of energy as a function of position in the glassy network is shown in Fig. 3. The experimentally observed activation energy for the glass is an average of the height of the barrier over which the ion must be thermally activated. The introduction of charged defects in the glass through radiation exposure modifies this energy coordinate plot, as is indicated by the dotted lines in Fig. 3. Note that this portion of the sodium ion path which passes near the negative portion of the radiation-induced defect is shifted downward, whereas that portion passing near the counter-part positive portion of the defect is shifted upward. In the present results, the average depth of the energy position plot is shifted from 96.6 kJ/mol for the unirradiated glass to as high as 117 kJ/mol for the glass with many defects. This effect has not been previously observed in alkali-containing glasses because the effect should be observable only when the number of defects is large compared to the alkali ion concentration. We thus conclude that the radiation-produced defects interact with the sodium ions in this glass to produce a trapping effect which is observed as an increase in activation energy for conduction and an increase in resistivity.

#### REFERENCES

- V. E. Cullen and H. E. Rexford, "Gamma Radiation Induced Conductivity in Glasses," Proceedings of the IEEE Conference on Dielectric and Insulating Materials, London, 1964.
- T. Minami, A. Yoshida, and M. Tanaka, "Gamma-Ray Induced Conductivity of Vitreous Semiconductors in the System As-S-Te and As-Se-Te," *J. Non-Cryst. Solids*, **7** [4] 328-36 (1972).
- F. Wakim, J. M. Lee, and D. L. Kinser, "The Effect of High Energy Gamma Radiation on the Electrical Properties of Iron Phosphate Glasses," *J. Non-Cryst. Solids*, **29** [3] 423-26 (1978).
- T. M. Mike, B. L. Steierman, and E. F. Degering, "Effects of Electron Bombardment on Properties of Various Glasses," *J. Am. Ceram. Soc.*, **13** [8] 405-407 (1960).
- E. J. Friebele and D. L. Griscom, pp. 257-351 in *Treatise on Materials Science and Technology*, Vol. 17, Edited by M. Tomozawa and R. H. Doremus. Academic, New York, 1979.
- J. Wong and C. A. Angell, *Glass Structure by Spectroscopy*, Marcel Dekker, New York, 1976; pp. 612-59.

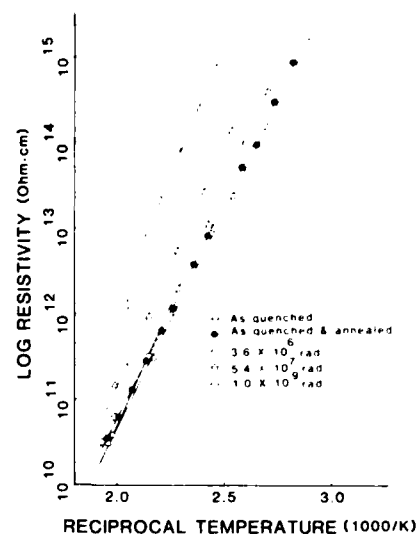


Fig. 2. Log of dc resistivity as a function of reciprocal temperature for a series of radiation doses and after annealing.

Table II. Summary of Activation Energy from Least-Squares Fit of Arrhenius Equation

Sample	Activation energy (kJ/mol) $\pm 1.9$
Virgin sample	97.6
$3.6 \times 10^6$ rad dose	97.6
$5.4 \times 10^7$ rad dose	107
$1 \times 10^9$ rad dose	117
Annealed	96.6

Note: 96.6 kJ/mol = 1 eV.

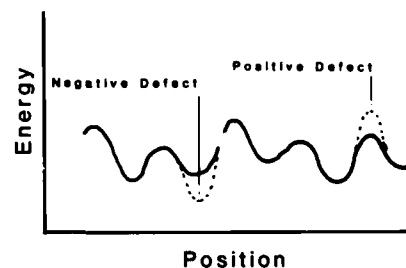


Fig. 3. Hypothetical plot of energy as a function of position for sodium ion moving through unirradiated glass (solid line) and irradiated (dotted line) glass.

- M. Stapelbroek, D. L. Griscom, E. J. Friebele, and G. H. Sigel, "Oxygen-Associated Trapped-Hole Centers in High-Purity Fused Silicas," *J. Non-Cryst. Solids*, **32** [1-3] 313-26 (1979).
- T. Purcell and R. A. Weeks, "Radiation-Induced Paramagnetic States of Some Intrinsic Defects in GeO<sub>2</sub> Glasses and Crystals," *Phys. Chem. Glasses*, **10** [5] 198-208 (1969).
- R. A. Weeks and T. Purcell, "Electron Spin Resonance and Optical Absorption in GeO<sub>2</sub>," *J. Chem. Phys.*, **43** [2] 483-489 (1965).
- G. H. A. M. Van der Steen and E. Papanikolan, "Introduction and Removal of Hydroxyl Groups in Vitreous Silica. Part II," *Philips Res. Rep.*, **30** [4] 192-205 (1975).
- J. E. Kelly III, J. F. Cordaro, and M. Tomozawa, "Correlation Effects on Alkali Ion Diffusion in Binary Alkali Oxide Glasses," *J. Non-Cryst. Solids*, **41** [1] 47-55 (1980).
- J. F. Cordaro and M. Tomozawa, "Possibility of Partial Dissociation of Sodium in High Purity GeO<sub>2</sub> Glasses Investigated by Electrical Measurements," *Phys. Chem. Glasses*, **21** [2] 74-77 (1980).
- Introduction to Ceramics, 2d ed. Edited by W. D. Kingery, H. K. Bowen, and D. R. Uhlmann. Wiley, New York, 1976; Ch. 17.

APPENDIX II.c.

The Effect of Fusion Conditions on the Intrinsic Paramagnetic States of GeO<sub>2</sub> Glasses

G. Kordas\*, R. Weeks, and D. Kinser

Vanderbilt University  
Nashville, Tennessee USA

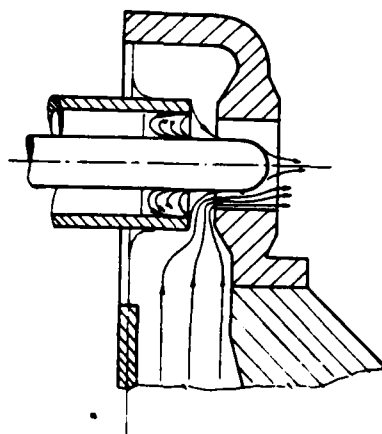


Fig. 1. Streamlines in the head and the tube

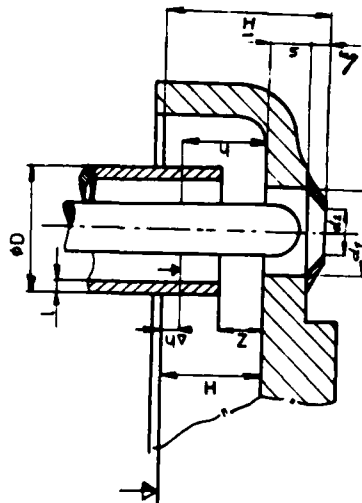


Fig. 2. Marking of the geometrical symbols

The defect center concentration of virgin and <sup>60</sup>Co irradiated GeO<sub>2</sub> glasses cooled at 10<sup>6</sup> C/s, 5 C/s and 0.2 C/s was determined with the ESR-method. In the virgin glasses, the E'-center concentration increases with increasing cooling rates. After  $\gamma$ -ray concentration a new defect center was obtained which was labeled H<sub>0</sub>-center. The concentration of this defect also increases with increasing cooling rates. The growth of the E'-center concentration with the irradiation dose indicates that further defect centers may exist in these glasses which inhibit the formation of the E'-center. However, these defect centers could not be characterized with the ESR-method because their detection was not possible.

### 1. Introduction

Absorption losses in optical fibers can be caused by impurities(1) and by intrinsic defect states(2). Impurities such as Fe, Cu, OH, etc. have been already reduced to an extremely low level through the introduction of new manufacturing processes(3,4) for optical fibers. Thus, losses caused by intrinsic electron states have become of greater significance. The losses due to defect centers can be minimized by an optimization of processing conditions, e.g. T<sub>f</sub>, P<sub>0</sub> and the drawing speed. The melting conditions affect the defect concentration (e.g. oxygen vacancies, peroxy radicals) and the drawing speed the strain (e.g. broken Si-O-bonds). This rupture was assumed to be the source of an absorption band at 630 nm. Large losses in phosphosilicate core fibers were attributed to the rupture of P-O-P-bonds which was assumed to produce an absorption peak at 530 nm(6). On the contrary, Ainslie, et al showed that in germanium doped silica fibers the transmission losses decreased with increasing drawing speed(7). More recently, Kordas et al(8) determined the defect concentration in virgin and  $\gamma$ -ray irradiated GeO<sub>2</sub> glasses fused at temperatures from 1200°C to 1650°C. In virgin GeO<sub>2</sub> glasses, only the E'-center was observed, the intensity of which has a minimum at a fusion temperature of 1550°C. After irradiation at a dose of 6.25 x 10<sup>18</sup>R, one oxygen related defect center was observed in

83K0024

addition to the E' center. While the oxyradical decreased monotonically with increasing fusion temperature  $T_f$ , the E' center concentration reached a maximum at  $T_f=1550^\circ\text{C}$ . The concentration of oxyradicals and E' centers were shown to be a function of fusion temperatures when the cooling rate was constant (5 C/s). As these defect centers may contribute to losses in GeO<sub>2</sub>-SiO<sub>2</sub>-optical fibers, a knowledge of the dependence of their concentration on various cooling rates is of practical importance. In the present paper, we report effects of variation in cooling rates on defect concentrations of the virgin and  $\gamma$ -ray irradiated GeO<sub>2</sub>-glasses.

### II. Experimental

Germania glasses were produced from electronic grade GeO<sub>2</sub> powder (Eagle-Pitcher, Inc.). The fusions were made in platinum crucibles in an electric furnace at 1650°C for three hours. A cooling rate of 5 C/s of the melts was achieved by placing the crucible from furnace on a heat sink (8). A piece of this glass was remelted at temperatures higher than 1700°C and cooled with rates 10<sup>6</sup> C/s (9) using an apparatus especially developed for this work. A third glass was produced with a cooling rate of 0.2 C/s. This cooling rate was achieved by turning off the furnace and cooling the glass in situ. The impurities of these glasses were measured by the neutron activation analysis and have been reported elsewhere (8). The ESR-spectra were recorded using a Varian V-4500 apparatus at 9 GHz and at 300 and 80K. Field strengths were measured with a NMR magnetometer.

### III. Results and Discussion

One ESR-spectrum typical for our virgin GeO<sub>2</sub> glasses is shown in Fig. 1.

It consists of an asymmetric line which was attributed to the E' center in the previous work (8) in as fused glasses. The dependence of the E' center concentration on cooling rate is shown in Table I. One can perceive from this table that the E' center concentration is highest in the splat cooled glass and lowest in the GeO<sub>2</sub> glass cooled at 0.2 C/s.

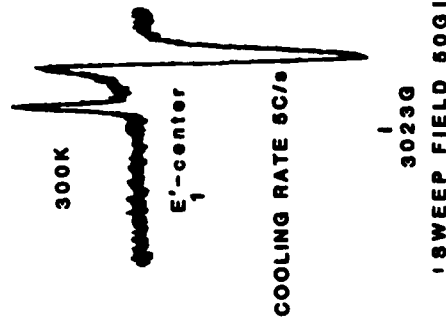


Fig. 1. ESR-Spectrum of GeO<sub>2</sub> glass.

TABLE I. E' Center Concentration in Virgin GeO<sub>2</sub> Glasses

Cooling rate (C/s)	10 <sup>6</sup>	5	0.2
E' center concentration/gr	1.45 x 10 <sup>16</sup>	1.9 x 10 <sup>15</sup>	1.4 x 10 <sup>14</sup>

Figure 2 shows the variation of the total defect center concentration after various  $\gamma$ -ray irradiation times. In these glasses the E' center is the dominant defect detected at room temperature. In the GeO<sub>2</sub> glass cooled at 5° C/s the E' center increases linearly with increasing irradiation time. However, the growth of the E' center concentration in the other glasses shows a more complex behavior

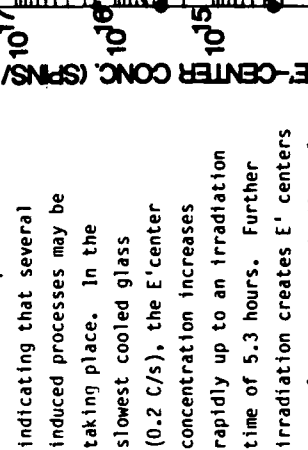


Fig. 2. E' center concentration as a function of cooling rates and  $\gamma$ -ray irradiation. 1) 10<sup>6</sup> C/s COOLING RATE 2) 5 C/s 3) 0.2 C/s

indicating that several induced processes may be taking place. In the slowest cooled glass (0.2 C/s), the E' center concentration increases rapidly up to an irradiation time of 5.3 hours. Further irradiation creates E' centers at a slower rate. In the splat cooled glass, the E' center remains unchanged up to an irradiation time of 255 hours and then suddenly increases with further exposure to  $\gamma$ -rays. In addition to these experiments, low temperature measurements were carried out in order to detect other components which were not detected at room temperature. The results of these measurements are summarized in Figure 3. This figure clearly shows a new well resolved line characterized by a g-value anisotropy ( $g_1=2.003$ ,  $g_2=2.007$ ,  $g_3=2.011-2.015$ ). This defect was labeled H<sub>0</sub>-center and was tentatively attributed to a hole trapped by a non-bridging oxygen.

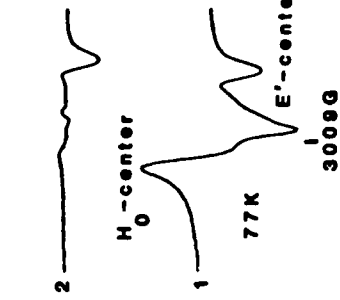


Fig. 3. Dependence of H<sub>0</sub>-center on the cooling rates

#### IV. Conclusions

The concentration of impurities in these glasses is practically invariant. Hence, the variation of the E'-center concentration (Table I) as a function of cooling rates among these GeO<sub>2</sub> glasses is attributed to broken Ge-O-Ge-bonds rather than to impurities. These results are supported by the experiments of Kaiser(5) and Yoshida et al(6) who found absorption bands characteristic of ruptured A-O-A-(A=Si,P) bonds increasing with increasing drawing speed of optical fibers. It is well known that during irradiation electrons and holes are released which can be trapped by different trapping sites in the GeO<sub>2</sub> glasses. The stability of the E' center concentration in the splat cooled glass up to an irradiation time of 255 hours indicates that in this glass a more efficient trapping center for electrons is formed. This electron center may have the H<sub>0</sub> center as reaction partner the intensity of which is higher in the splat cooled samples than in the other glasses. This center is saturated at an irradiation time of 255 hours because the E' center concentration starts increasing. Almost the opposite behavior is present in the slowest cooled glass (0.2 C/s). In this glass, the E' center concentration grows rapidly in a first stage, then increases much more slowly with continuing time greater than 5.3 hours. On the contrary, the E' center concentration in the glass cooled at 5 C/s increases linearly with increasing irradiation time. The E' center concentration in the splat cooled glass and in the glass cooled at 5 C/s do not differ significantly as is expected from the "strain bond" hypothesis(10). Because of the very large differences in cooling rates, we do not believe this hypothesis is applicable to our glasses.

#### Acknowledgements

The authors would like to acknowledge their appreciation of the financial support under ARON Contract #DAAG-29-81-K-0118.

#### REFERENCES

1. H. G. Unger, *Optische Nachrichten Technik*, Elsevier-Verlag, 1976, Berlin 33.
2. F. T. Stone and B. K. Taryal, *J. Non-Cryst. Solids*, 42 (1980) 247-260.
3. M. Shibata, M. Kawachi and T. Edahiro, *T. IECE Japan*, EG3, 12(1980)837-841.
4. B. Bendow and S. S. Mitra, *Advances in Ceramics, Physics of Fiber Optics*, Vol. 2, 1981, Columbus, OH.
5. P. Kaiser, *J. Opt. Soc. America*, 64, 4 (1974), 475-481.
6. K. Yoshida, S. Sentsui, *T. IECE Japan*, G1, 3 (1978) 181-184.
7. B. Ainslie, K. Reales, C. Day & J. Rush, *IEEE J. Q.E.* QE-17, 6(1981) 854-857.
8. G. Kordas, R. Weeks and D. Kinser, submitted to *J. Appl. Phys.*
9. A. E. Owen, *Electronic & Structural Properties of Amorphous Semiconductors*

APPENDIX II.d.

PARAMAGNETIC DEFECTS IN GERMANIUM SULFUR GLASSES

G. Kordas\*, R. Weeks, D. Kinser, and R. Quarles  
Department of Mechanical and Materials Engineering  
Vanderbilt University  
Nashville, Tennessee USA

ESR-studies were conducted at 9.5 GHz on  $\text{GeS}_{2+x}$  glasses ( $x=0,0.1$ ). Glasses were melted at 683°C, 789°C and 895°C in Vycor tubes which were evacuated and sealed before fusion. The ESR-spectra of the virgin glasses are characterized by a narrow symmetric ( $g=2.0037$ ,  $\Delta H_{pp}=3\text{G}$ , A-component) and a broad asymmetric line ( $g=2.0113$ ,  $\Delta H_{pp}=17\text{G}$ , B-component). The narrow line was not detected in the  $\text{GeS}_{2+x}$  glasses fused at 895°C and in the  $\text{GeS}_{2.1}$  glass fused at 796°C. The narrow line intensity of the sulfur deficit glass is approximately two times the corresponding intensity of the stoichiometric and sulfur excess glass. The intensity of the asymmetric line is negligibly small in the GeS glasses fused at 638°C. It dominates in the spectra of the GeS glasses fused at 789°C, and triples in the GeS glasses fused at 895°C. Structural models for the defect centers which cause the detected lines have not yet been developed by us.

I. INTRODUCTION

Paramagnetic defect centers in GeS glasses have been studied extensively by many researchers(1-5). Several species were identified, the concentration of which is sensitive to the stoichiometry of the GeS glasses(1-5). According to Mott et al(6), the paramagnetic states ( $D^0$ ) frozen in at a certain glass composition are in equilibrium with two diamagnetic charged states ( $D^+$  and  $D^-$ ) as given by the reaction:



The fusion temperature variations in the present glasses is designed to examine the kind and concentration of the defect center as a function of this equilibrium. In the present paper, we report preliminary results of a study in which the paramagnetic defect centers have been examined as a function of the stoichiometry and the fusion temperature of these glasses.

II. Experimental

$\text{GeS}_{2+x}$  glasses with  $x=0$  and 0.1 were prepared from pure Ge metal (electronic grade) and reagent grade sulfur powder. Twenty grams of powder of the desired

Also presented at The Conference  
on Glass Science, Clausthal,  
West Germany, July, 1983

composition were fused in evacuated Vycor ampules in a rocking furnace at temperatures of 683°C, 796°C and 895°C. After a fusion time of three hours, the melts were quenched in water. The Vycor tubes were opened in a dry box for further handling. For ESR-measurements, glasses in granular form (D = 2mm and ~150mg in weight) were placed in quartz tubes which were immediately evacuated and sealed in a dry box. The ESR-spectra were recorded with a Varian V-4500 spectrometer operating at 9.5GHz.

### III. Results

ESR-spectra of the  $\text{GeS}_2$  glasses fused at 683°C, 796°C and 895°C are shown in Figure 1. Two different ESR signals were detected which will be referred to as A ( $g=2.0037$ ,  $\Delta H_{pp}=3.26\text{G}$ , symmetric) and B ( $g=2.0113$ ,  $\Delta H_{pp}=17\text{G}$  asymmetric) signals in the following discussion. Figure 1 shows that the intensity of the A-signal decreases with fusion temperature whereas the intensity of the B-signal increases. The ESR-spectra of  $\text{GeS}_{2-x}$  glasses reveals that the intensity of the A- and B-signal also depends on the stoichiometry of these glasses. The intensity of the A-signal gradually decreases with increasing sulfur content.

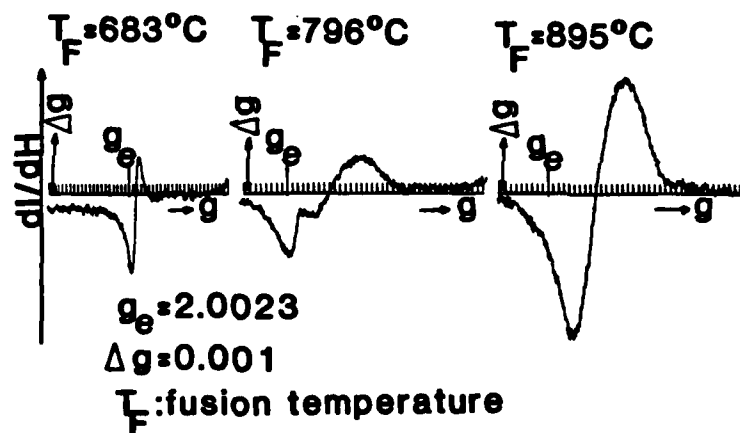


Figure 1

EPR Spectra of  $\text{GeS}_2$  Glasses melted at 683, 796 & 895°C.

However, the B-signal reaches the maximum in the  $\text{GeS}_2$  glasses. These results are tabulated in Table I. Furthermore, the line width of the A-signal depends on the stoichiometry of the glasses, Table I.

Linewidth of the A resonance, $\Delta H_{pp}$ (Gauss)						
x =	0.1		0.0		-0.1	
Fusion T (°C)						
683	1.89		3.26		2.09	
789	3.75		4.00		ND*	
895	ND*		ND*		ND*	
*ND = not detected						
Intensity of the A and B resonances in arbitrary units ( $I = I_{pp} \cdot \Delta H^2$ )						
Fusion T (°C)	A	B	A	B	A	B
683	9.7	ND*	5.1	ND*	4.9	weak
789	4.5	10	1.9	13	ND*	8.5
895	ND*	33	ND*	46	ND*	41

Table I. Dependence of the linewidth of the A- and B-signal and of the intensity of the A-signal on the stoichiometry of the  $\text{GeS}_{2\pm x}$  glasses

#### IV. Discussion

Prior researchers have also reported the A- and B-ESR components(1-5). The A component has been attributed to a  $\equiv\text{GeS}^\bullet$  specie, i.e. a hole located on a non-bridging sulfur ion(1). One component has been observed in carbon disulfide with insoluble sulfur(7). However, its g-value (2.0044), its linewidth ( $\Delta H_{pp}=9.56$ ) and its asymmetry indicate that it differs significantly from the A-component in our glasses. An analysis by Chen and Das(8) indicates that "it is unlikely that the signals stem from such free chain ends". Thus, we reject models which involve non-bridging sulfur ions or chain ends of sulfur chains. Our data show that the intensity of the A component decreases with increasing sulfur. This decrease is particularly evident in the glasses melted at 683°C. Also, this component is not observed in the glass with sulfur excess fused at 796°C, and it is not detected in the glasses fused at 895°C. Thus, its presence is clearly related to the melting temperature. If the A-component is due to an electron state of Ge we would expect g-values less than g-free electrons. For example, in  $\text{GeO}_2$  glasses the E' has g-values  $g_{\perp}=1.9944$  and  $g_{\parallel}=2.001(g)$ . Thus, we expect that the corresponding configuration in the  $\text{GeS}_{2\pm x}$  glasses would have similar g-values. Thus, the E'-center is not an appropriate model for this component. In view of the fact that this center is observed in the  $\text{GeS}_{2.1}$  glass melted at 683°C, we attribute it to a configuration of sulfur ions as yet unspecified. Since the intensity decreases with increasing melting temperature, the concentration of this configuration decreases with increasing melting temperature. We do not believe that this component is due to an impurity since the raw materials were the same for all glasses and since the component is not

observed in some of the glasses. The peaks of the derivative curve of the B-component have g-values of 2.0066 and 2.0166 while the point of maximum intensity has a g-value of 2.0113. The asymmetrical shape of the derivative curve shows that the low field intensity encompasses a spread of g-values. These values fall within those reported in the literature(1-5). Černý and Furmar(4) described this component by a hole located on a non-bridging sulfur. In the GeS<sub>2</sub> glass, the intensity increases with melting temperature. In the glasses melted at 895°C, its intensity is also highest in the GeS<sub>2</sub> glass. Thus, both melting temperature and composition determine the intensity of this component. According to Mott et al(6), the relation between neutral paramagnetic states D<sup>0</sup> and charged diamagnetic states D<sup>+</sup> and D<sup>-</sup> given in the introduction favors the diamagnetic states in chalcogenide glasses. If the paramagnetic state causing the B-component is related to sulfur ions (4), then it appears that this assumption is not valid for this defect center.

## REFERENCES

1. Y. Akagi, A. Kawamori and H. Kawamura, J.Phys.Soc.Jap., 51(1982)4, pp.1041-1042.
2. I. Watanabe and T. Shimizu, Sol.Stat.Comm., 25(1978)pp.705-707.
3. K. Arai and H. Namikawa, Sol.Stat.Comm., 13(1973)pp. 1167-1170.
4. V. Černý and M. Furmar, J.Non-Cryst.Solids, 33 (1979) pp.23-39.
5. I. Watanabe, M. Ishikawa and T. Shimizu, J. Phys.Soc.Jap., 45(1978) 5, pp. 1603 - 1609.
6. N. F. Mott and R. A. Street, Phil. Mag., 36 (1977)1, pp. 33-52.
7. A. G. Pinkus and L. H. Piette, J. Phys. Chem., 63 (1959), pp. 2086-2087.
8. I. Chen and T. P. Das, J. Chem. Phys., 45 (1966) 10, pp. 3526-3535.
9. T. Purcell and R. A. Weeks, Phys. Chem. Glass., 10 (1969) 5, pp. 198-208.

APPENDIX II.e.

THE INFLUENCE OF FUSION TEMPERATURE ON THE DEFECT CENTER  
CONCENTRATION OF GeO<sub>2</sub> GLASS

G. Kordas, R.A. Weeks, and D.L. Kinser  
Vanderbilt University  
Nashville, Tennessee 37235

ABSTRACT

Paramagnetic resonance spectra of virgin glasses and  $\gamma$ -ray irradiated GeO<sub>2</sub> glasses were studied with the Electron-Spin-Resonance (ESR) method as a function of fusion temperatures. Fusions were made in air at temperatures between 1200°C and 1650°C and cooled at constant rate. In virgin glasses, only the E'-center was detected at concentrations of about 10<sup>15</sup>/gr. After a  $\gamma$ -ray irradiation, a new resonance at the low field side (lfs) of the E'<sub>1</sub>-center and a symmetric line with  $g = 1.91$  were observed. Measurements at various temperatures, power levels, and frequencies provide a basis for resolving the overlapping resonances. We labeled the paramagnetic center causing the lfs-signal the H<sub>0</sub>-center. The  $g$ -values of the H<sub>0</sub> center are the basis for attributing this center to a hole located on a non-bridging oxygen. The  $g = 1.91$  resonance is attributed to Cr<sup>5+</sup> or Mn<sup>5+</sup> impurities in the GeO<sub>2</sub> glasses. At constant  $\gamma$ -ray dose, the H<sub>0</sub>-center concentration decreased and the E'<sub>1</sub> center concentrations increased with increase of fusion temperature.

## 1. INTRODUCTION

When extremely low loss optical waveguide fibers are exposed to ionizing radiation, their light transmittance is affected by the generation of color centers<sup>(1)</sup>. The concentrations and types of irradiation induced defect centers depend both on composition and thermal history of the fibers. In the past, much research has been done to characterize centers that are generated in optical fibers<sup>(2)</sup>. A connection has already been established between coloration and composition, particularly impurities, of an optical fiber<sup>(2,3)</sup>. On the other hand, very little is known about the influence of fabrication conditions on concentrations of various types of defects. Vergano and Uhlman<sup>(4)</sup> attributed the intensity variations of an optical absorption band, characteristic of GeO<sub>2</sub> glasses, to variations in stoichiometry with increasing fusion temperatures, T<sub>f</sub>. Using the Electron-Spin-Resonance spectroscopy, Weeks and Purcell showed<sup>(5)</sup> that the E'-center concentration is greater in GeO<sub>2</sub> glasses melted in vacuum ( $p_{O_2} = 10^{-6}$  atm) than in normal atmosphere ( $p_{O_2} = 0.2$  atm). Recently, Weeks and co-workers determined the accumulation kinetics of the E'-center in GeO<sub>2</sub> glasses with cooling rates 5°C/s and ~10<sup>6</sup>°C/s<sup>(6)</sup>. These experiments showed that among the virgin glasses, glasses cooled at ~10<sup>6</sup>°C/s have more E'centers than glasses cooled at 5°C/s. The E'-center concentration of the rapidly cooled GeO<sub>2</sub> glasses remains unchanged after a dose of 7.7 x 10<sup>5</sup> R while in the slowly cooled glasses increases of about two orders of magnitude were measured.

Based on various models which have been proposed for intrinsic paramagnetic states of  $\text{GeO}_2$  glasses, the intensity variations of these states as a function of fusion temperature and subsequent irradiation with energetic photons will provide indirect evidence of their thermodynamic properties.

It is the aim of this work to detect and characterize the paramagnetic states of virgin and irradiated  $\text{GeO}_2$  glasses as a function of fusion temperatures. The melts were made in air and cooled at a constant rate. In this work, the  $\text{GeO}_2$  glasses were chosen because they can be easily melted and are very often used for the fabrication of the optical fibers<sup>(7,8)</sup>.

## 2. EXPERIMENTAL PROCEDURE

Commercially available electronic grade  $\text{GeO}_2$  (Eagle-Pitcher, Inc.) was used for the production of the glasses. They were fused in platinum crucibles in an electric furnace. The time of fusion was varied between 3 and 270 hours depending on the fusion temperature in order to achieve an equilibrium with the atmosphere in the glass melt. After melting, the crucibles were removed from the furnace and placed on a heat sink which gave an average cooling rate from melt temperature to  $400^\circ\text{C}$  of 5 C/s. Trace element analysis of the samples were obtained by neutron activation<sup>(9)</sup> and the OH content was estimated using the 2.7 micron IR band with the extinction coefficients as reported for  $\text{SiO}_2$  glasses<sup>(10)</sup>. These are given in Table I. Specimens of approximately 11mm in length weighing 0.1 grams

were used for the 9.5GHz measurements. For the 35GHz measurements, sample dimensions were 5x1x1 mm. The 9.5GHz studies were carried out with a Varian V4500 spectrometer. The microwave frequency was measured with a counter (Syntron Danner Counter 1017/1255A) and the magnetic field with a NMR magnetometer (ANAC-SENTEC 1001). The spin concentration was calculated by the comparison technique using a Varian strong pitch standard. The irradiation of the specimens was made with a  $^{60}\text{Co}$  source with a dose rate of  $1.5 \times 10^5$  R/h.

### 3. ESR SPECTRA OF THE UNIRRADIATED $\text{GeO}_2$ GLASSES

Figure 1 shows the ESR-spectrum of an unirradiated  $\text{GeO}_2$  glass melted at  $1200^\circ\text{C}$ . This spectrum consists of an axial symmetric resonance. The estimated g-values of this resonance are shown in Table II. In the same table, g-values for the  $\text{E}'\text{-GeO}_2$ -center are entered. One can perceive from this table that the g-values of the measured spectrum agree with the published g-values for the  $\text{E}'$ -center within experimental error.(11,12). From this comparison, it can be concluded that the resonance of Figure 1 is caused by an  $\text{E}'$ -center. We calculated the  $\text{E}'$ -center spin concentration for the glass fused at  $1200^\circ\text{C}$  to be  $1.17 \times 10^{15}/\text{gr}$ . The ESR-spectra of several  $\text{GeO}_2$  glasses melted at various temperatures were recorded and we calculated the  $\text{E}'$ -center concentration of these glasses. Two glasses were melted at the same temperature in order to test the reproducibility of the  $\text{E}'$ -center concentration obtained at a certain fusion temperature. Figure 2 summarizes our results. The paramagnetic defects detected in the virgin glasses represent only one of the defects present in these glasses.

Additional paramagnetic defects can be generated by exposing these glasses to  $\gamma$ -ray irradiation.

#### 4.1 ESR SPECTRA AFTER $\gamma$ -RAY IRRADIATION

After exposure to  $\gamma$ -ray, the  $\text{GeO}_2$  glasses showed two additional resonances, one on the low-field side (lfs) and the other on the high-field side ( $g=1.91$ ) of the  $E'$ -center. These resonances are shown in Figure 3. The intensity of the  $g = 1.91$  component is less than 0.01 the  $E'$ -center intensity. The lfs-signal overlaps with the resonance of the  $E'$ -center. For a precise determination of the  $g$ -values of the centers which cause this lfs-signal, separation of the overlapping signals is useful. These  $g$ -values of the lfs-resonance can provide a basis from which a structural model can be developed. We labeled the center causing the lfs-signal  $H_0$ -center.

#### 4.2 35 GHz MEASUREMENTS

One possibility for the separation of overlapping signals consists in the observation of these signals at higher frequencies because the resolution of a spectrometer increases with increasing frequency. For this purpose, we measured the ESR spectra of a sample fused at  $1650^\circ\text{C}$  at 35 GHz at room temperature. Figure 4 shows the 35GHz spectra. Two well resolved resonances are evident in this figure, one of which is due to the  $E'$  center. The other resonance is caused by the  $H_0$ -center shown in Figure 3 and is characterized by the  $g$ -values given in Table III. The  $g_3$ -component cannot be precisely measured from the spectrum because the shoulder determined by  $g_3$  is poorly resolved.

## 5. MEASUREMENTS AT 77 K

The  $\text{GeO}_2$  glasses investigated in this work contain 1376 ppm chlorine, 200 ppm OH and several other impurities (Table I). It can be assumed that these impurities and even intrinsic defects may have paramagnetic states after irradiation which could have very short relaxation times. Thus, their ESR-spectra may not be detected at room temperature. In order to examine this possibility, low temperature measurements were carried out. Figure 5 shows the spectrum of a  $\text{GeO}_2$  glass fused at  $1200^\circ\text{C}$  recorded at 300k and 77k. This figure clearly demonstrates the changes of the spectra occurring from the variation of the temperature of the measurements.

In order to improve resolution and to detect other paramagnetic states, the low temperature spectra shown in Figure 5 were recorded at two microwave power levels. These experiments are based on the fact that different species possess different spin-lattice relaxation times and therefore their contribution to a spectrum is different at different microwave powers. Thus, in the case that saturation broadening does not occur, different species may be identified by varying the microwave power. For a better resolution of changes occurring as a function of microwave power, the spectra were normalized to the maximum amplitude of the curves. The coincidence of the curves demonstrates that no substantial changes of the resonances were obtained with variation of microwave power. Thus, the conclusion can be drawn that only one species contributes to the low temperature spectra of Figure 5. The g-values describing this resonance are given in Table III and within the experimental errors are the same as those obtained

for the  $H_0$ -center in the 35GHz measurements. As the g-values of this center are greater than the g-values of the free electron, it can be assumed that the paramagnetic state is hole-type.

6. THE DEPENDENCE OF FUSION TEMPERATURE ON THE DEFECT CENTER CONCENTRATION

$GeO_2$  glasses fused at various temperatures were irradiated and their spectra at room temperature and at 77 K were recorded. Figure 6 shows the measured spectra. It can be seen from this figure that the room temperature ESR-spectra are dominated by the  $E'$ -center. The estimation of the  $E'$ -center concentration was made on the basis of these measurements. The defect concentration of the  $H_0$ -center was made from the 77 K measurements. For these calculations, we first generated the low temperature spectra  $I(H, \text{fusion } T)$  of Figure 6 with the ESR-spectra of the  $H_0$ -center (Figure 5) and of the  $E'$ -center (Figure 1) using the equation:

$$I(H, \text{fusion } T) = c(H_0, \text{fusion } T) * f(H_0, H) + c(E', \text{fusion } T) * f(E', H)$$

with:

$I(H, \text{fusion } T)$ ,  $f(H_0, H)$  and  $f(E', H)$  normalized and

$$c(H_0, \text{fusion } T) + c(E', \text{fusion } T) = 1$$

and where  $I(H, \text{fusion } T)$  is the measured amplitude and  $c(H_0, \text{fusion } T)$  and  $c(E', \text{fusion } T)$  are the contributions of the  $H_0$  and  $E_0$  centers to the measured ESR-signal.

By knowing the real contribution of the  $H_0$ -center to the ESR spectrum, its concentration can be calculated by a double integration of the signal:

$$I(H_0, H, \text{fusion } T) = c(H_0, \text{fusion } T) * I(H, \text{fusion } T)$$

With this method, the spin concentration of the  $H_0$ -center was estimated. Figure 7 summarizes the results of the calculation of the  $H_0$ - and  $E'$ -center concentration.

## 7. DISCUSSION

### 7.1 Model for the $H_0$ -center:

Based on the 9 and 35 GHz spectra and the low temperature measurements, the  $H_0$ -center can be described as a hole having  $S=1/2$ . This hole may be located on an intrinsic point defect because of the following facts:

1. The impurities with the highest concentration in our glasses are chlorine and hydrogen. Paramagnetic states arising from molecule ions or ions of these elements in glasses can be easily identified because they have a non-zero nuclear spin in high natural abundance. It is well known that an interaction of paramagnetic state  $S=1/2$  with an nuclear spin can cause  $n=2*I+1$  equidistance lines with equal intensity. Such hfs-splitings due to Cl and H have been well identified in the literature<sup>(12-16)</sup>. The spectrum of the  $H_0$ -center does not provide any evidence of a hfs-splitting.

2. The concentrations of the  $H_0$  and  $E'_1$  centers exceed by more than an order of magnitude the concentrations of any detected impurity except Cl and H.

3. Alkali metals can serve as hole traps in glasses<sup>(17)</sup>

However, their spectra are obtained after irradiation at 77 K<sup>(17)</sup>.

Thus, we attribute the  $H_0$  center to an intrinsic state of  $GeO_2$  glass. The structure of the  $GeO_2$  glass may contain several paramagnetic states involving oxygen ions such as  $O^-$ ,  $O_2^-$ ,  $O_3^-$ , etc. The g-values of these radicals have been well characterized in many glasses and crystals<sup>(6,11,19)</sup>. Table IV gives characteristic g-values of these paramagnetic centers in many materials. The  $O_3^-$  complex can be ruled out because its g-values differ from those obtained for the hole center. Furthermore, the peroxyradical can be eliminated because the typical shoulder at  $g = 2.05$  has not been resolved in our spectra. Based on the present data, the oxyradical on non-bridging oxygen ion is the most probable candidate for the  $H_0$  center, However, further experimental and theoretical work is needed for a precise interpretation of this paramagnetic state.

## 7.2 MODEL FOR THE $g=1.91$ RESONANCE

Chromium and molybdenum are the most abundant transition metal impurities in our glasses. The +5 and +3 valence states of these ions have been well identified with the ESR-method<sup>(20-22)</sup>.  $Cr^{5+}$  and  $Mo^{5+}$  have a  $d^1$  electron and consequently  $S = 1/2$ . Based on prior research, the  $g=1.91$  signal is consistent with the experimental observations of  $Cr^{5+}$  and  $Mo^{5+}$  in oxide glasses<sup>(20,21)</sup>.

### 7.3 EFFECTS OF VARIATIONS OF FUSION TEMPERATURE

In all of the glasses which have been prepared, E' centers are present in concentrations,  $n(E'_1)$  that are  $10^{14} \text{ gr}^{-1} < n(E'_1) < 3 \times 10^{15} \text{ gr}^{-1}$ . These concentrations are less than the concentration of any of the impurities which have been detected. However, in all of the glasses for which data are given in Figure 2 and 7 and for other  $\text{GeO}_2$  glasses prepared in a similar manner, each impurity listed in Table I have a maximum range of  $\pm 10\%$  from the average concentration. The variation shown in Figure 2 and 7 is much larger than the variation in any impurity. Thus we attribute the variation in E'-center concentration in the as-fused samples to variation in  $T_f$  (Fig. 2). As  $T_f$  increases from  $1200^\circ\text{C}$  to  $1550^\circ\text{C}$ , the  $E'_1$ -center concentration decreases. However, for a  $T_f = 1650^\circ\text{C}$ , it increases. Gamma-ray irradiation of all of these glasses produces an increase in  $n(E')$ . Hence, in addition to the initial concentration of E' centers, there are precursor sites in the glasses which can become E' centers upon electronic excitation. For a constant  $\gamma$ -ray dose, the magnitude of this increase is a function of  $T_f$ , increasing with increase of  $T_f$  from  $1200^\circ\text{C}$  to  $1450^\circ\text{C}$ , unchanged from  $1450^\circ\text{C}$  to  $1550^\circ\text{C}$ , and decreasing for  $1650^\circ\text{C}$  (Figure 7). This change between  $1550^\circ\text{C}$  and  $1650^\circ\text{C}$  is correlated with the change observed in  $n(E')$  in the as-fused samples. Thus, the concentration of E' precursor sites is also a function of fusion temperature.

In the as-fused samples, the  $H_0$  center has not been detected. However, after irradiation its concentration exceeds that of the E' center except for the  $1650^\circ\text{C}$  sample. The concentration of the  $H_0$  center decreases with increasing  $T_f$  with a dependence that is inverse

of the E' center dependence with the exception of  $T_f = 1650^\circ\text{C}$ . For this  $T_f$  the E' concentration after irradiation is less than in the  $1550^\circ\text{C}$  sample, but in the as-fused sample increases by almost an order of magnitude and the  $H_0$  center concentration decreases by a similar order. Thus we conclude that there is a strong correlation between the concentration of  $H_0$  centers and  $T_f$  and between the concentrations of  $H_0$  and E' centers. For both  $H_0$  and E'<sub>1</sub> centers, the precursor concentration decreases sharply at  $T_f = 1650^\circ\text{C}$ .

The processes by which the E'<sub>1</sub> and  $H_0$  centers and their precursor sites are formed during fusion are thermal and consequently their concentration,  $n$ , should have a temperature dependence

$$n = n_0 e^{-E/kT}$$

where  $n$  is the number of sites,  $n_0$  is the number of sites from which either the centers or their precursors can be formed,  $E$ ,  $k$  and  $T$  are the activation energy, Boltzman constant and absolute temperature respectively. It is evident from both Figure 2 and 7 that there may be several thermally activated processes involved in the formation of E' and  $H_0$  centers and their precursors. It is also evident that there is a change in these processes which begins at  $1550^\circ\text{C}$  and this change becomes more evident at  $1650^\circ\text{C}$ .

## 8. CONCLUSIONS

With increase of fusion temperature, the concentration of E' centers after irradiation to a constant dose ( $8.25 \cdot 10^5$  R) increases. On the other hand, the concentration of the  $H_0$  center decreases.

These changes can be interpreted as a change in the stoichiometry of the glass with fusion temperature<sup>(4)</sup>. The fact that the concentration of the  $H_O$  center exceeds the alkali concentration indicates that the alkali is not the sole determinant of the concentration of nonbridging oxygen. Despite its relatively high concentration, we have not detected any paramagnetic states in which Cl is a constituent. Because of its high concentration, we think that Cl may play some indirect role in determining the concentrations of  $H_O$  and  $E'$  centers. However, the concentrations of Cl and H do not vary with fusion temperature, thus the variations in  $H_O$  and  $E'$  centers are primarily determined by fusion temperatures and not by H and Cl concentrations.

The fact that the concentration of  $H_O$  centers is much greater than that of  $E'_1$  may indicate that these glasses are not deficient in oxygen. This data may indicate an excess of oxygen in these glasses, although this is contrary to the conclusions of other investigators. If there is a deficit of oxygen then same fraction, nonetheless, is present as non-bridging ions. Since the Cl concentration exceeds the maximum concentration of  $H_O$ -centers, it may be in part the compensation for the oxygen deficit and also permit the formation of non-bridging oxygens.

#### ACKNOWLEDGEMENT

The authors wish to express their appreciation for financial support of this work under AROD Contract #DAAG-29-81-K-0118. We also would like to thank Dr. L. Wilson of the Electrical Engineering Department at Vanderbilt University for the use of the ESR apparatus and R. Magruder and M. Wells for supplying samples.

## REFERENCES

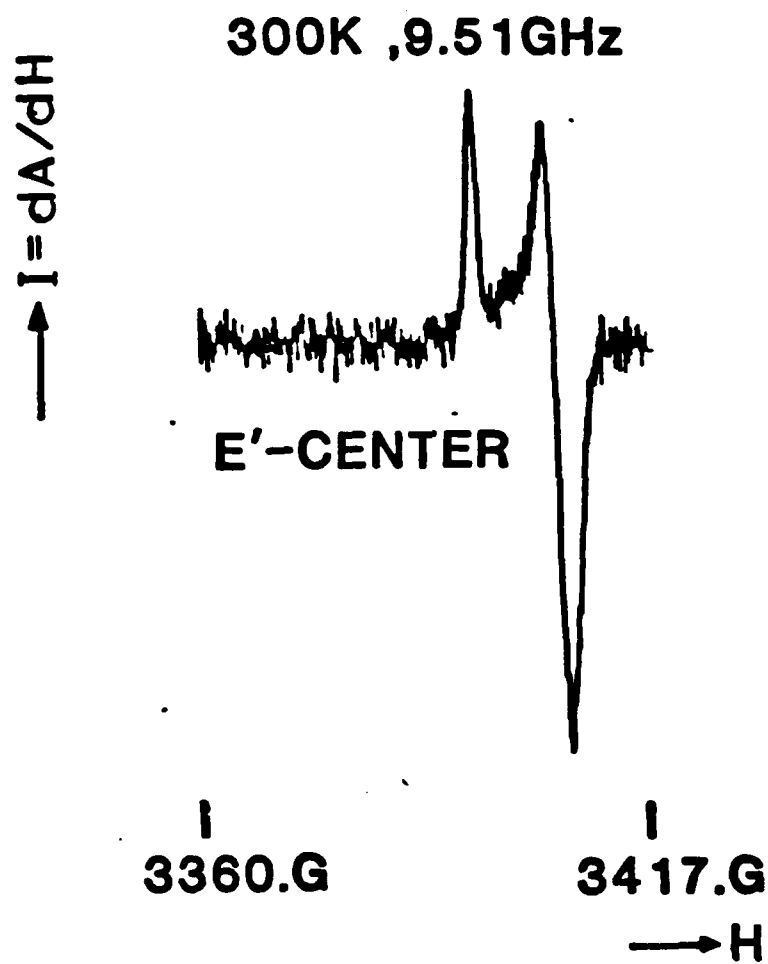
1. B. D. Evans and G. H. Siegel, Jr., IEEE Trans., Nucl. Science 21, 113 (1974).
2. E. J. Friebale, D. L. Griscom and G. H. Siegel, Jr., J. Appl. Physics, 45 3424 (1974).
3. H. G. Unger, Optische Nachrichtentechnik, (Elitera-Verlag, Berlin 33, 1976).
4. P. Vergano and D. R. Uhlmann, Phys. Chem Glasses II (2), 39 (1970).
5. R. A. Weeks and T. Purcell, J. Chem. Phys. 43 483 (1965).
6. R. A. Weeks, D. L. Kinser, G. Kordas, R. Magruder, and M. Wells, J. Physique, to be published.
7. N. Shibata, M. Kawachi and T. Edahivro, Trans. IEEE Japan, 63 (12), 837 (1980).
8. B. J. Aylile, K. J. Beales, D. M. Cooper, C. R. Day, and J. D. Rush, J. Non-Crystalline Solids, 47 (2), 243 (1982).
9. Neutron activation analysis performed by Lamont Bate of Oak Ridge National Laboratories.
10. G.H.A.M. Van der Steen and E. Papanikolau - Phillips Research Reports 30, 192-205 (1975).
11. T. A. Purcell and R. A. Weeks, Phys. Chem. Glasses, 10, 198 (1969).
12. G.F.J. Garlick, J. E. Nicholls, and A. M. Ozer, J. Phys. C. 4, 2230 (1971).
13. D. L. Griscom, J. Chem. Phys. 51, 5186 (1969).
14. R. Berger and G. Vignaud, C. R. Acad. Sc. Paris, t. 287, B-329 (1978).
15. E. B. Zvi, R. A. Beaudet and W. K. Wilmarth, J. Chem. Phys. 51, 4166 (1969).
16. A. V. Shendrik and D. M. Yudin, Phys. Stat. Sol. (b) 85, 343 (1978).
17. D. L. Griscom, J. Non-Cryst. Solids, 13, 251-285 (1973/74).
18. G. Kordas, B. Camara and H. J. Oel, J. Non-Cryst. Solids 50, 79 (1982).
19. N. E. Wong and J. H. Lungsford, J. Chem. Phys. 56 (6), 2664 (1972).
20. N. S. Garif'yanov, Sov. Phys. Sol. State 4 (9), 1795 (1963).
21. A. Bals, J. Kliava and J. Purans, J. Phys. C: Solid St. Phys., 13, L437-41 (1980).
22. J. Wong and C.A. Angell, Glass structure by spectroscopy, (Marcel Dekker, Inc., New York, 1976), pp.555.

## FIGURES

1. ESR-spectrum of a virgin  $\text{GeO}_2$  glass melted at  $1200^\circ$ .
2. Dependence of the  $E'_1$ -center concentration on the fusion temperature of unirradiated  $\text{GeO}_2$  glasses. The temperature is plotted as  $1/T$  and the concentration as log concentration in order to show that the concentration is not due to any single activated process
3. ESR-spectrum of a  $^{60}\text{Co}$  gamma-ray irradiated  $\text{GeO}_2$  glass ( $10^6\text{R}$ ).
4. Room temperature 35GHz ESR-spectrum of a  $^{60}\text{Co}$  gamma-ray irradiated  $\text{GeO}_2$ -glass fused at  $1650^\circ\text{C}$ . The symbols 1x and 5x are relative gains of the amplifier. The term "lfs-signal" is used in the text.
5. Spectra of  $\text{GeO}_2$  glass fused at  $1200^\circ\text{C}$  and irradiated with  $^{60}\text{Co}$  gamma-ray to a dose of  $8.25 \cdot 10^5\text{R}$ .
  - a) The symbol 5.9x indicates the relative amplifier gain.
  - b) Curve 2 was recorded at a microwave power 10 time that for curve 1. The maximalization procedure is described in the text.  
The symbol 1x indicates relative amplifier gain.
6. Spectra of irradiated  $\text{GeO}_2$  glasses ( $8.25 \cdot 10^5\text{R}$ ) recorded at room temperature and at 77 K.
7. Dependence of the  $\text{H}_o$ - and  $E'_1$ -center concentration on the fusion temperature.

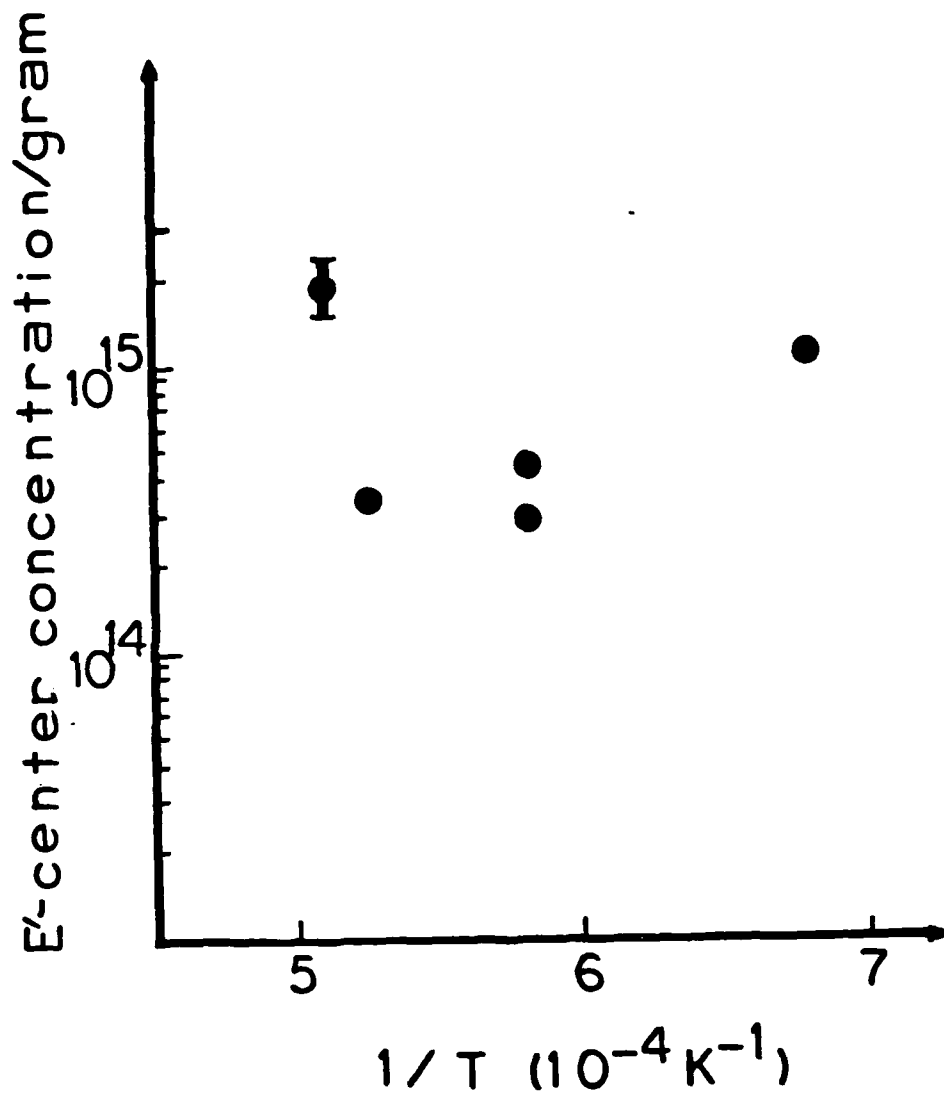
TABLES

- I. Impurities in  $\text{GeO}_2$  from Neutron activation and IR analysis ( $2.7 \mu\text{m}$  OH absorption)
- II.  $g$  - values of the  $E_1'$ -center in our glasses and  $g$ -values of  $E_1'$ -centers in crystalline and glassy  $\text{GeO}_2$  reported in the literature.
- III.  $g$ -values of the  $H_0$ -center.
- IV. Characteristic  $g$ -values of  $O^-$ ,  $O_2^-$ , and  $O_3^-$  paramagnetic complexes reported in the literature.



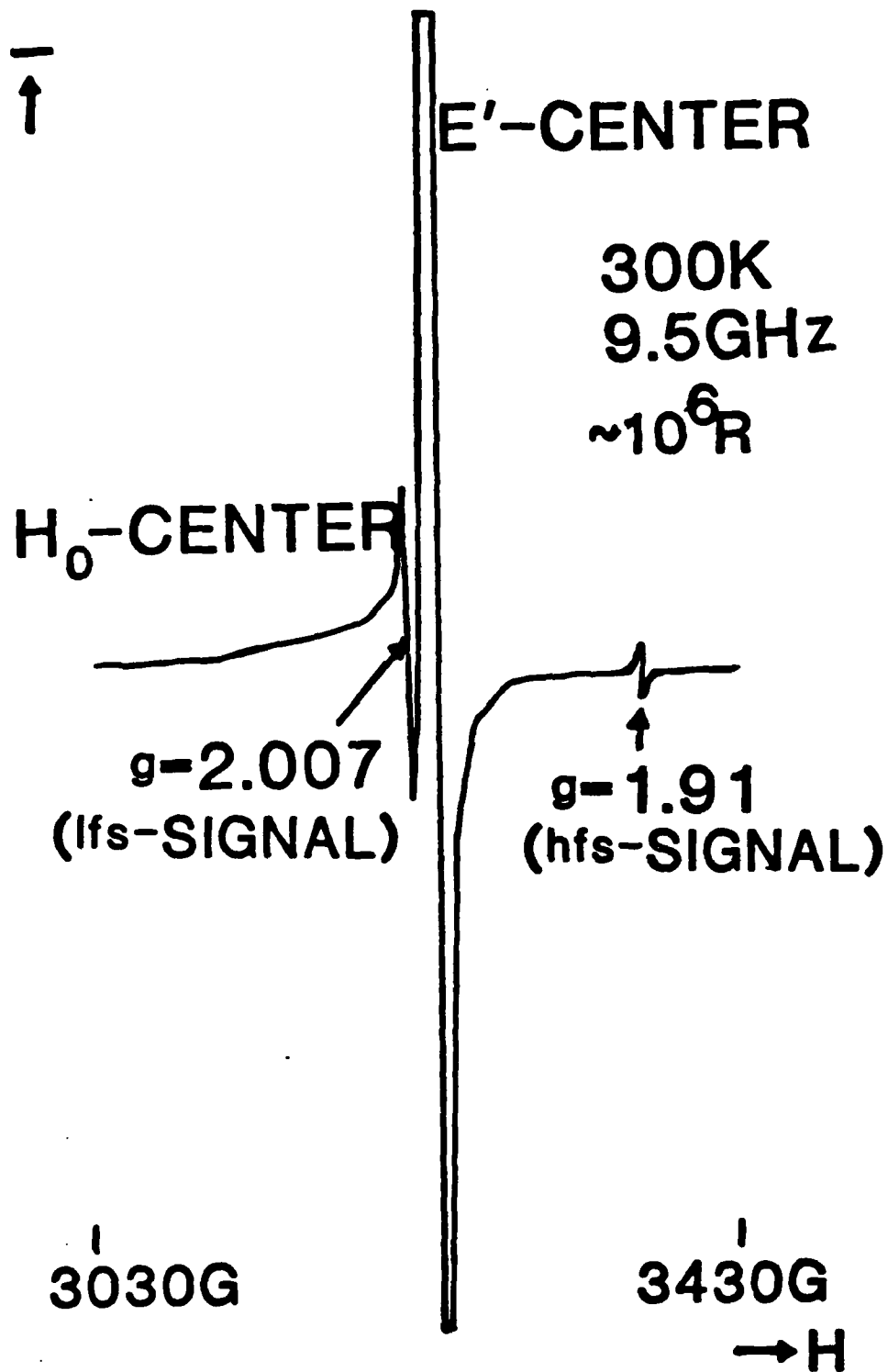
FIGURE

1. ESR-spectrum of a virgin  $\text{GeO}_2$  glass melted at  $1200^\circ$ .



FIGURES

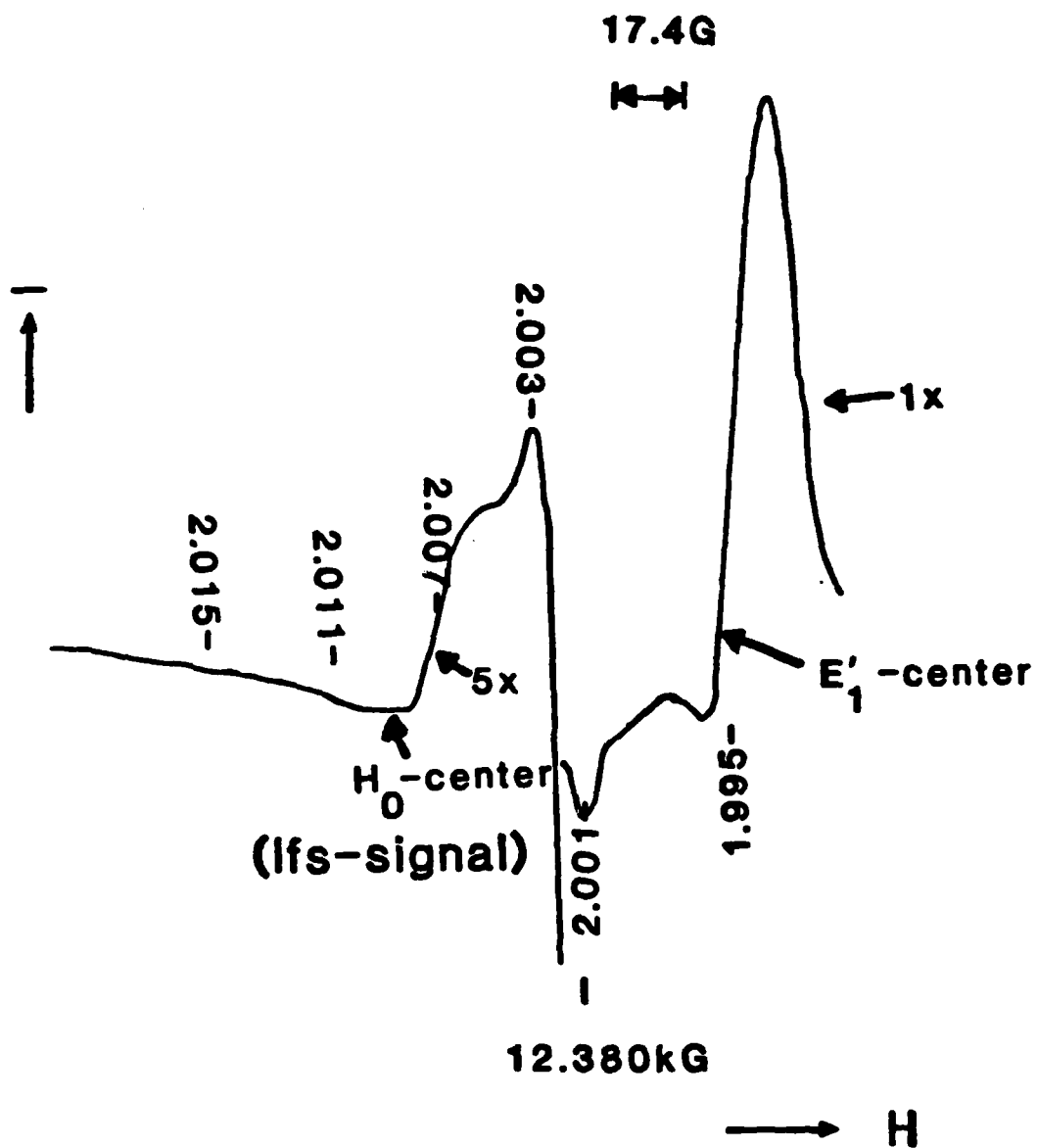
2. Dependence of the  $E'_1$ -center concentration on the fusion temperature of unirradiated  $\text{GeO}_2$  glasses. The temperature is plotted as  $1/T$  and the concentration as log concentration in order to show that the concentration is not due to any single activated process



FIGURE

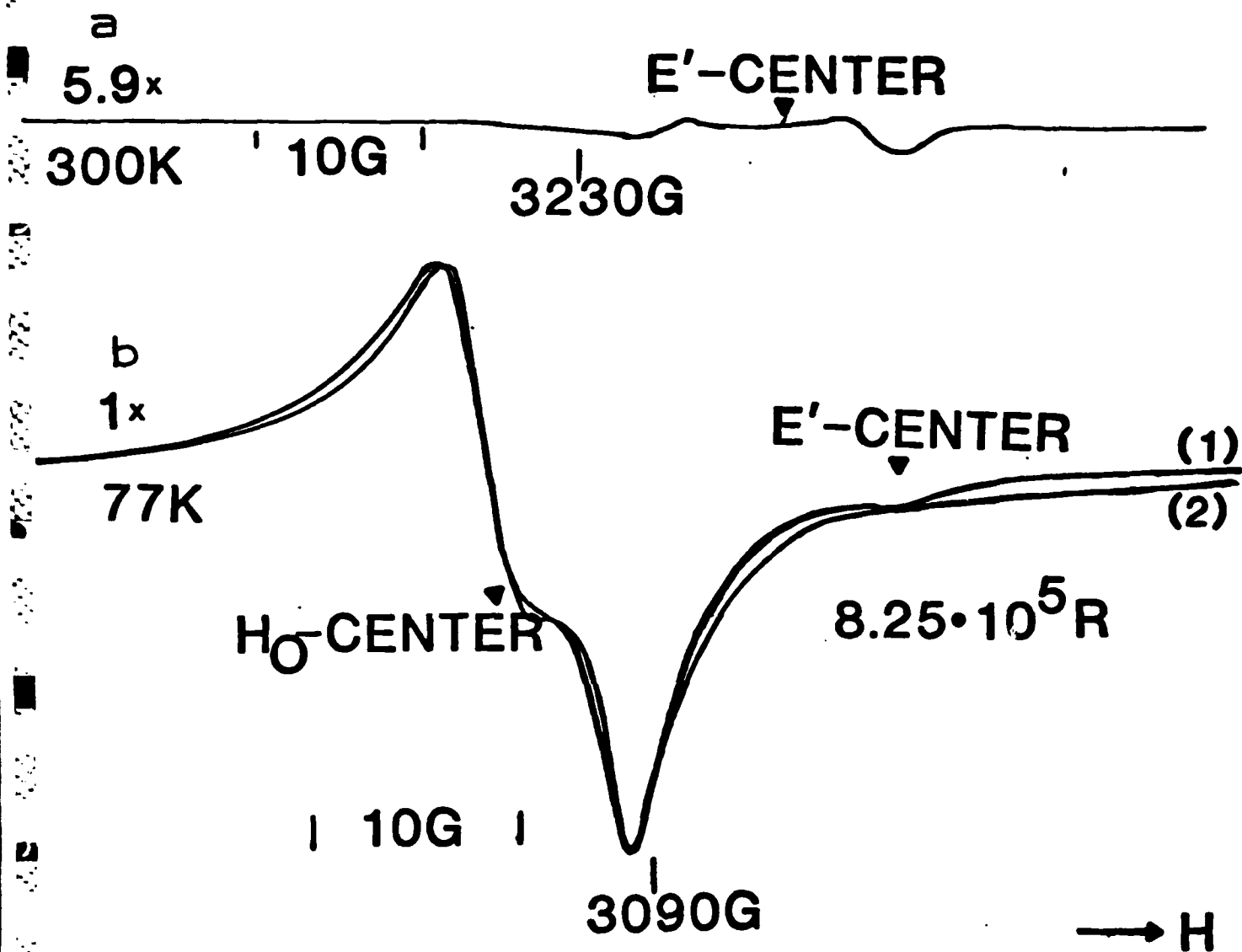
3. ESR-spectrum of a  $^{60}\text{Co}$  gamma-ray irradiated  $\text{GeO}_2$  glass ( $10^6 R$ ).

34.67GHz, 300K



FIGURE

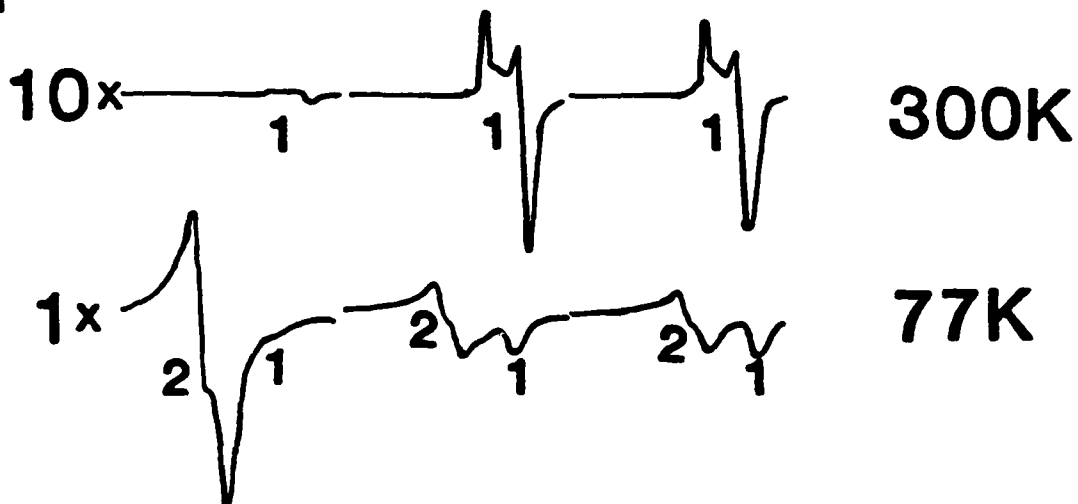
4. Room temperature 35GHz ESR-spectrum of a  $^{60}\text{Co}$  gamma-ray irradiated  $\text{GeO}_2$ -glass fused at  $1650^\circ\text{C}$ . The symbols 1x and 5x are relative gains of the amplifier. The term "lfs-signal" is used in the text.



FIGURE

5. Spectra of  $\text{GeO}_2$  glass fused at  $1200^\circ\text{C}$  and irradiated with  $^{60}\text{Co}$  gamma-ray to a dose of  $8.25 \cdot 10^5 \text{R}$ .
- a) The symbol 5.9x indicates the relative amplifier gain.
- b) Curve 2 was recorded at a microwave power 10 time that for curve 1. The maximalization procedure is described in the text. The symbol 1x indicates relative amplifier gain.

$T_F = 1200^\circ\text{C} \ 1450^\circ\text{C} \ 1550^\circ\text{C}$



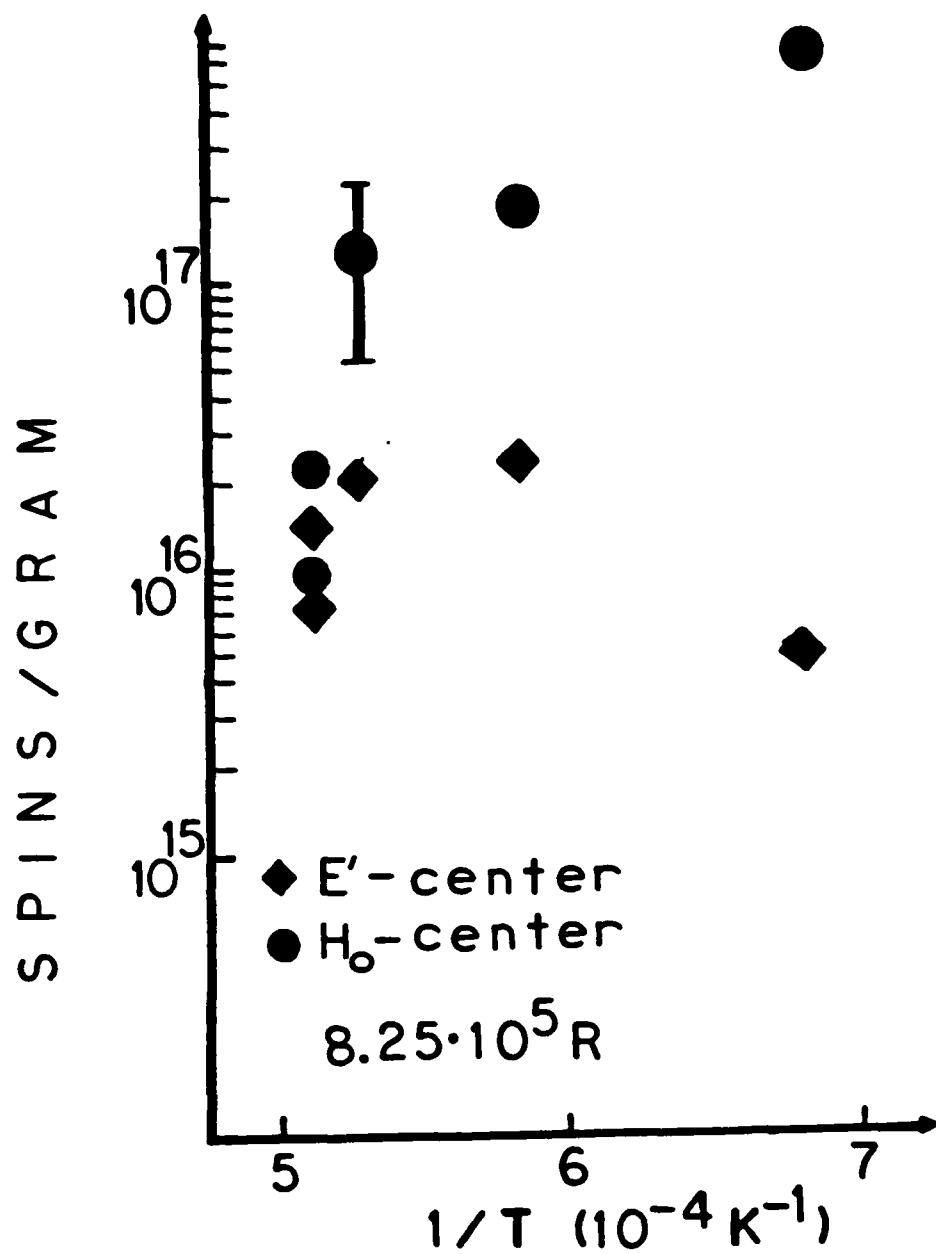
$T_F$  : FUSION TEMPERATURE

1 : E'-CENTER

2 : H<sub>0</sub>-CENTER

FIGURE

6. Spectra of irradiated  $\text{GeO}_2$  glasses ( $8.25 \cdot 10^5 \text{R}$ ) recorded at room temperature and at 77 K.



**FIGURE**

7. Dependence of the H<sub>0</sub>- and F'<sub>1</sub>-center concentration on the fusion temperature.

TABLE I.

Impurities in GeO<sub>2</sub> from Neutron activation  
and IR analysis (2, 7 μm OH absorption)

<u>Element</u>	<u>Level (parts per million by weight)</u>
Na	18.4 ±0.3
Cl	1376 ±16
Al	14 ±1.3
Fe	<15
Cr	13.1 ±2.0
K	<70
Mg	<60
Ca	<31
Ti	<70
Sr	<50
Mo	30.4 ±4.8
Ni	<19
OH	200
Others	<15

	$g_{\parallel}$	$g_{\perp}$
GeO <sub>2</sub> -GLASS (THIS WORK)	2.0010	1.9952
GeO <sub>2</sub> -GLASS (10) *	2.0010	1.9944
GeO <sub>2</sub> -CRYSTAL (11) *	2.0015	1.9940

\* REFERENCES

Table II. g-values of the E'<sub>1</sub>-center in our glasses and g-values of E'<sub>1</sub>-centers in crystalline and glassy GeO<sub>2</sub> reported in the literature.

MEASUREMENTS	$g_3$	$g_2$	$g_1$
AT 35GHz AND 300K	2.011-2.015*	2.007	2.003
AT 9.5GHz AND 77 K	2.01-2.015*	2.007	2.003

The g values are purely resolved in the spectra and consequently a range of possible values are given

Table III. g-values of the  $H_0$ -center.

**2 . 0 1 9**

**2.0090**

**2 . 0 1 9 6**

**2 . 0 1**

**2.051**

**2.008**

**2.0172**

**2.0100**

APPENDIX II. f.

The Effect of Melt Temperature on the DC Conductivity of GeO<sub>2</sub> Glasses

R. H. Magruder, III, D. L. Kinser, R. A. Weeks, and J. M. Jackson

Vanderbilt University

Nashville, Tn 37235 USA

ABSTRACT

The DC electrical properties of a series of high purity GeO<sub>2</sub> glasses fused and equilibrated at various temperatures ( $T_{\phi}$ ) in air were measured.  $T_{\phi}$  ranged from 1200°C to 1690°C. The observed changes are not correlated changes in concentration of any of the impurities as determined by neutron activation analyses or IR measurements of OH concentrations.

The resistivity was found to obey an Arrhenius function with enthalpy of activation of approximately 1.0 eV for all  $T_{\phi}$ 's except for  $T_{\phi} = 1200^{\circ}\text{C}$ . The charge carrier was concluded to be the Na<sup>+</sup> ion. The mobility of the Na<sup>+</sup> ion was calculated and was found to be a function of  $T_{\phi}$ .

We suggest that the change in  $T_{\phi}$  results in a change in the configurational coordinates of the average interstitial sites through which the Na<sup>+</sup> ion moves. This change results in differences in the vibrational energy structure of the interstitial sites. These differences are manifested in the entropy of activation.

With changes in the entropy of activation, the pre-exponential term changes producing the variation in mobilities which is observed.

Alkali ion motion under electrical fields has been the subject of continuing research in the century since the 1884 work of Warburg<sup>(1)</sup>. Most of the early investigations were restricted to the commercial glasses of the period. In the past two decades substantial interest has been focused upon simple glass systems which, for the most part, have been of high alkali compositions. This literature is reviewed by Doremus<sup>(2)</sup>, Morey<sup>(3)</sup>, Owen and Hughes<sup>(4)</sup> and Owen<sup>(5)</sup>.

Relatively little research has been conducted on high purity simple glass compositions. Owen and Douglas<sup>(6)</sup> examined four commercially pure fused silicas and found a good correlation between resistivity and sodium content.

Doremus<sup>(7)</sup> examined the electrical conductivity of high purity fused silica glasses with trace levels of sodium, lithium and potassium. He concluded that the activation energies for conduction ions were approximately equal for the three alkalis. The effect of fusion conditions upon fused silicas has not been examined to the authors' knowledge because of the difficulty of preparing these glasses with appropriate controlled compositions at the required temperatures.

The influence of fusion conditions upon the physical properties of  $\text{GeO}_2$  glasses have been a subject of continuing interest. Garinia-Canino<sup>(8)</sup> examined the effect of fusion conditions and subsequent thermal treatments

on an optical absorption band at  $\sim 245$  nm in  $\text{GeO}_2$  glasses. He observed that the intensity of this band increased with fusion temperature and suggested that it was due to an oxygen vacancy. Cohen and Smith<sup>(9)</sup> examined the effect of fusion temperature as well as ultraviolet bleaching upon this peak and corroborated the results of Garinia-Canino. Vergano and Uhlmann<sup>(10)</sup> reported on the crystallization kinetics of  $\text{GeO}_2$  glasses and concluded that reduced glasses had higher crystallization rates. The degree of reduction was found to be a function of the temperature at which the liquid was equilibrated. Purcell and Weeks<sup>(11)</sup> have described some of the intrinsic paramagnetic defects in  $\text{GeO}_2$  crystals and glasses and characterized their concentrations as a function of thermal history. They concluded that one of the defects observed is due to singly charged oxygen vacancies. Bohm<sup>(12)</sup> measured the dc conductivity of low sodium germania glasses and concluded that the conduction mechanism is a thermally activated motion of sodium with an Arrhenius behavior and activation energy of 1.0 eV. Cordaro et al<sup>(13)</sup> have confirmed that result and, additionally, reported that the OH content affect the conductivity.

There are numerous reports<sup>(14-20)</sup> in the literature which conclude or can be interpreted to argue that the structure of a glass is dependent upon the structure of the liquid from which it was cooled. The local environment of the sodium ion does not totally relax to a structure characteristic of a glass transition temperature but instead retains a structure determined by the equilibrium established in the liquid at a temperature,  $T_\phi$ , from which it was quenched. This argument is, of course, contrary to the conventional view that the structure of a glass is in metastable equilibrium at temperatures above the glass transition.

This argument is supported by the work of Galeener et al<sup>(14)</sup> who reported Raman measurements of GeO<sub>2</sub> glasses held in the liquid state at different temperatures but quenched through the glass transition regime at the same rate. They concluded that the Raman results indicate differences in structure among glasses quenched in such a fashion. Bohm<sup>(15,16)</sup> reports differences in photoconductivity and thermoluminescence in GeO<sub>2</sub> glasses held at different temperatures in the liquid state. We interpret these observations as indicating that the electronic structure associated with these processes is influenced by the temperature at which the liquid was equilibrated and that the electronic structure differences necessarily require that atomic structural differences also exist.

Kordas et al<sup>(17)</sup> have measured the electron paramagnetic resonance spectra of a series of GeO<sub>2</sub> glasses held in the liquid state at different temperatures and quenched at a constant rate. Several paramagnetic defects are reported whose functional dependence upon melting temperature is not Arrhenius. They suggested that this result indicates that the defect concentrations are not controlled by oxidation/ reduction equilibria exclusively but are also influenced by structural differences in the liquid which are a function of melting temperature.

Primack<sup>(18)</sup> reviewed the Douglas and Isard<sup>(19)</sup> density measurements upon SiO<sub>2</sub> glasses with differing glass transition temperatures and concluded that remnants of the high temperature structure are responsible for the observed density differences. Douglas and Isard stated that "the high temperature phases are readily quenched" and Primack added the observation that clearly these configurational differences are quite stable at lower temperatures.

Hetherington et al<sup>(20)</sup> have reported a survey of the viscosity of SiO<sub>2</sub> in which they defined a term "equilibrium viscosity." The viscosity of a

glass held for a long period of time at a particular temperature is said to be the equilibrium value but after a change in temperature the equilibrium viscosity is reached only after times from 2 to 50,000 hours depending upon these new temperatures. We argue that these equilibration times reflect the time dependent structural rearrangement when the "melt temperature" is changed and thus the structure characteristic of a liquid equilibrated at a given temperature can be expected to persist during cooling to room temperature. Our objective is to determine the effects of fusion temperature on the alkali ion mobility of a series of glasses.

#### Experimental Procedure:

A series of  $\text{GeO}_2$  glasses was prepared by melting high purity  $\text{GeO}_2$  powder (electronic grade from Eagle Pitcher Corporation) in a platinum crucible in an electrically heated furnace with air atmosphere for various times which were dependent upon the melt temperature. The melt times are tabulated in Table I. The crucible with glass was removed from the furnace and cooled to room temperature at an average rate of  $5^\circ\text{C}/\text{sec}$ . from fusion temperature to  $400^\circ\text{C}$ . The cooling rate below  $400^\circ\text{C}$  was less. Samples were removed from the crucibles by core drilling a cylinder approximately 17 mm in diameter from the center. This cylinder was then cut into discs approximately 1 mm thick. Wafers were polished with petroleum lubricants through 400 grit abrasive, then washed with ethanol. Samples were then placed in a vacuum evaporator and heated at  $230^\circ\text{C}$  for approximately 30 minutes after which gold electrode samples were vapor deposited. The guarded configuration gold electrodes were annealed for one hour at  $300^\circ\text{C}$ . DC measurements were made with the samples in a chamber which permitted

measurements under a vacuum of approximately 30 microns over the temperature range from room temperature to 300°C. Computer control of the DC measurements was employed. Predetermined target temperatures were chosen so that they were equally spaced in  $1/T$  between the extremes of the measurement temperatures. The present experiment used 30 target temperatures. A three modes proportional control algorithm was used to calculate the percent duty cycle of the heating element with the design characteristic of minimum overshoot with reasonable convergence time. Temperatures were scanned from lowest to highest to minimize annealing processes during measurement.

The sample temperature was measured every 10 seconds and when the rms deviation from the target temperature of the last 50 of these measurements was less than 1°K, then the convergence criterion is met. With this the sample temperature was stable over a period of 500 seconds which is consistent with the relatively long thermal time constant of the system.

After the sample temperature had converged to the target temperature, the applied sample voltage was switched on for 30 seconds to allow for polarization processes. Immediately following this, the electrometer was activated and auto ranged to the appropriate scale.

To enhance accuracy, 10 current measurements were taken at each measurement temperature. The recorded current value was the computed root mean square average of these values and the rms error was stored for subsequent statistical calculations.

At the completion of the run, the data was converted to resistivity and the rms errors in current were similarly transformed. To effect the statistical

analysis and determine the preexponential and exponent for the Arrhenius fit, the equation is linearized and the data plotted as  $1/T$  vs.  $\log$  Resistivity. For the statistical analysis, the measurement error in  $T$  is assumed to be negligible ( $< \pm 0.5C^\circ$ ) and error bars corresponding to uncertainties in resistivity are plotted. The parameters are determined by a Chi square fit to the linearizing function with the individual resistivity uncertainties propagated through the calculations to give the uncertainties in pre-exponential and exponent(21).

Analyses for trace elements were made by neutron activation analysis at ORNL<sup>22</sup>. The OH content was determined by measurements of the intensity of the 2.7 IR absorption band<sup>(23)</sup>. Results of the analysis are given in Table I.

#### RESULTS:

The DC resistivity of two samples with differing Na concentration with  $T\phi$  equal to  $1650^\circ C$  are shown in Figure 1. The data show a proportional decrease in resistivity with increase in Na concentration. The activation enthalpy was calculated for both samples using a least square fit to the Arrhenius equation:

$$\rho = \rho_0 \exp^{-\Delta S/k} \exp^{\Delta H/kT} \quad (1)$$

and is given in Table I with Na concentrations, pre-exponential factor  $\rho_0$  and OH concentration.

The mobility of the Na ion as calculated from the equation

$$\mu = 1/ne\rho \quad (2.)$$

is plotted as a function of temperature for glasses with  $T\phi$  equal to 1200, 1450, 1550, and 1690 C. Measurements made on glasses with  $T\phi$  at intermediate temperatures and omitted for clarity. The mobility of the sodium as measured at 1440 on samples with  $T\phi$  equal to a series of temperatures is plotted as a function of  $T\phi$  in Figure 3.

The sodium ion mobility exhibits a maximum at approximately 1450 C. The lowest Na ion mobility was calculated for the samples fused at 1200°C. The activation energy for these samples is 1.19 ev while all other samples have an activation energy of 1.01 ev.

#### Discussion

The equation for resistivity as derived from reaction rate theory is discussed by Moynihan et al(24,25) and is given by them in the form of equation 1 with

$$\rho_o = ne^2d^2h/6 \quad (3.)$$

Substituting equation 2 in 3, the mobility is expressed as

$$\mu = e^2d^2/6h \exp \Delta S/h \exp -\Delta H/kt \quad (4.)$$

where  $e$  is the charge of the carrier,  $d$  the jump distance,  $k$  Boltzman's constant, and  $T$  the temperature.  $\Delta S$  and  $\Delta H$  are the entropy of activation and enthalpy of activation respectively. In order to rationalize the dependence of  $\mu$  on  $T\phi$ , we discuss the variables in the above expression. The variables in the expression above are  $\Delta S$  and  $\Delta H$  and  $d$ .

If the variation in mobility is attributed to a variation in jump distance, then the jump distance  $d$  must range over a factor of 2, i.e. up to 10 Å. Such a large jump distance would require a great deformation of the structure. We assume that the jump distance is of the order of the distance between interstitial sites i.e. approximately 5 Å. It is physically unreasonable to expect the jump distance sites to be larger. The activation enthalpy,  $\Delta H$ , is invariant with  $T\phi$  except in the 1200 melt. The inconsistent behavior of the  $T\phi = 1200$  sample may be a consequence of either the anomalous high potassium content or unrationalized behavior with  $T\phi$ . Hence, we assume the short range order is the same in these glasses. A consequence of this assumption is that the "doorway" through which the ion must pass from one site to another is invariant with  $T\phi$ . We suggest, then, that the changes seen in mobility of the glasses with  $T\phi$  between 1690°C and 1350°C are due to changes in the entropy of activation  $\Delta S$ . Table III lists the value calculated for  $\Delta S$ .

Entropy can be expressed as

$$S = k \ln \omega \quad (5.)$$

where  $\omega$  represents the probability that a given state will exist. In accord with this definition of entropy,  $\Delta S$  the entropy of activation represents the probability that an activated state will be reached, i.e.

$$\Delta S = k \ln \omega^A \quad (6.)$$

where  $\omega^A$  represents the probability of the activated state being occupied. The probability of the transition to an activated state is dependent upon the density of energy levels available. This density is not independent of the energy<sup>(24)</sup>. Table III shows that  $\Delta S$  increases

with decrease in  $T\phi$ . Thus, we suggest that the probability of reaching an activated state increases with decreasing fusion temperature. To reach an activated state, an ion must gain sufficient energy from the phonon spectrum supplied by the vibrational modes of the local environment of the Na ion. Thus, the change in  $\Delta S$  implies a change in the local structure around the Na ion. A model for this change is discussed in the following.

We consider the sodium ions as occupying a series of "interstitial" wells in the glass structure. The existence of the interstitial wells has been documented by the studies of Shackleford et al (26,27). While there is a statistical distribution of well depths, we restrict the following discussion to a statistically average well.

These wells represent minimum in the potential energy curve for the Na ion. They are caused by the ion fields of the oxygen surrounding the interstitial sites in the glass. These ion fields cause a  $U(r)$  potential where  $r$  is a configurational coordinate as seen in Figure 4.

$U(r)$  is an aperiodic potential function in that the oxygen ion configuration around each site is variable as are the dimensions of each site resulting in no translational symmetry. However, depth of the wells is determined by the energy required to stretch the GeO bond to allow passage of the  $Na^+$  ion. This energy, from measurements of DC conductivity, is found to be constant.

A Taylor series expansion of  $U$  for a particular potential well yields:

$$U(x) = U_{x=0} + (dU/dx)x + 1/2!(d^2U/dx^2)x^2 + 1/3! (d^3U/dx^3)x^3 + \dots \quad (7.)$$

Following the treatment of Barrow<sup>(28)</sup>  $U_{x=0} = 0$  and  $(dU/dx)_{x=0}$  is 0.

The resulting expression for  $U(x)$  becomes

$$U(x) = 1/2! (d^2U/dx^2)_{x=0} x^2 + 1/3! (d^3U/dx^3)_{x=0} x^3 + \dots \quad (8.)$$

The first term on the right is the same term obtained for Hooke's law

where  $K$  the force constant is given by

$$(d^2U/dx^2)_{x=0} = K$$

The second term on the right will then determine the anharmonicity induced in the system.

Using the potential in Equation 7, Schrodinger's equation can be solved for the energy levels giving

$$\epsilon_n = h \omega (n+1/2) - h \omega x_e (n+1/2)^2 + \dots \quad (9.)$$

$$\text{where } \omega = 1/2\pi\sqrt{k/m} \quad \text{and } k = (d^2U/dx^2)_{x=0}$$

$x_e$  is the anharmonicity constant and is related to  $(d^3U/dx^3)_{x=0}$ . In contrast to a simple harmonic oscillator whose energy levels are equidistant in energy, the anharmonic term causes the spacing levels to decrease with increasing  $n$  as seen from equation 9. The  $x_e$  term then determines the spacing of the energy levels and affects the symmetry of the function as seen in Figure 5.

The ( $d^2U/dx^2$ ) term would determine the well structure in the absence of the anharmonic term. The change from the parabolic structure is then determined by the  $d^3U/dx^3$  term and as a consequence affects the energy level density of the well. Barrow comments that as the well structure is broadened, "... (it) confines the vibrating particle less closely than would a parabolic curve. Such loosening of the restriction on the motion of particles always leads to more closely spaced allowed energy levels."

The average well seen by the sodium ion is characterized by the force constant that determines the depth of the well and by the anharmonic term that determines its departure from a true harmonic oscillator. We thus argue that a change in the glass structure is manifested in the anharmonic term. This change in the anharmonic term results in a difference in the energy level spectrum of the well in which the Na ions reside. These differences change the statistical average value of the vibrational modes of the well. As the Na ion moves through the glass structure, it encounters wells characteristic of the melt temperature. As we shift the melt temperature, the vibrational excitation of the well changes in accord with energy level changes induced by changing the shape of the well.

From Boltzmann statistics, it is known that the fractional occupancy of a particle between energy states is given by

$$f_a = \exp(-\epsilon_a/kt) / \sum \exp(-\epsilon_n/kt) \quad (10.)$$

where  $\epsilon_a$  is the level of interest,  $E_n$  is the energy level in general. The denominator in Equation 10 is the partition function  $L$ .

$$L = \sum_n \exp(-\epsilon_n / kt) \quad (11.)$$

As  $n$  increases, i.e. the density of states increase, the partition function must increase causing the fractional occupancy at a particular temperature to decrease. Hence, the structure of wells is broadened as shown schematically in Figure 5.

Changes in  $T\phi$  change the density of energy levels in the Na sites. These changes produce a change in the partition function. This change in the partition function causes a change in the average fractional occupancy of the activated states in the glass. With  $f_a$  decreasing the probability of reaching the activated state decreases, then  $\Delta S$  decreases in accordance with Equation 6. resulting in a mobility decrease.

From the  $\Delta H$  value given in Table III, we argue that the short range order in the glasses with  $T\phi$  from 1690°C to 1350°C is essentially the same. This short range order in the configuration of the ions determines the height of the potential barrier. If, however, as the fusion temperature is changed, slight changes in the bond angles as suggested by Primack or change the density as can be inferred from Bruckner's index of refraction data, then we can reasonably expect the potential well size to change. It is this change in well size that results in the change in the anharmonic term. Additional evidence for the above model comes from computer modeling of Angel et al(29).

## CONCLUSIONS

The average well structure is a function of the temperature of the liquid ( $T\phi$ ) from which the glass was quenched. The depth of the well, which is a function of the energy required by an ion to pass through a "doorway" to the next interstitial site, is invariant with  $T\phi$ . The fundamental change produced by changes in  $T\phi$  are in the configuration coordinates of the interstitial sites. These differences in anharmonicity are then manifested in the entropy of activation. With changes in the entropy of activation, the pre-exponential term changes producing the variation in mobilities which is observed.

Thus we conclude that DC conductivity of  $\text{GeO}_2$  glasses with low levels of sodium depends upon the  $T\phi$  temperature of a glass.

## ACKNOWLEDGEMENTS

The authors gratefully acknowledge the financial support of the U.S. Army Research Office/Durham under contract #DAAG 29-81-K-0118.

## REFERENCES

1. E. Warburg, *Ann. Physik. Chem.* 21, 622 (1884).
2. R. H. Doremus, *Journal of Electrochemical Society*, 115, 181, (1968).
3. G. W. Morey, *The Properties of Glass* (Am. Chem. Soc. Monograph), Reinhold, NY (1954), pp. 465-501.
4. K. Hughes and J. O. Isard, *Physics of Electrolytes*, J. Hladik, ed., Academic Press, London (1972), pp. 351-400.
5. A. E. Owen (*Progress in Ceramic Science*, Vol. 3, J. E. Burke, ed. Macmillan Co., NY (1963), pp. 77-196.
6. A. E. Owen and R.W.Douglas, *Journal of Society of Glass Technology*, 43, 159 (1959).
7. R. H. Doremus, *Physics and Chemistry of Glasses*, 10, 28 (1969).
8. V. Garina-Canina, *Comptes Rendus de la Academy of Sciences*, 247, 593 (1958).
9. A. J. Cohen and H. L. Smith, *Journal of Physics and Chemistry of Solids* 7, 301 (1958).
10. P. J. Vergano and D. R. Uhlmann, *Physics and chemistry of Glasses*, 11, 30 (1970).
11. T. Purcell and R.A. Weeks, *Physics and Chemistry of Glasses*, 10, 198 (1969).
12. H. Bohm, *Journal of Applied Physics*, 43, 1103 (1972).
13. J. F. Cordaro, J. E. Kelly, III and M.Tomozawa, *Physics and Chemistry of Glasses*, 22, 90 (1981).
14. F.L. Galeener and R. H. Geils, *The Structure of Non-Crystalline Materials*, P. H. Gaskell, editor, Taylor and Francis, London, 1977, p. 223.
15. H. Bohm, *Journal of Non-Crystalline Solids*, 7, 192 (1972).
16. H.Bohm, *Physics and Chemistry of Glasses*, 11, 177 (1977).
17. G. Kordas,R. A.Weeks and D. L. Kinser,*Journal of Applied Physics*, 54, 5394 (1983).
18. W. Limak, *Physics and Chemistry of Glasses*, 24, 8 (1983).
19. R.W.Douglas and J. O. Isard, *Journal of Society of Glass Technology*, 35, 206 (1951).

20. G. H. Hetherington, K. H. Jack and J. C. Kennedy, *Physics and Chemistry of Glasses*, 5, 130 (1964).
21. Phillip R. Bevington, *Data Reduction and Error Analysis for the Physical Sciences*, McGraw-Hill, 1969, pp. 56-61 and pp. 180-185.
23. G.H.A.M. Van der Steen and E. Papanikolan, *Philips Res. Rep.*, 30, 192, (1975).
22. The analyses were made by Lamont Bates of Oak Ridge National Laboratories.
24. R. Syed, D.L. Govin and C.T. Moynihan, *J.Am.Cer. Soc.*, C129 (1982).
25. C. T. Moynihan, D. L. Gavin and R. Sayed, *Physics of Non Cryst. Solids, Proceedings of the 5th Intl Conf. J. Zarzycki, ed. (1982)*
26. J. F. Shackelford and J. S. Masaryk, *Journal of Non-Crystalline Solids*, 30, 127 (1978).
27. J. F. Shackelford and B. D. Brown, *Journal of Non-Crystalline Solids*, 44, 379 (1981).
28. G. M. Barrow, *Introduction to Molecular Spectroscopy*, McGraw-Hill, Kogakusha Ltd, Tokyo (1962).
29. C. A. Angell, P. A. Cheeseman, and S. Tamaddon, *J. Am. Cer. Soc.* C129 (1982).

TABLE I

Trace Elements in GeO<sub>2</sub> Glasses from Neutron activation analysis and  
Infrared Analysis in ppm

T <sub>φ</sub> (°C)	1690	1650	1550	1450	1350	1200
Equilibration Time (hrs)	1	3	3	110	185	275
Na	20.3	12.2	8.7	14.9	13.9	39.5
Cl	1.41x10 <sup>3</sup>	1.21x10 <sup>3</sup>	1.60x10 <sup>3</sup>	1.27x10 <sup>3</sup>	1.47	1.66x10 <sup>3</sup>
Al	a	4.8	a	4.4	7.9	a
Li	a	a	a	a	a	a
K	a	a	a	a	a	138
OH	214	181	238	206	190	165

a-less than detectable limit

TABLE II

Summary of sodium concentration and pre-exponential factors  
for two glasses fused at 1650°C. for 3 hrs. in air

Na(ppm)	$\rho_o$ (ohm/cm)	OH(ppm)	$\Delta H$ (ev)
12.3	1.18	181 ppm	1.02
37.3	0.370	204	1.02

TABLE III

Summary of activation entropy and enthalpy for series  
of glasses

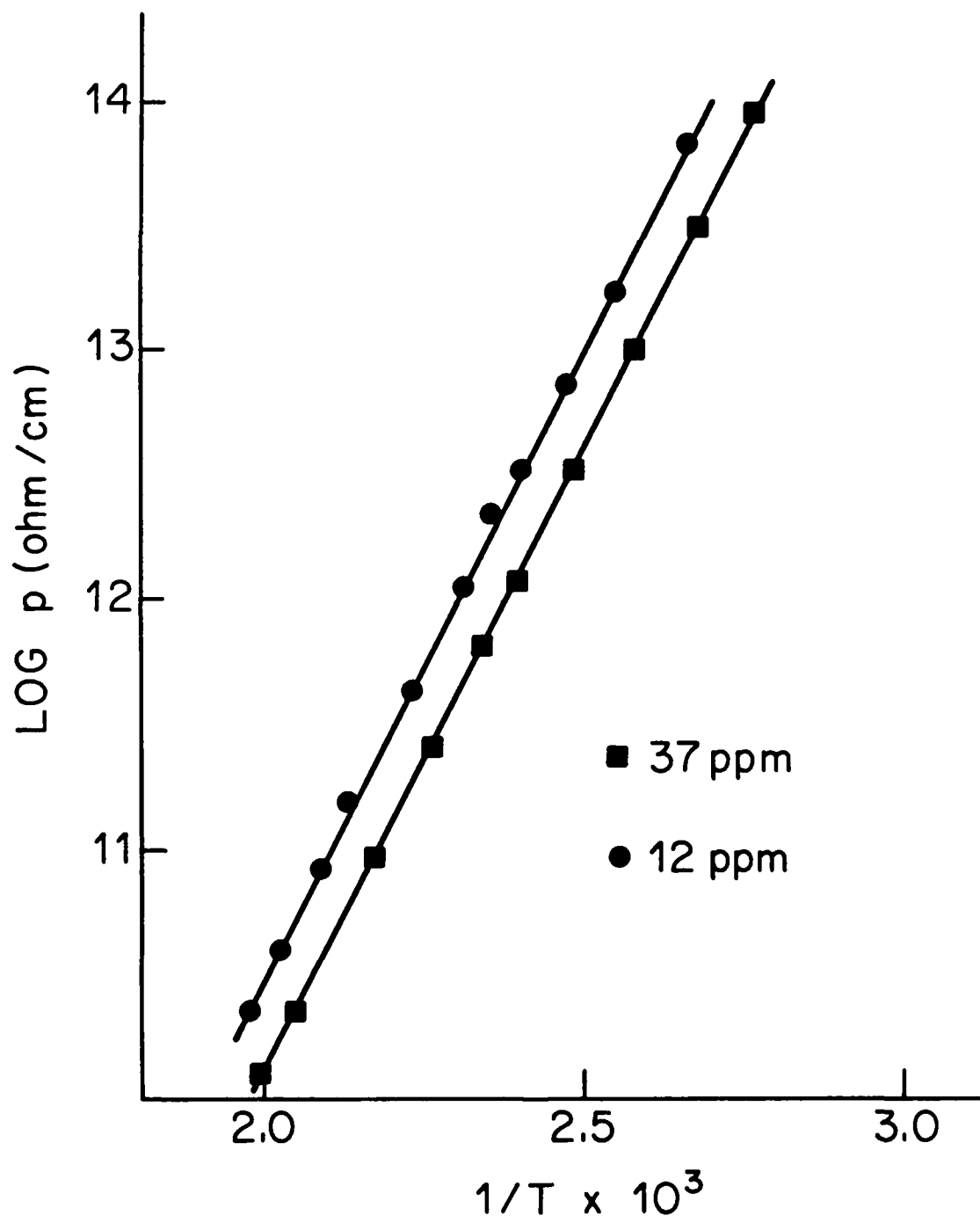
$T\phi$	$\Delta S$ (ev/°K) <sup>a</sup>	$\Delta H$ (ev) <sup>b</sup>
1690	$1.2082 \times 10^{-2}$	1.01
1650	1.2149	1.02
1550	1.2164	1.01
1450	1.2191	1.00
1350	1.2176	1.00
1200	1.2466	1.19

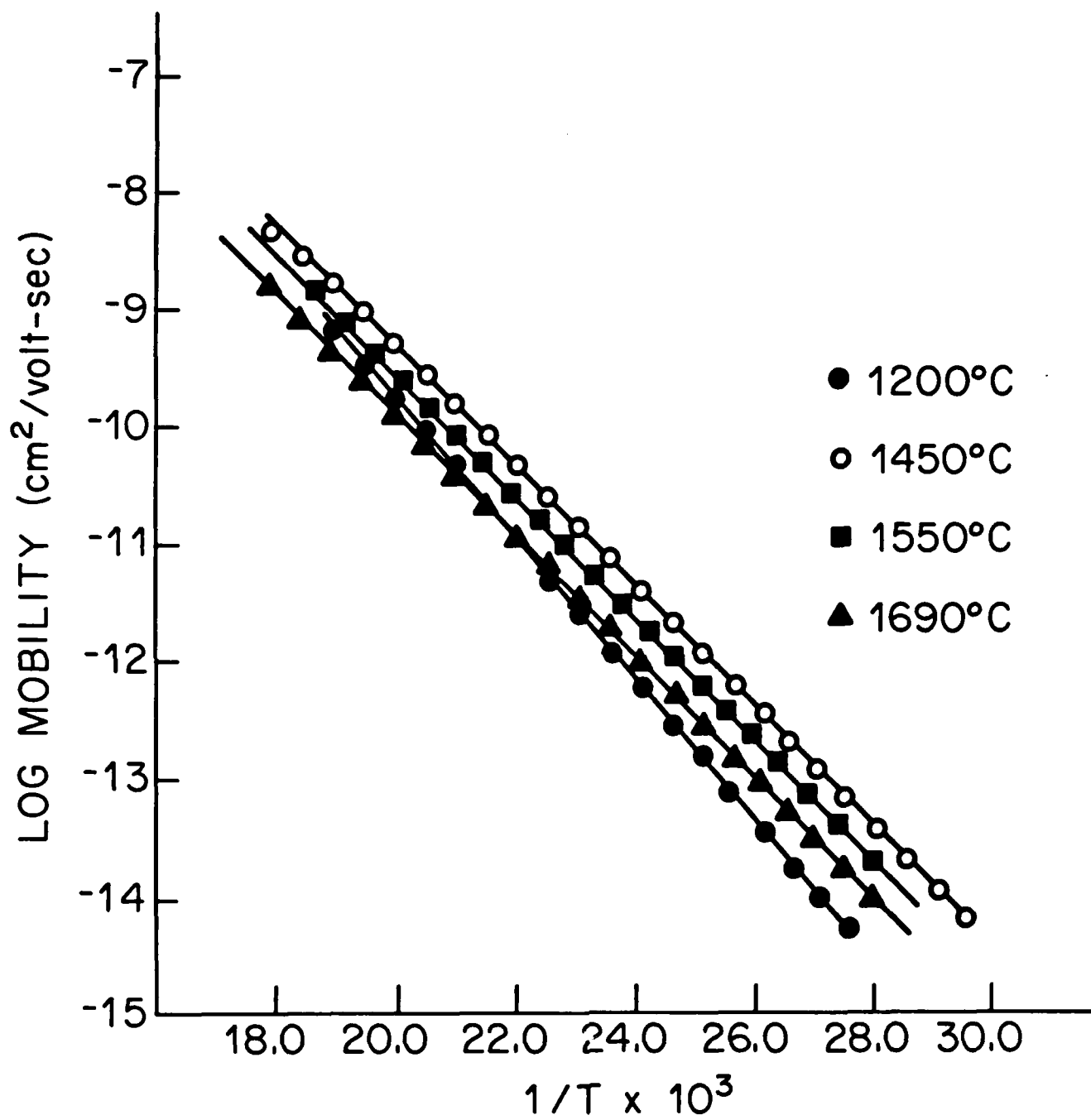
<sup>a</sup> The error in these values as determined by differences  
between two melts is  $\pm 0.0006$

<sup>b</sup> The rms error as determined by least square fit calculations  
to the Arrhenius equation is  $\pm 0.0003$

## List of Figure Captions

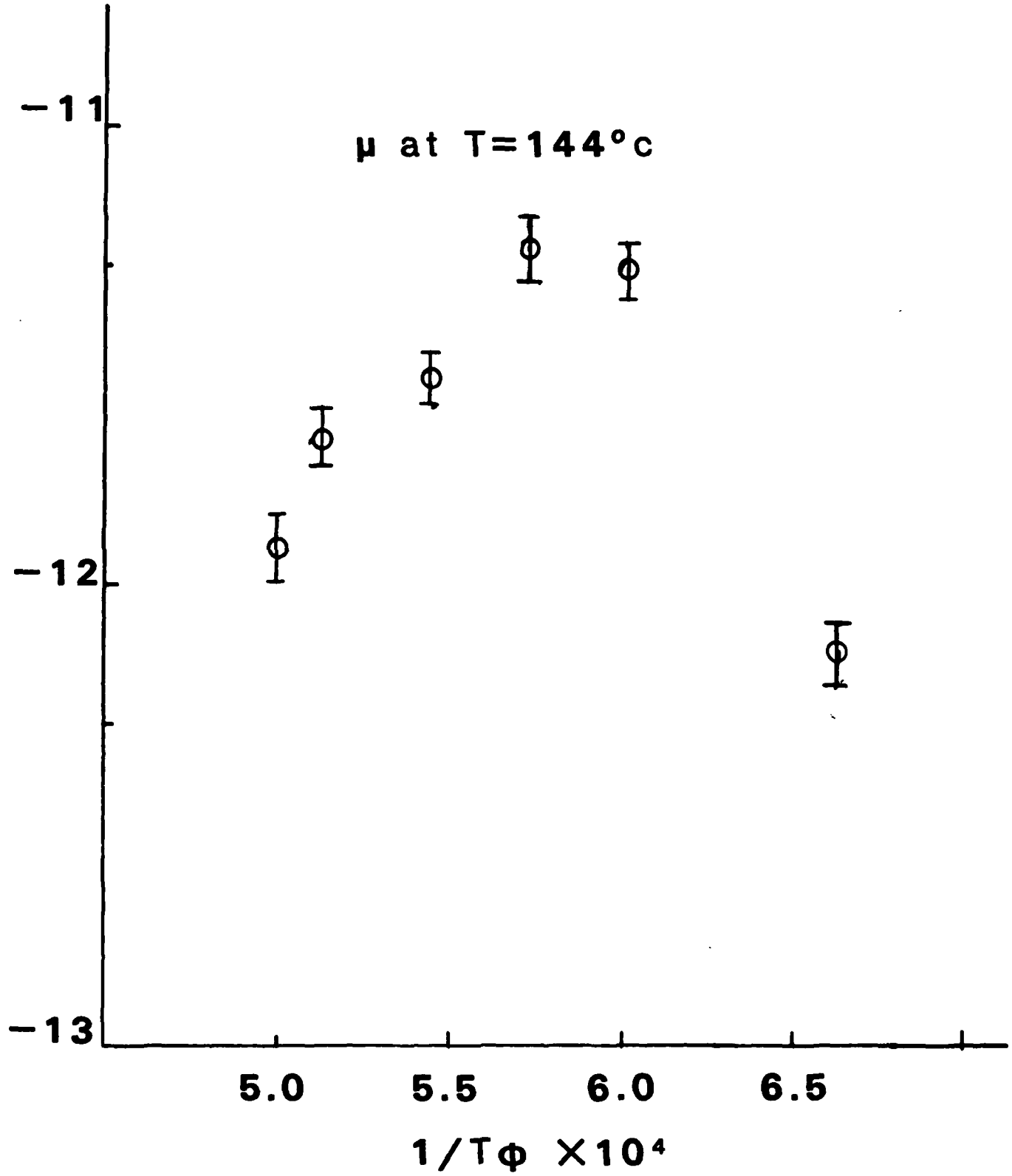
- Figure 1. Temperature dependence for resistivity  $\rho$  glasses with  $T_{\phi} = 1650^{\circ}$  and varying  $\text{Na}^{+}$  concentration.
- Figure 2. Temperature dependence of mobility for a series of glasses with varying  $T_{\phi}$ .
- Figure 3. Mobility versus  $T_{\phi}$  for a series of glasses fired from  $1690^{\circ}$  to  $1200^{\circ}\text{C}$ .
- Figure 4. Potential energy versus distance ( $r$ ) from equilibrium  
dashed curve represents simple harmonic oscillator  
solid curve represents anharmonic oscillator.
- Figure 5. Potential energy  $u(r)$  versus  $r$  distance from equilibrium position for 2 curves of anharmonic oscillator with different  $\chi_e$ .

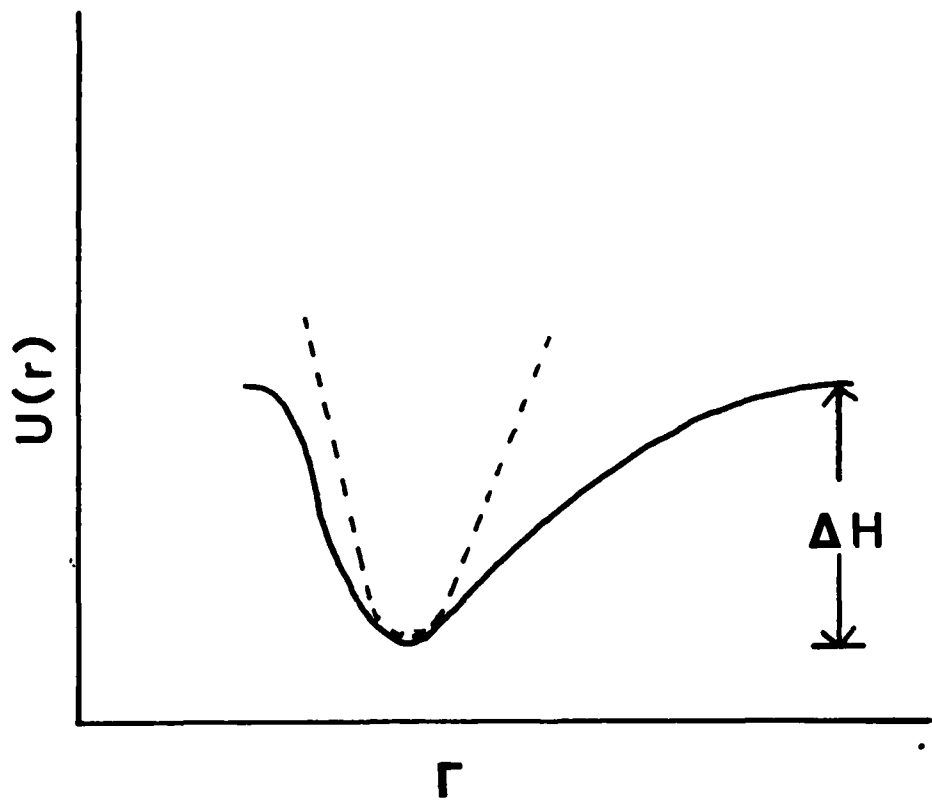


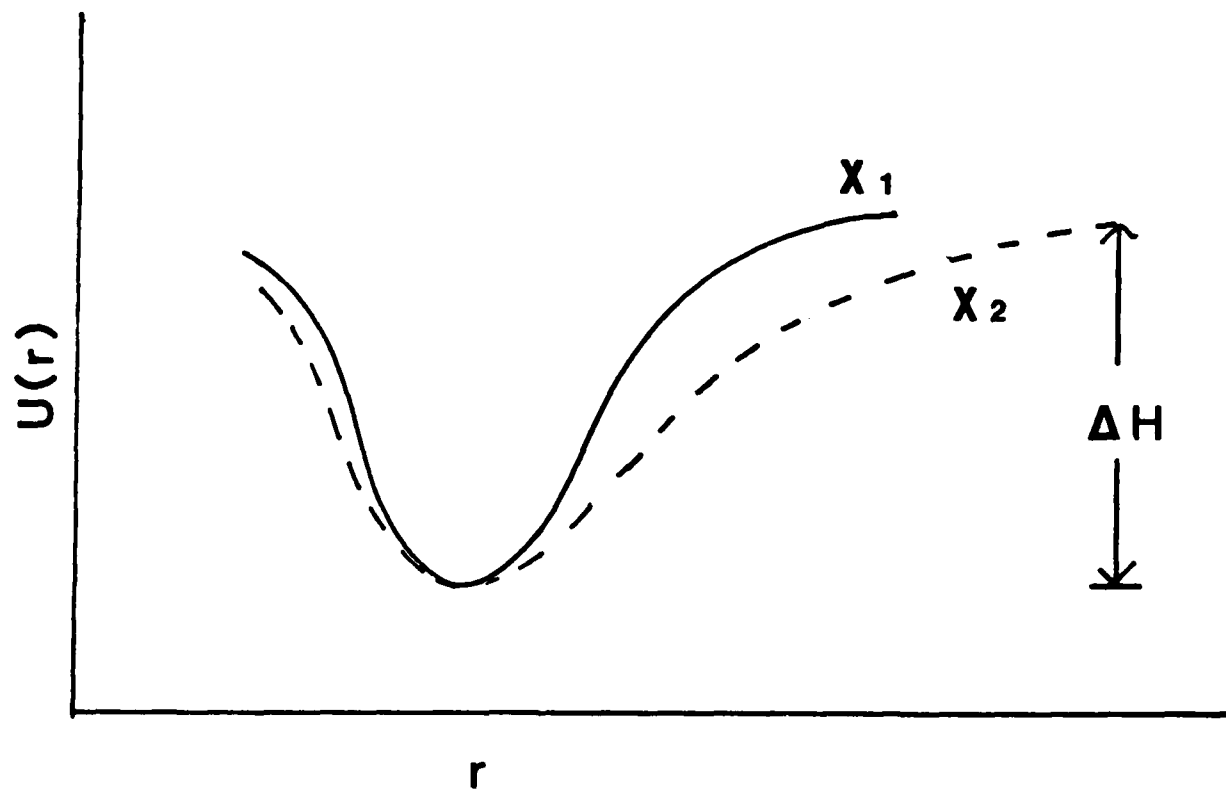


$\mu$  at  $T=144^{\circ}\text{C}$

LOG MOBILITY ( $\text{cm}^2/\text{volt}\text{-sec}$ )







APPENDIX II.g.

EFFECTS OF DENSIFICATION CONDITIONS ON THE DEFECT CENTER CONCENTRATION  
IN GERMANIUM-DOPED SILICA OPTICAL FIBER PREFORMS

G. Kordas, D. L. Kinser and R. A. Weeks

Department of Mechanical and Materials Engineering  
Vanderbilt University  
Nashville, TN 37235.

ABSTRACT:

Electron-Spin-Resonance(ESR)-studies were carried out on unirradiated and  $^{60}\text{Co}$   $\gamma$ -ray irradiated  $\text{GeO}_2$ - $\text{SiO}_2$ -fiber optic preforms which were densified (sintered) at  $1550^\circ\text{C}$  and  $1625^\circ\text{C}$  in air and in vacuum ( $10^{-6}$  Torr) for 75 minutes.

In the unirradiated preforms only those densified in a vacuum furnace exhibit an asymmetric line attributed to the  $\text{GeO}_2$ - $\text{E}'$  center. After irradiation three types of germanium  $\text{E}'$ -center were detected [ $\text{Ge}(0)$ ,  $\text{Ge}(2)$  and  $\text{Ge}(3)$ ], the concentration of which is sensitive dependent upon the densification conditions. The  $\text{Ge}(0)$  and  $\text{Ge}(2)$   $\text{E}'$ -centers were observed in the air sintered preforms. However, the  $\text{Ge}(3)$ - $\text{E}'$ -center was obtained in the vacuum densified preforms only. Saturation of the defect center concentration is obtained at about  $6 \times 10^5$  R. The total defect center concentration at  $12.3 \times 10^6$  R increases with increasing temperature of densification [ $c(\text{E}'_1\text{-center}, 1625^\circ\text{C}, \text{air},) = 724 \times 10^{15}$  spins/gr,  $c(\text{E}'_1\text{-center}, 1550^\circ\text{C}, \text{air},) = 330 \times 10^{15}$  spins/gr and is lowest in the vacuum densified preform ( $c \text{E}'_1\text{-center}, 1550^\circ\text{C}, 10^{-6}, \text{Torr}) = 288 \times 10^{15}$  spins/gr).

Thus, we recommend densification of preforms in vacuum at low temperatures for high radiation resistant optical fibers.

Currently, extremely low loss optical fibers are fabricated using germania-doped silica glasses. Their production demands a rigorous control of the processing variables such as the oxygen partial pressure, and the drawing temperature and speed. The proper setting of the processing variables requires knowledge of the relationship between fabrication conditions and intrinsic loss mechanisms of the fiber.

Ainslie et. al. (1,2) studied the effects of drawing temperature and speed on the total transmission loss of the  $\text{SiO}_2\text{-GeO}_2$ -fiber. They showed that the increase of fusion temperature leads to an increase of transmission loss. The major contributions to the loss was caused by the tail of UV absorption edge which is affected by the redox states ( $\text{Ge}^{4+}, \text{Ge}^{2+}$ ) of germanium (1,2). However, the loss decreases with increasing drawing speed (1,2). The transmission loss of fibers have also been studied as a function of the core diameter at fixed germania concentration (1) and at variable  $\text{GeO}_2$ - dopant concentration (3). The results of these studies showed that loss is inversely proportional to the core diameter at constant  $\text{GeO}_2$  concentration and increases proportionally to  $\text{GeO}_2$  concentration (3). Transmission loss can also be caused by Ge-OH impurities which have absorption maxima at 1.389 nm and 1.410 nm (3). The generation of defect centers caused by ionizing radiation generates additional loss.

Friebele et. al. (4) using Electron-Spin-Resonance (ESR)-spectroscopy detected defect centers after  $^{60}\text{Co}$   $\gamma$  -ray irradiation of a Corning  $\text{GeO}_2\text{-SiO}_2$ -optical fiber. Four types of germanium  $\text{E}'_1$ -centers were produced.

The radiation sensitivity of treated germania doped silica fiber has also been determined (5). At a  $^{60}\text{Co}$   $\gamma$ -ray irradiation dose of  $10^6$  rad the defect concentration was highest ( $425 \times 10^{15}$  spins/gr) in an oxygen atmosphere and lowest ( $173 \times 10^{15}$  spins/gr) in a hydrogen atmosphere treated fiber.

In the present communication, we report results of a study of the effects densification conditions (sintering) of the preforms. Samples of a preform were sintered at  $1625^\circ\text{C}$  and  $1550^\circ\text{C}$  in air and in vacuum ( $10^{-6}$  Torr) for 75 minutes. The ESR spectra of defects obtained before and after irradiation were detected at 9GHz and Room temperature. (V4500-Varian spectrometer). The magnetic field was measured with a NMR-Anac/Sentec 1001 field tracking gaussmeter and the microwave frequency with a Syntron/Dannar (1017/1255A)-counter. The data were collected on line with a digital PDP11/03 computer permitting signal averaging.

The defect concentration was determined by comparing the double integrals of the first derivative ESR-resonances of the samples with a Varian strong pitch standard. The samples were exposed to  $^{60}\text{Co}$   $\gamma$ -rays ( $1.5 \times 10^5$  R/h).

Among the unirradiated samples only those sintered in the vacuum furnace showed an asymmetric resonance (fig. 1 a). This resonance is due to germanium  $E'_1$ -center (6). After irradiation a new signal was detected the lineshape of which is independent of the irradiation dose level. However, the intensity of this signal increases up to a  $^{60}\text{Co}$   $\gamma$ -ray dose of about  $6 \times 10^5$ R and then remains practically

unchanged (fig. 2). The intensity and lineshape of this absorption are altered by the temperature of the treatments and the oxygen partial pressure. Fig. 3 shows the spectra obtained as a function of the sintering temperature and the oxygen partial pressure. The defect concentration increases [ $c(E'_1\text{-center}, 1625\text{ C, air}, 12.3 \times 10^6\text{ R}) = 724 \times 10^{15}\text{ spins/gr}$ ,  $c(E'_1\text{-center}, 1550^\circ\text{ C, air}, 12.3 \times 10^6\text{ R}) = 330 \times 10^{15}\text{ spins/gr}$  with increasing sintering temperature. However, at constant sintering temperature, the defect concentration ( $c(E'_1\text{-center}, 1550^\circ\text{ C, air}, 12.3 \times 10^6\text{ R}) = 330 \times 10^{15}\text{ spins/gr}$ ,  $c(E'_1\text{-center}, 1550\text{ C}, 10^{-6}\text{ Torr}) = 12.3 \times 10^6\text{ R}) = 288 \times 10^{15}\text{ spins/gr}$ ) decreases slightly with decreasing oxygen partial pressure.

The lineshape of the spectra of the samples sintered in air at  $1550^\circ\text{ C}$  and  $1625\text{ C}$  is similar. However, the differences of the spectra are more profound between the samples treated in air and in vacuum. Based on the shape of the spectra (fig. 3) and the dependence of the lineshape of the spectra (fig.3) on various post heat treated samples at elevated temperatures (7) we suggest that a superposition of resonances of different defect centers is present. The lineshape of these signals have not yet been determined. However, the principal g-values of the resonances detected elsewhere (4,6,8) in a  $\text{GeO}_2\text{-SiO}_2$  fiber are marked on figure 3. Some of these correspond to signals in our samples. According to Friebele et. al. (4) four types of germanium  $E'_1$ -centers may be obtained in germanium doped silica fibers named as  $\text{Ge}(n, n=0,1,2,3)$  centers. The index n indicates the number of the next nearest neighbors of the  $E'_1$ -center bonded with the bridging oxygens. From the spectra of fig 3., it is evident that the  $G(0)$ -

and G(3)-defects may be present in all samples. The G(1)-center probably appears in the air sintered samples but not in the samples sintered in vacuum. In the vacuum sintered preforms, the G(2)-center is created. At the present time, we believe that the  $\text{SiO}_2\text{-E}'_1$ -center is of minor importance in all samples.

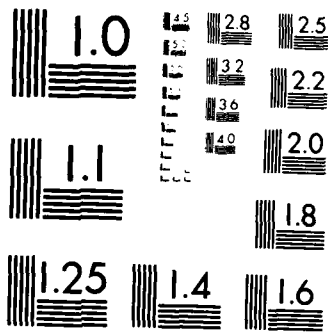
Summarizing, the results of the present study,  $\text{E}'_1$ -centers are observed in the vacuum sintered preforms. A high concentration of these defects was present after irradiation of our samples. Type and extent of these defects can be controlled by both sintering temperature and atmosphere.

In the air densified preforms only the Ge(0) and Ge(3)- $\text{E}'_1$ -centers were detected. However, the Ge(1) and Ge(2)  $\text{E}'_1$ -centers were identified additionally in the  $\text{GeO}_2\text{-SiO}_2$  optical fiber. We believe that the Ge(1) and Ge(2)  $\text{E}'_1$ -centers in the  $\text{GeO}_2\text{-SiO}_2$ -fibers results from the drawing process. Furthermore, Friebele et al (5) reported much lower  $\text{E}'_1$ -center concentration in the  $\text{GeO}_2\text{-SiO}_2$  optical fibers than the defect center concentration of the  $\text{GeO}_2\text{-SiO}_2$ -preforms of our investigation.

We attribute this decrease of defect center concentration in the  $\text{GeO}_2\text{-SiO}_2$  optical fiber to the drawing process in accordance with the observations of other investigators (1,2). Our results clearly indicate that the densification process affects the defect center concentration and, moreover, the transmission loss in an optical fiber. For low radiation induction of defects densification (sintering) of preforms in vacuum at low temperatures appears desirable.

The authors would like to thank Dr. D.K. Nath (ITT Electro-Optical Products Division) for supplying the preform. This work was performed under financial support of AROD under contract DAAG-29-81-K-0118.





MICROCOPY RESOLUTION TEST CHART  
NATIONAL BUREAU OF STANDARDS-1963 A

## REFERENCES

1. B.J. Ainslie, K.J. Beales, D.M. Cooper and J. D. Rusch,  
J. Non-Cryst. Sol. 47,2(1982) 243-246.
2. B.J. Ainslie, K.J. Beales, C.R. Day, and J. D. Rusch,  
IEEE J. Quant. Electr., QE-17, 6(1982) 854-857.
3. N. Shibata, M. Kawachi, and T. Edahiro, Trans. IECE Japan, E63, 12  
(1980) 837-841.
4. E.J. Friebele, D.L. Griscom, and G.H. Sigel, Jr., J. Appl. Phys.,  
45,8(1974) 3424-3428.
5. E.J. Friebele, R.J. Ginther, and G.H. Sigel, Jr., Appl. Phys. Lett.,  
24,9(1974) 412-414.
6. T.A. Purcell and R.A. Weeks. J. Phys. Chem. Glasses, 10, (1965) 198;  
R.A. Weeks and T.A. Purcell, J. Chem. Phys., 43, (1965) 483.
7. G. Kordas, D.L. Kinser, and R.A. Weeks, unpublished data.
8. F.J. Feigl and J.H. Anderson, J. Phys. Chem. Solids, 31,(1970) 575 .

## FIGURES

- Fig. 1. ESR-spectra of unirradiated (a) and  $^{60}\text{Co}$   $\gamma$ -ray irradiated (b)  $\text{GeO}_2\text{-SiO}_2$ -preforms sintered at  $1625^\circ\text{C}$  in a vacuum ( $10^{-6}$  Torr) furnace.
- Fig. 2. The radiation kinetics of paramagnetic defect states observed in a preform sintered at  $1625^\circ\text{C}$  and  $p\text{O}_2=10^{-6}$  Torr.
- Fig. 3. The spectra of  $^{60}\text{Co}$   $\gamma$ -ray irradiated preforms exposed to various treatments. The marks (two: for axial symmetry, and three: for total g-value anisotropy) indicates the positions of principal g-values reported in previous publications (a: reference 8, b: reference 6, and c: reference 4) for the germanium (b,c) and silicon (a)  $\text{E}'_1$ -centers).

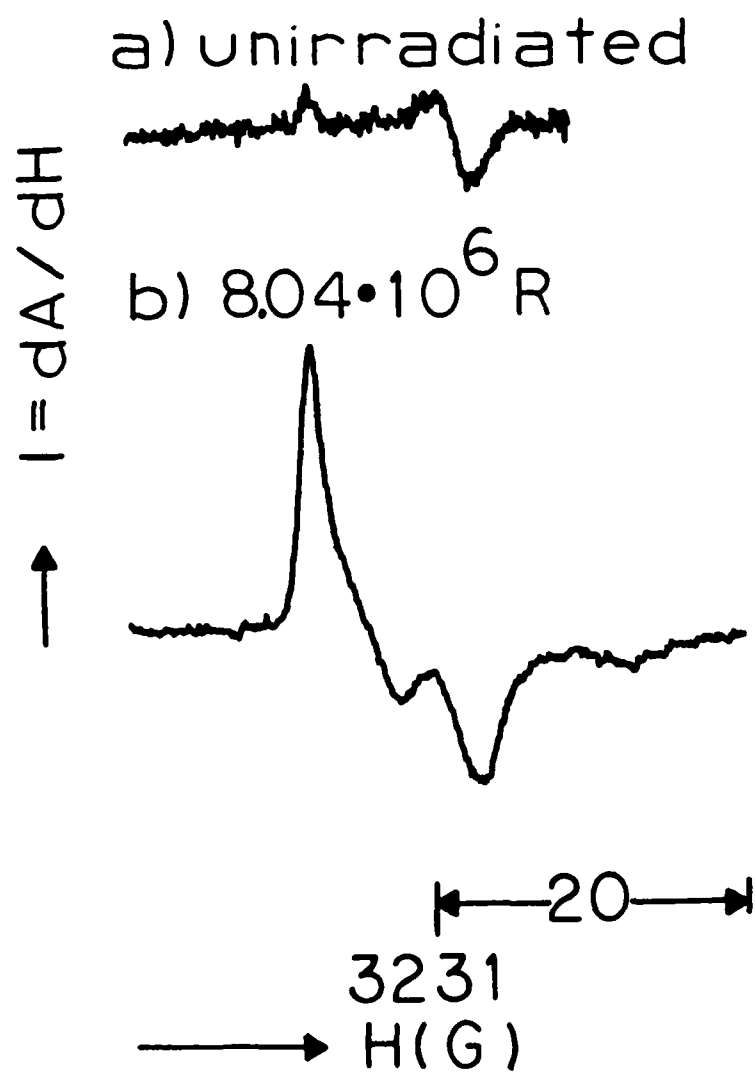


fig. 1

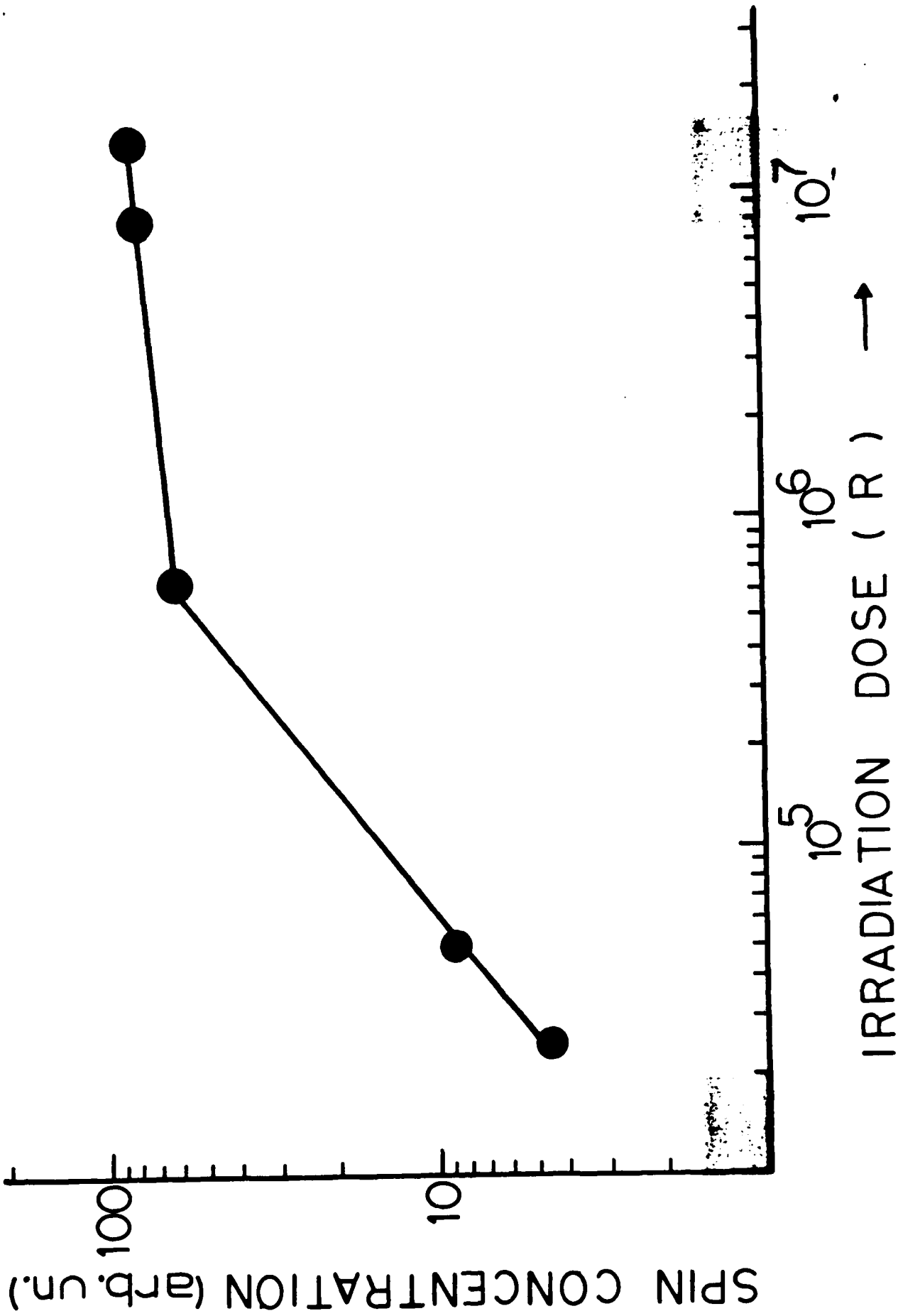


fig.2

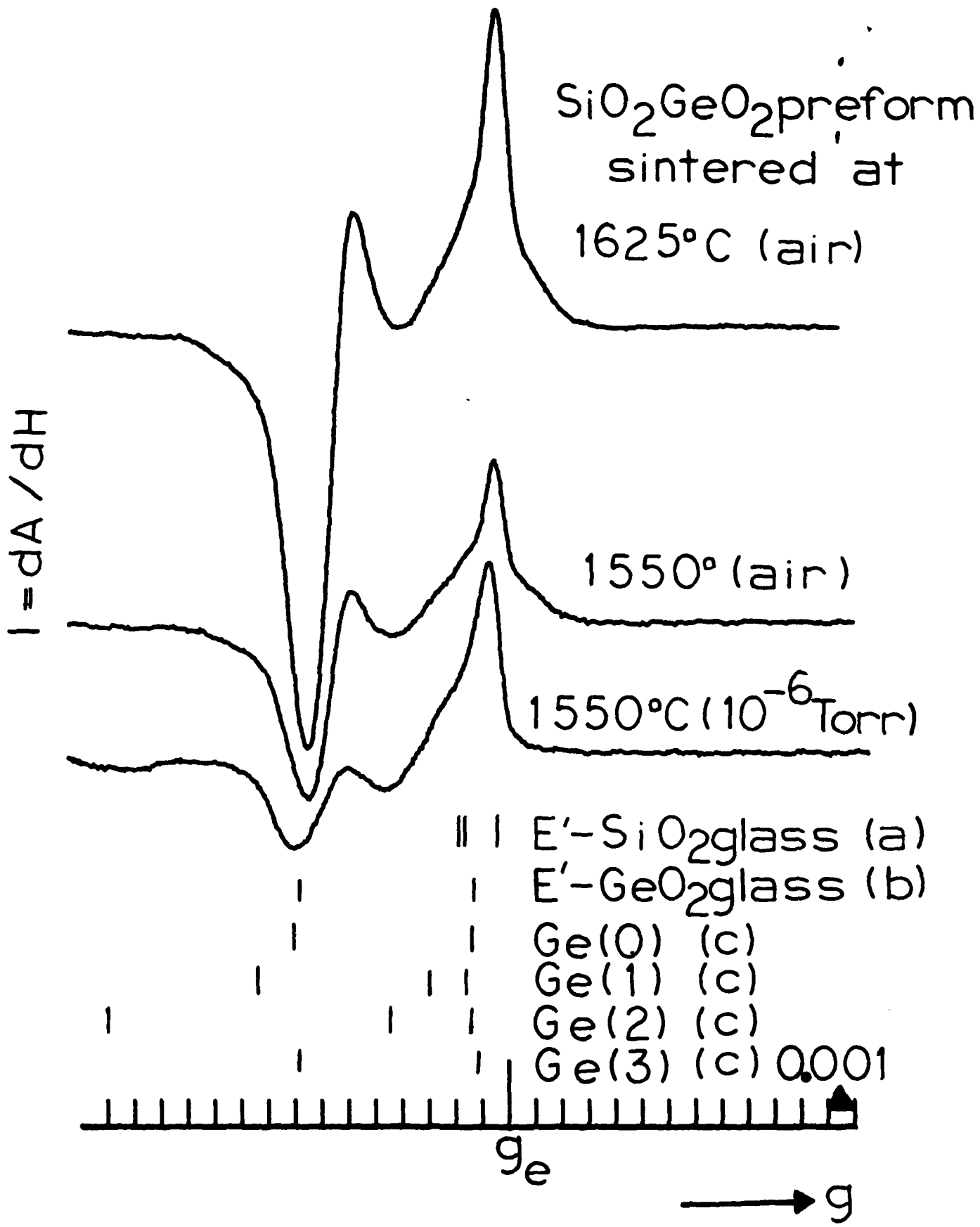


fig.3

APPENDIX II.h.

Paramagnetic Conduction Electrons in GeS<sub>x</sub>-Glasses.

G. Kordas, R.A. Weeks, and D.L. Kinser

Vanderbilt University, Nashville, IN 37235, USA

ABSTRACT

The 9.5 and 35GHz spectra of GeS<sub>x</sub>-glasses with x=1.25-2.01 synthesized in evacuated Vycor ampules between 683°C and 895°C exhibit a symmetric narrow line (A-component: g<sub>eff</sub> = 2.003, ΔH<sub>pp</sub> (9.5GHz) = 3G, ΔH<sub>pp</sub> (35GHz) = 4.8G) and an asymmetric broader resonance (B-component: X-Band, g<sub>eff</sub> = 2.0112, ΔH<sub>pp</sub> = 16.25G, Q-Band: g<sub>eff</sub> = 2.0045, ΔH<sub>pp</sub> = 11G). The line width of the A- and B- components was measured between 10K and 300K. For the A component the ΔH<sub>pp</sub> vs. temperature of measurements, T<sub>M</sub>, and ln(ΔH<sub>pp</sub>) vs. T<sub>M</sub><sup>-1/4</sup> plots were best fitted assuming two straight lines in the ranges from 34K to 77K and from 77K to 300K. The line width of the B-component is invariant with temperature of measurements from 10K to 300K. On the basis of the frequency and temperature behavior of these lines we suggest that the A-component is due to a paramagnetic electron hopping between different sites and attribute the B-component to conduction electrons in Ge rich regions in the glass.

## 1. Introduction

The electron spin resonance spectrum of amorphous germanium (a-Ge) exhibits a symmetric line at  $g=2.021$  (1-5). The line width of this ESR-signal is about 3/G below 77K and increases linearly with the increase of the temperature of measurements,  $T_M^{-1/4}$  (1-5). The plot of  $\ln(\Delta H_{pp})$  versus  $T_M$  could also be fitted to a straight line between 77K and 300K. This behavior of the line width with  $T_M$  led numerous investigators to attribute the a-Ge-signal to unpaired electrons hopping between different sites (1-5).

Shimizu et. al. (6) studied the change of the symmetric a-Ge-signal by doping a-Ge with sulfur. Based on these measurements Shimizu et. al. (6) concluded that the B-component detected in  $GeS_2$ -glasses is caused by electrons localized on germanium dangling bonds. The B-component was also reported by Cerny et. al. (7) who attributed this defect to sulfur dangling bond. Akagi et. al. (8) measured, in  $GeS_{2.5}$ -glasses, the A-component and assumed that this signal is caused by a  $GeS^{\cdot}$ -defect centers.

In the present work we report the temperature and frequency variation of the A- and B- components and we discuss their relation to the paramagnetic states causing the a-Ge-signal.

### 2. Experimental Procedures.

The sample preparation technique and ESR-apparatus are described in previous publication. <sup>(9)</sup> The glass compositions were determined by X-ray energy dispersive spectroscopy using a Hitachi scanning electron microscope and a Princeton gamma tech spectrochemical analyzer and are given in table 1. Metallic germanium and pyrite were used as standards for the analysis of the glass compositions. The impurities were determined by the neutron activation analysis and are given in table 2.

### 3. Results

From the data in table 1. One can percieve that the glass compositions differ from the batch compositions.

Fig. 1 shows the ESR-spectra of three glasses equilibrated at temperatures  $T$ , of  $683^{\circ}\text{C}$ ,  $796^{\circ}\text{C}$  and  $895^{\circ}\text{C}$ . The A-component was detected in the glasses with  $T = 683^{\circ}\text{C}$  and  $796^{\circ}$ . The B-component is not detected in the glass with  $T = 683^{\circ}\text{C}$  and increases with the increaae of  $T$ . The intensity variation of these components in  $\text{GeS}_x$ -glasses with  $x$  was reported elsewhere <sup>(9)</sup>.

The temperature variation of the peak-to-peak line width

of the A-component is shown in fig. 2. One can notice from this figure that the line width varies linearly with  $T_M$ . In fig. 2b the logarithm of the peak-to-peak line width is plotted as  $T_M^{-1/4}$ . It is clear that also the  $\ln(\Delta H_{pp})$  is linear with respect to  $T_M^{-1/4}$ .

The line width of the B-component is 16.25G between 10K and 300K. Fig. 3 displays the B-component recorded at 35GHz and at 300K. The peak-to-peak line width of the B-component is 11G and that of the A-component is 4.8G at 35GHz and at 300K.

Fig. 4 shows the values of the double integrals of the differentiated ESR-signals recorded at various  $T_M$  as a function of  $1/T_M$ .

#### 4. Discussion.

The impurities determined by the neutron activation analysis have valence states which are paramagnetic and exhibit well defined ESR-signals <sup>(10)</sup>. These differ in several respects from the signals of the A- and B- components (fig. 1,2). Therefore, we attribute the defects causing the A- and B- components to intrinsic defects of the GeS<sub>x</sub>-glasses. An appropriate model for the A- and B- components must explain the frequency and

temperature variation of their line widths. For example, a  $S=1/2$  paramagnetic state with anisotropic g-values will have a line width at 35GHz four times greater than at 9.5GHz (11)

The line width of a  $S>1/2$  paramagnetic state is independent of the frequency of measurements provided the line width is not appreciably affected by spin lattice relaxation effects. In the case of the A component  $\Delta H_{pp}(35\text{GHz})/\Delta H_{pp}(9.5\text{GHz})=1.6$  for the B component  $\Delta H_{pp}(35\text{GHz})/\Delta H_{pp}(9.5\text{GHz})=0.68$ . These data indicate that the A- and B- components cannot be explained by unpaired electrons localized on sulfur or germanium dangling bonds (6-8)

For the modeling of the paramagnetic defect centers in a-Ge and a-Si the peak-to-peak line width variation with  $T_M$  of the ESR-signal was of great importance. The a-Ge-ESR-line width can be expressed in a temperature-independent  $\Delta H_{pp}$  and temperature-dependent  $dH_{pp}(T)$  contribution (1-5). The  $dH_{pp}(T)$ -contribution was related to unpaired electrons hopping between different sites. Thomas et. al. (3) found that the a-Si-paramagnetic center obeys the Curie law. The line width of the a-Ge- and a-Si- signals increases slightly with increase of frequency from 9.5GHz to 35GHz (3). The behavior of the A-component (fig.2) is compatible with the behavior of the a-Ge- and a-Si- signals reported in the literature. Therefore, it is

reasonable to assume that the A-component is due to unpaired electrons hopping between different sites in Ge-clusters of the GeS<sub>1.25</sub>-glasses. .

The decrease of the line width of the B-component with the frequency of measurements is important for understanding the origin of this signal. Overhauser<sup>(11)</sup> found that the peak-to-peak line width of conduction electrons interacting with the currents arising from translational motion of conduction electrons is proportional to  $\ln(\text{constant}/\text{applied magnetic field } H)$ . This mechanism may be the one producing the decrease of the line width of the B-component with increase of the applied magnetic field.

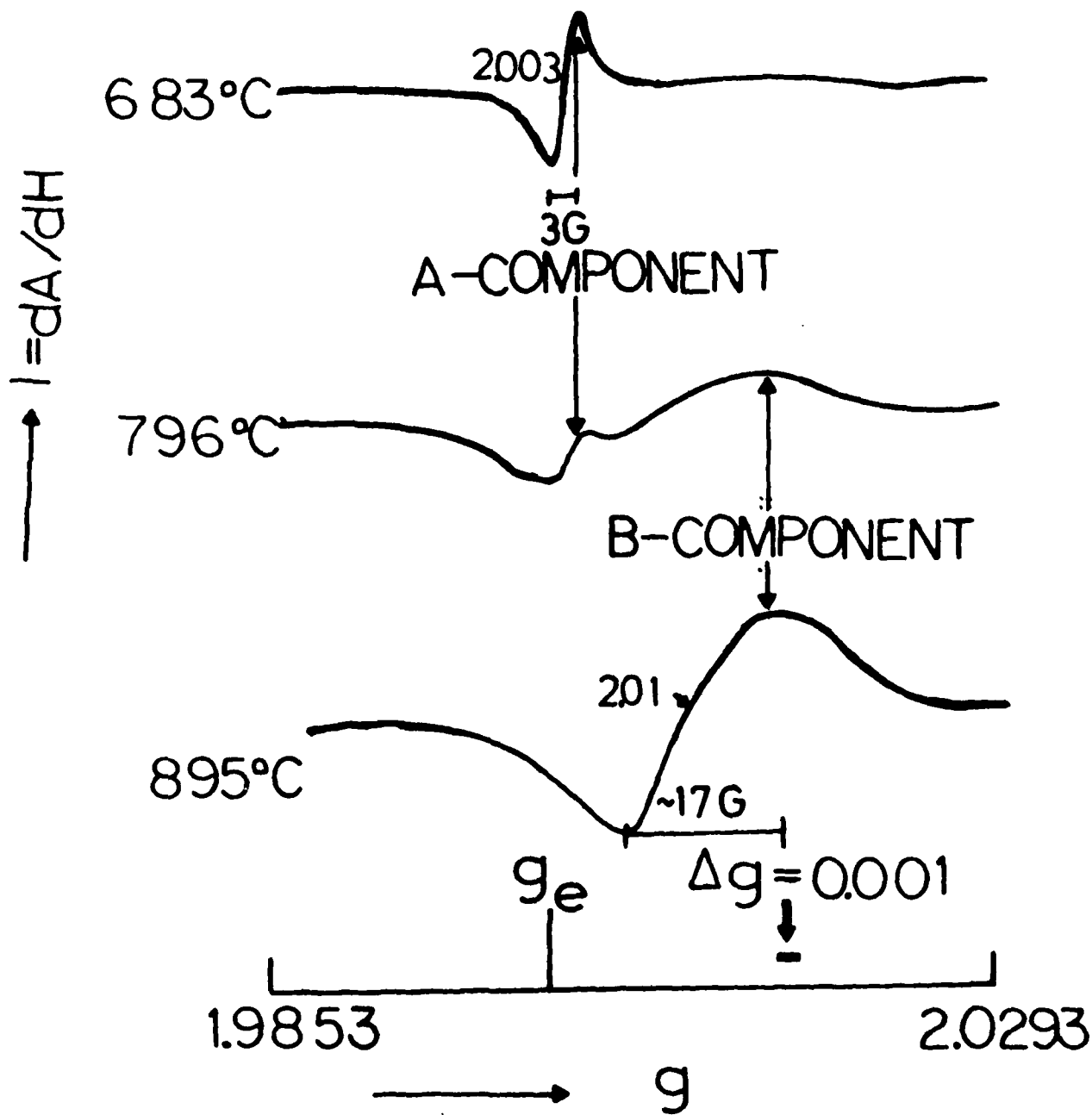
## CONCLUSIONS

The composition of the germanium sulfide glasses is not the same as their batch compositions. The ESR-spectra of the germanium sulfide glasses displays two components which we have labeled A and B. The relative intensity of these components is a function of T. The A component is explained by an unpaired electron hopping between different germanium sites. The B component is attributed to a paramagnetic conduction electron.

## ACKNOWLEDGEMENT

The authors wish to express their appreciation for financial support of this work under AROD Contract #DAAG-29-81-K-0118.

GeS<sub>2</sub>  
300K  
(as fused)

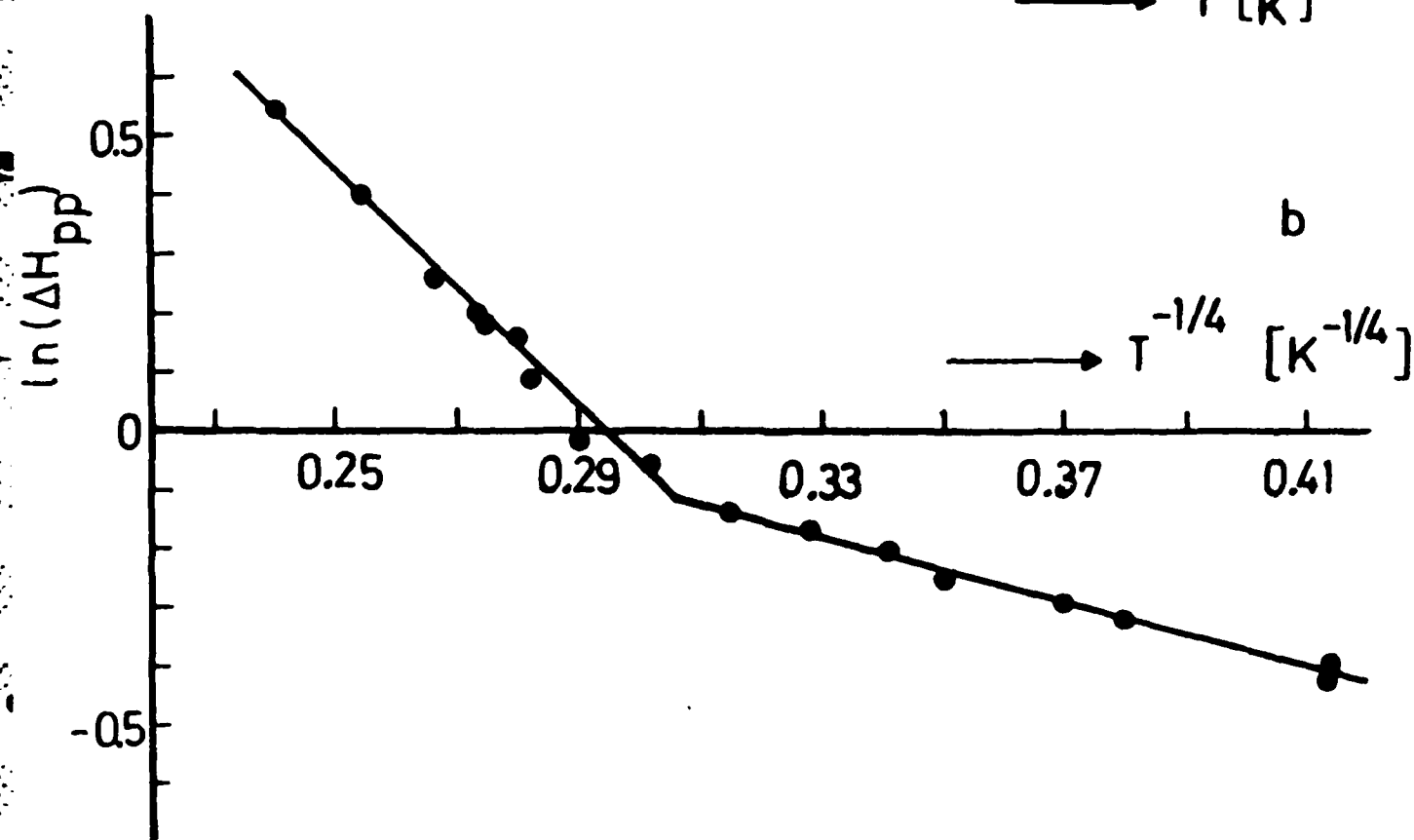
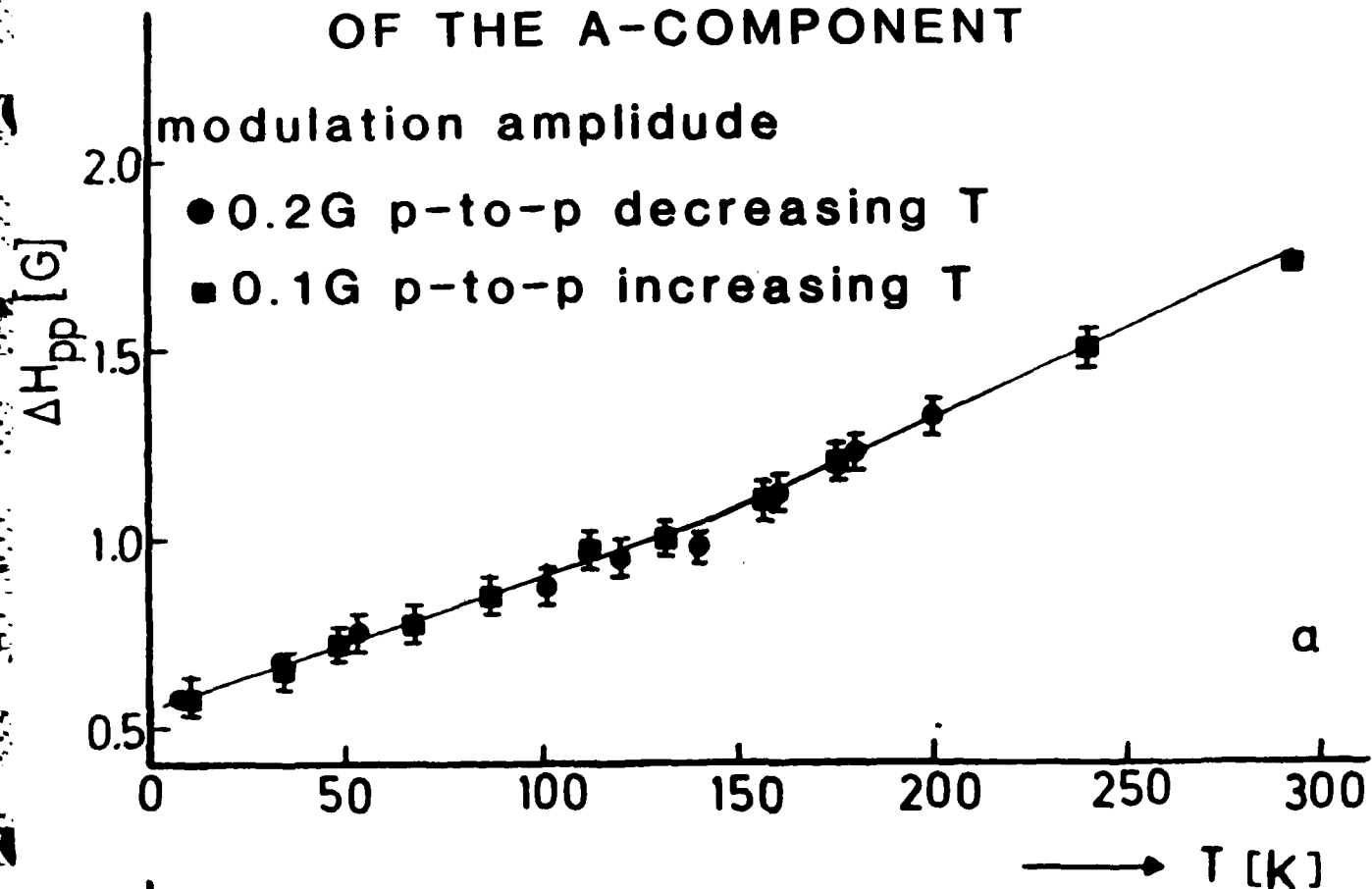


# TEMPERATURE DEPENDENCE OF THE LINE WIDTH OF THE A-COMPONENT

modulation amplitude

● 0.2G p-to-p decreasing T

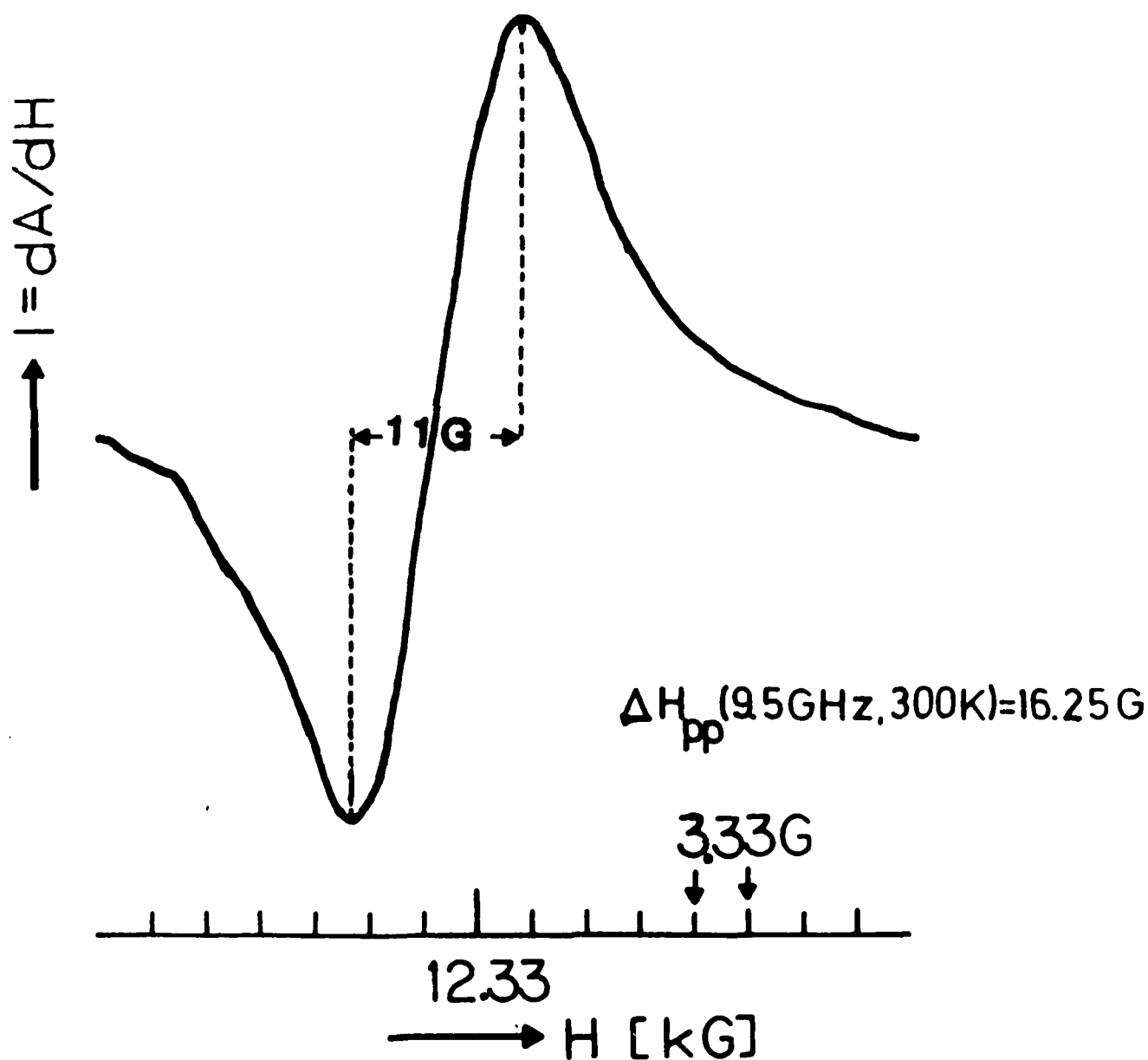
■ 0.1G p-to-p increasing T

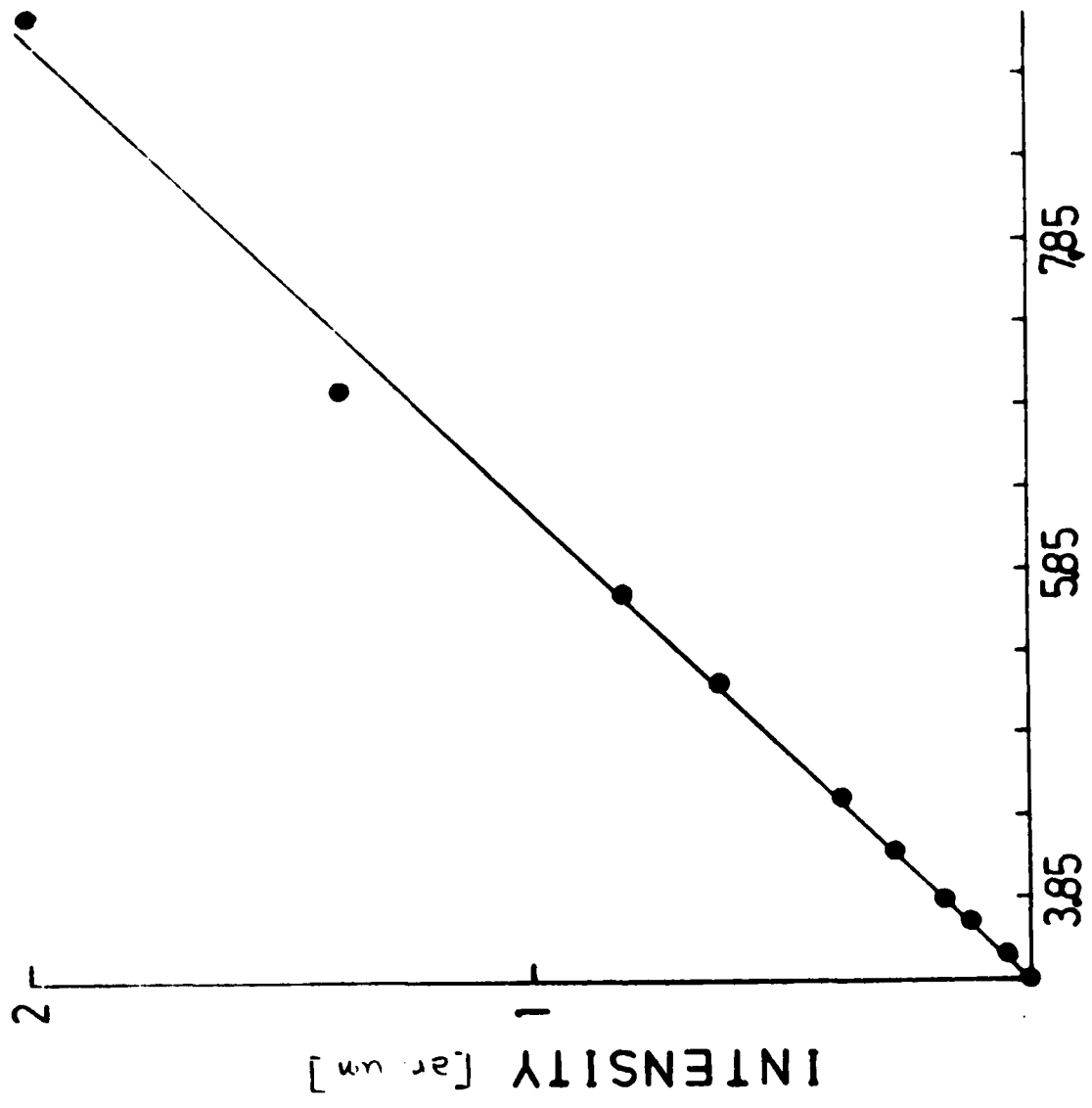


# Q-BAND SPECTRUM OF B-COMPONENT

$\text{GeS}_{2.02}$

35GHz, 300K,  $T_m = 895^\circ\text{C}$





$1/T$  [ $10^{-4} \text{ K}^{-1}$ ]

**GeS<sub>x</sub> GLASS COMPOSITION**

$T_{\phi}$

BATCH COMPOSITION	683° C	796° C	895° C
1.9	1.25	1.89	1.71
2.0	-	2.02	1.81
2.1	-	1.96	1.84

T.1.

**TRACE ELEMENTS GIVEN in ppm**

	Na	Mg	Al	Ti	Fe	Se
GeS <sub>2.02</sub> Sample	76.0	490.0	113.0	70.0	3.0	0.49

- 2

APPENDIX II.i.

Presented at Conference "Effects of Modes  
- of Formation on the Struct. of Glass" & -  
to be published in J. Non-Cryst. Solid, '85

Electron-Spin-Resonance (ESR) Study of Sol-Gel-Glasses.

G. Kordas and R.A. Weeks

Vanderbilt University, Nashville, TN 37235, USA

L. Klein

The State University of New Jersey RUTGERS, New Jersey, USA

## ABSTRACT

The 9.5GHz ESR-spectra of gamma-ray irradiated  $\text{SiO}_2$  vacuum dried gels, produced with 2, 4, 8 and 16 mole of water per mol tetraethylorthosilicate (TEOS) and gels heat treated at temperatures between 400 C and 1000 C were recorded at 77K and 300K. A broad asymmetric line ( $\text{DH}_{\text{pp}} = 20.5\text{G}$ ,  $g_{\text{eff}} = 2.006$ ) dominated the room temperature spectra of the dried gels. The ESR-spectra of these gels recorded at 77K consist of a well resolved signal characterized by  $g_1 = 2.004$ ,  $g_2 = 2.01$  and  $g_3 = 2.04$ . We tentatively attribute this resonance to  $\text{O}_2^-$ -ions. The resonance of this  $\text{O}_2^-$ -specie dominates the spectra of the gels treated up to 500 C. The spectrum of the vacuum dried gel heat treated at 900 C exhibit the resonance of the  $\text{E}'_1$ -center and non-bridging oxygens. The spectrum of the gel heat treated at 1000 C is composed of several lines attributed to  $\text{O}_2^-$  radicals having different ligand fields.

## 1. Introduction

It has been recognized that optical wave guide fibers can be produced more economically by the sol-gel process than by the MCVD- or VAP- method<sup>(1)</sup>. Besides the economical aspect, the sol-gel process offers technological advantages for the fabrication of optical fibers such as<sup>(1)</sup>:

1. easy fabrication of preforms in a wide range of homogeneous glass compositions,
2. low temperatures of production which result in a low concentration of thermal activated defects,
3. easy modification of the defect structure by a variation of starting solutions, of drying, and of densification procedures.

A recent publication reported attenuation losses of 6dB/km at 850nm in SiO<sub>2</sub>-sol-gel fibers<sup>(1)</sup>. These attenuation losses were due to OH overtone absorptions and intrinsic defect centers<sup>(1)</sup>.

The removal of water from the sol-gel glasses, necessary to reduce the OH overtone absorption bands, requires heat treatments with Cl<sub>2</sub> at high temperatures<sup>(2)</sup>. The absorption losses caused by intrinsic defect centers can be reduced by an optimization of the fabrication conditions of the sol-gel glasses. The defect structure of the sol-gel glasses can be modified by the pH of the starting solutions and by densification conditions.

The raman spectra showed that the 487cm<sup>-1</sup> and 600cm<sup>-1</sup>

scattering bands caused by defects <sup>(3-5)</sup> are present in the gels as well as in the sol-gel glasses <sup>(6)</sup>. The effects of variation in pH, of starting solutions and of densification conditions on the formation of defects in gels as well as sol-gel glasses has not been studied.

In the present work we report the paramagnetic defect centers obtained after irradiation of the SiO<sub>2</sub> based vacuum dried gels produced with various water contents. The water content was chosen to be 2, 4, 8, and 16 moles per mole TEOS (Si(OC<sub>2</sub>H<sub>5</sub>)<sub>4</sub>). The ESR spectra observed during the gel-to-glass transformation of the gel with 16 mole water per mole TEOS was measured. The gel was vacuum dried and then heat treated at temperatures between 400 °C and 1000 °C. The sample preparations and experimental procedures have been described in previous publications <sup>(7,8)</sup>.

## 2. Results.

Fig. 1 shows the room temperature ESR-spectrum of a gel gamma-ray irradiated at room temperature and recorded while exposed to air and while in vacuum (about 10<sup>-5</sup> m pressure). An asymmetric broad resonance was detected in this gel having a line shape, line width and intensity independent of

the atmosphere in which the sample was measured. This signal observed in all the other gels is independent of the water content of the initial solutions from which the vacuum dried gels were produced.

Fig. 2 shows the ESR-spectrum at 77K of the gamma-ray irradiated 2 mole water/mole TEOS gel. The g-values characterizing this defect are given in table 2.

Fig. 3 displays the 77K ESR-spectra of the gels produced with 16 mole of water per mole TEOS as a function of the temperature of heat treatments,  $T^{\circ}$ , between 80 C and 500 C (fig. 4). The asymmetric line characterizing the 77K spectra of the irradiated vacuum dried gels is also observed at 77K in the gels heat treated at 80 C, 400 C and 500 C.

The spectrum of the sample heat treated  $T^{\circ} = 900$  C consists of a narrow and broad asymmetric line (fig. 4a). The narrow line is shown on an expanded scale in fig. 4b in order to exhibit its line shape, line width and g-values.

Fig. 5 displays the spectra of the vacuum dried gel heat treated at 1000 C. We measured this spectrum at various microwave power levels. These measurements indicated the presence of three components due to defects created when the temperature of heat treatments was greater than 900 C. The spectrum shown in fig. 6 is complex, however, there are three low field shoulders at  $g=2.1143$ ,  $g=2.0457$  and  $g=2.0335$ . In addition two shoulders on the high field side

of the spectrum are well resolved with g-values of  $g=2.0027$  and  $2.0004$ . There are additional inflections in the region of maximum intensity. We attribute this spectrum to the presence of three components due to defects created at  $T_H$  higher than  $900^\circ\text{C}$ .

### 3. Discussion.

The paramagnetic defect centers may be due to impurities or intrinsic defect centers. Since the starting solutions were  $\text{Si}(\text{OC}_2\text{H}_5)_4$ ,  $\text{H}_2\text{O}$  and  $\text{HCl}$  the formation of oxygen radicals is possible. The g-values of the radicals listed in table 1 are not the same as those determined from the spectra of our samples (table 1). Based on this fact we believe that intrinsic defect centers account for the recorded signals (fig. 1,2,3,4,5).

The g-values of the defect detected in vacuum dried gels and gels with  $T_H$  below  $500^\circ\text{C}$  correspond to those of an oxygen related center (table 2). In table 2 the ESR spectra of g-values of the ESR spectra of  $\text{O}_2^-$  ions obtained in  $\text{MgO}$ ,  $\text{ZnO}$  and Zeolites containing oxygen are also given. We suggest that the correspondance of the g-values for the low field shoulder and of the peak of the absorption intensity

with those for  $O_2^-$  ions indicates a similar source for the spectra of vacuum dried gels and those heat treated at  $T_H$  less than  $500^\circ C$ . We have also shown that the atmosphere surrounding the sample (fig. 1) does not affect the spectra. Hence the defect does not appear to be located on the surface of the gels.

In addition the line shape of the resonance in our samples depends on the temperature of measurements (fig. 1,2). We suggest that this temperature dependence of the signals is due to a tumbling motion of the  $O_2^-$  ions. The tumbling rate decreases as the temperature of measurements decreases. Thus, a better resolution of the spectra is obtained at 77K than 300K (fig. 1,2).

The narrow line detected in the vacuum dried gels heat treated at  $900^\circ C$  has about the same g-values as those reported for the  $E'_1$ -center (fig. 5) <sup>(9)</sup>. Therefore, we attributed this defect to oxygen vacancies. The broad signal recorded in this sample (fig. 5) has about the g-values which have been reported <sup>(10)</sup> for the non-bridging oxygens. We attribute this defect to a paramagnetic non-bridging oxygen.

The spectra of the vacuum dried gels heat treated at  $1000^\circ C$  consists of a complex array of resonances. There appears to be three different distinct spectra (fig. 6). We

result to those observed for  $O_2^-$  in different oxides and zeolites<sup>(11)</sup> are consistent with this explanation (table 3).

### CONCLUSIONS

The paramagnetic centers detected in vacuum dried gels and gels heat treated up to 500<sup>o</sup> were attributed to  $O_2^-$  ions in interstitial positions. Major changes occur at  $T_H$  from 500<sup>o</sup> C to 900<sup>o</sup> C. These changes favor the formation of non-bridging oxygens and  $E'_1$ -centers. Further increase of  $T_H$  induces three different  $O_2^-$  radicals present in different interstitial sites.

### ACKNOWLEDGEMENT

The authors wish to express their appreciation for financial support of this work under AROD Contract #DAAG-29-81-K-0118.

## REFERENCES

1. K. Susa, I. Matsuyama, S. Satoh, and T. Suganuma, *Elect. Lett.*, 18(1982)499.
2. N. Shibata, M. Kawachi and T. Edahiro, *Trans. IEEE of Japan*, Vol. E 63, 12(1980)837.
3. F.L. Galeener and G. Luckovsky, *Phys. Rev. Lett.*, 37,22(1976)1474.
4. J.C. Mikkelsen, Jr. and F.L. Galeener, *J. Non-Cryst. Sol.*, 37(1980)71.
5. J. Bates, R.W. Hendricks and L.B. Shaffer, *J. Chem. Phys.*, 61,10(1974)4163.
6. A. Bertoluzza, C. Fagnano, M. A. Morelli, V. Gottardi and M. Guglielmi, *J. Non-Cryst. Sol.*, 48(1982)117.
7. G.J. Garvey and L.C. Klein, *J. Physique*, C9,43(1982)271.
8. G. Kordas, R.A. Weeks and D.L. Kinser, *J. Appl. Phys.*, 54,9,(1983)5394.
9. R.A. Weeks and C.M. Nelson, *J. Appl. Phys.*, 31,9(1960)1555.
10. G. Kordas and H.J. Oel, *Phys. Chem. Glasses*, 23,5(1982)179.
11. J.H. Lunsford, *Catalysis Review*, 8(1973)135.
12. D.B. Chesnut, *J. Chem. Phys.*, 29(1958)43.
13. T. Cole, *Proc. Natl. Acad. Sci.*, 46(1960)506.
14. E. Clementi, C.C. Roothaan and M. Yoshimine, *Phys. Rev.*, 127(1962)1618.
15. T. Cole, C. Heller, and H.M. McConnell, *Proc. Natl. Acad. Sci.*, 45(1959)525.

## FIGURE CAPTURES

Fig. 1 Room temperature ESR-spectrum of a gamma-ray irradiated vacuum dried gel (2 mole water/mole TEOS) recorded in air and in vacuum.

Fig. 2 77K ESR-spectrum of the gamma-ray irradiated vacuum dried 2 mole water/mole TEOS gel.

Fig. 3 77K ESR-spectra of the 16 mole water/mole TEOS gels heat treated at 80 C, 400<sup>o</sup> and 400<sup>o</sup> C.

Fig. 4 a) 77K spectrum of vacuum dried gel (16 mole water/mole TEOS) heat treated at T = 900<sup>o</sup> C.

b) Resonance of the E'<sub>1</sub>-centers recorded in the 16 mole water/mole TEOS gel with T = 900<sup>o</sup> C.

Fig. 5 77K ESR-spectra of the irradiated vacuum dried (16 mole water/mole TEOS) gel with T = 1000<sup>o</sup> C.

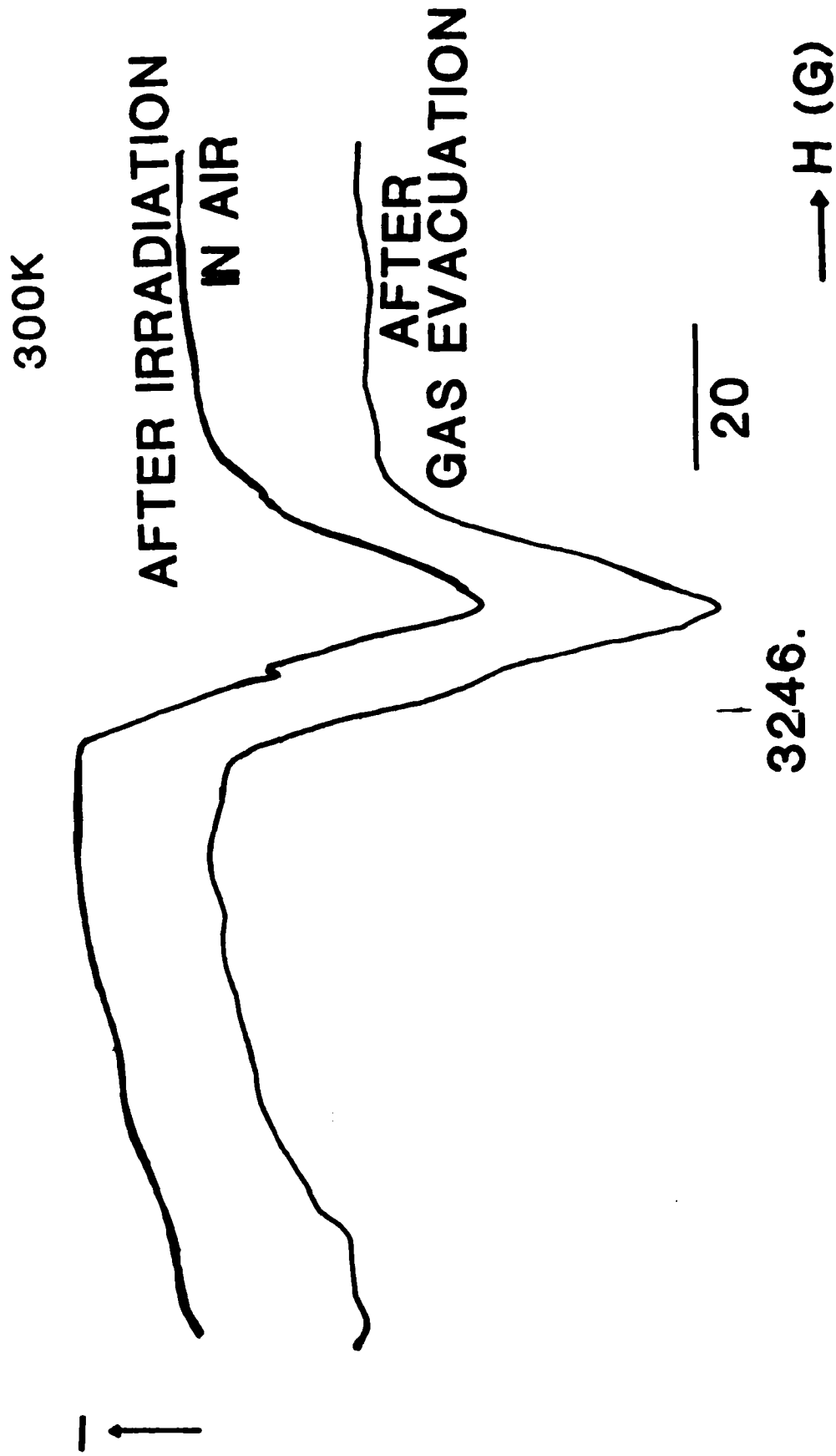
## TABLES

Table 1 The g-values of the  $O_2^-$  ions in MgO, ZnO and Zeolites.

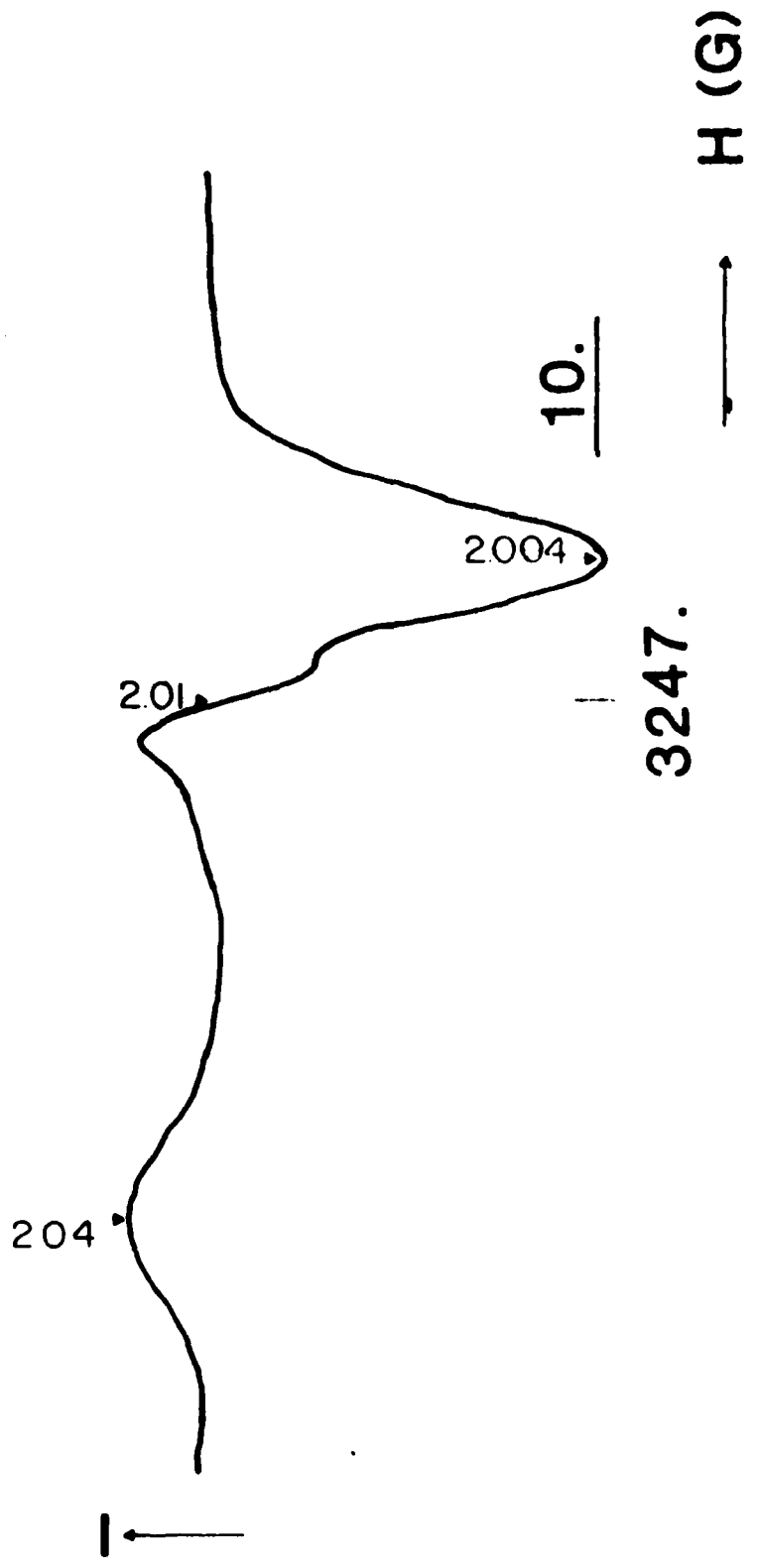
Table 2 The g-values of radicals which can be formed after gamma-ray irradiation of the gels.

Table 3 The g-values of the  $O_2^-$  ions obtained in oxides and zeolites as a function of the energy separation,  $U$ , between the ground state and the next lower energetic state of these ions.

The intensity of the X-band ESR-spectrum as a function of the atmosphere of measurements  
2 mole water/mole TEOS

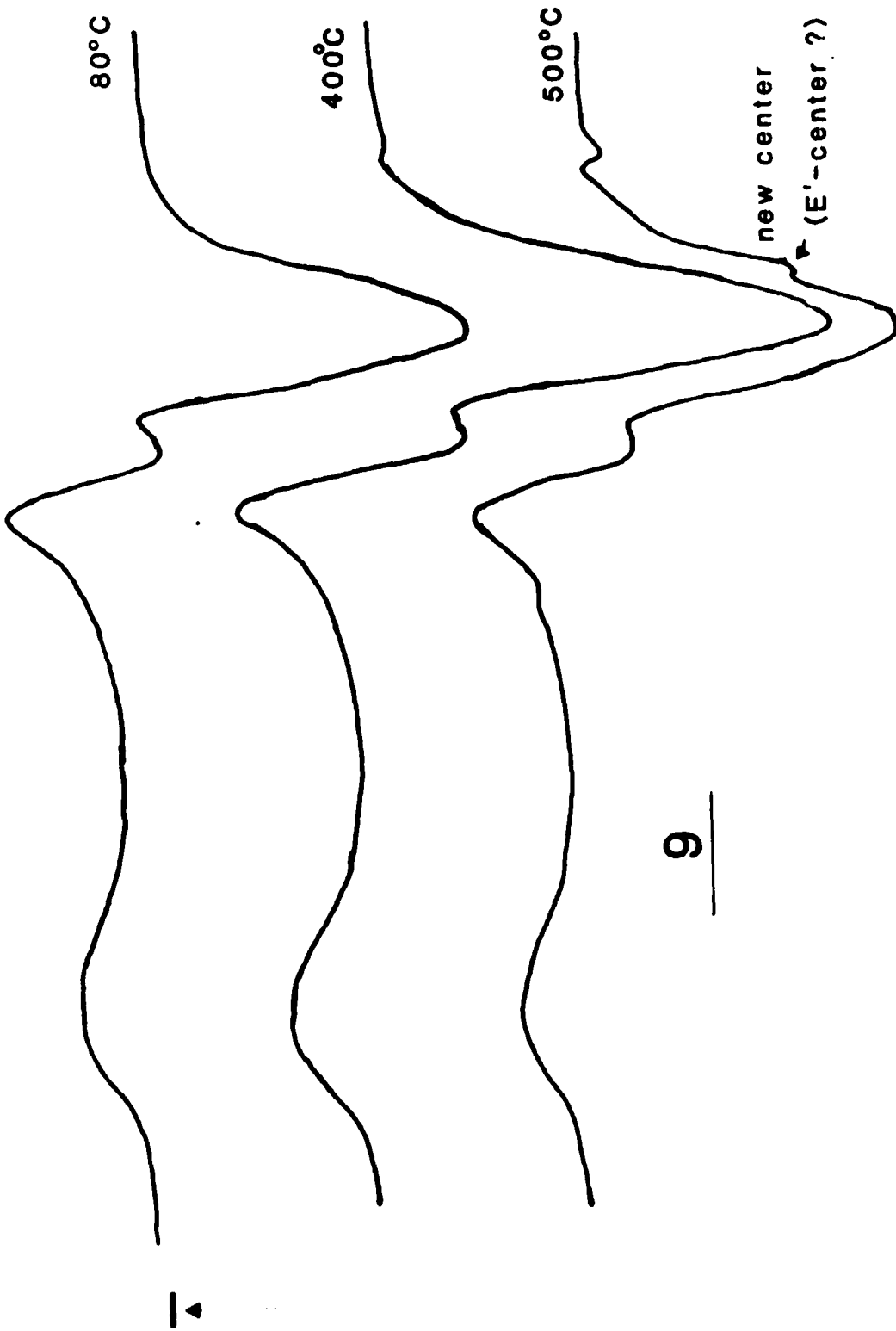


The 9.5GHz ESR-signal of the gamma-ray irradiated vacuum dried gel ( $n=2$ ) recorded at 77K



ESR-Spectra of irradiated gels heat treated at 80, 400, 500°C

77K



9

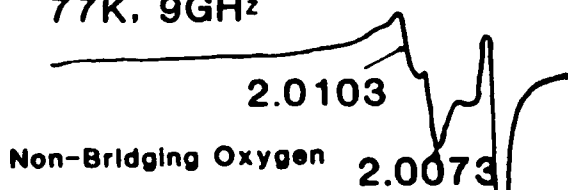
3247.

→ H(G)

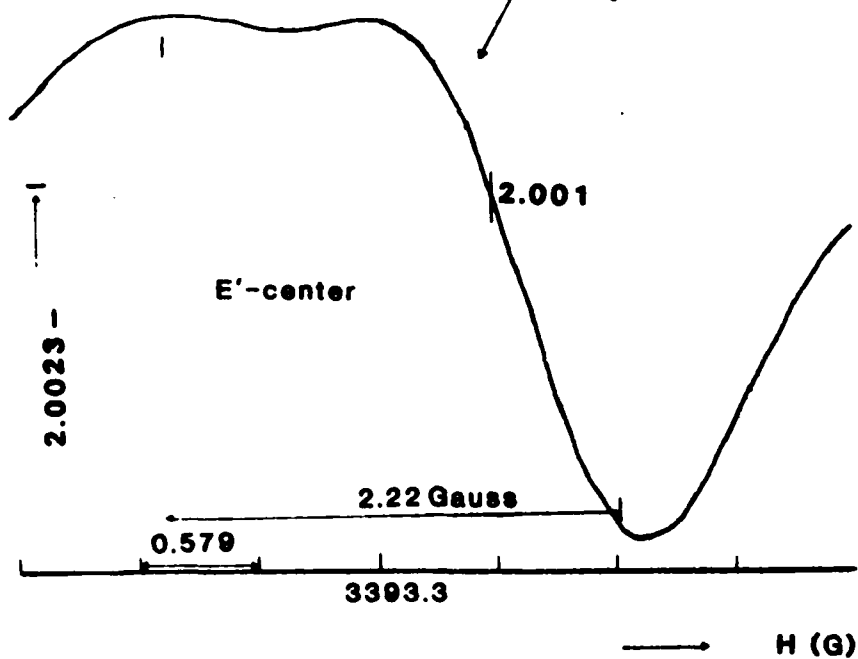
1 2 3 4 5 6 7 8 9 10 11 12 13 14 15 16 17 18 19 20 21 22 23 24 25 26 27 28 29 30 31 32 33 34 35 36 37 38 39 40 41 42 43 44 45 46 47 48 49 50 51 52 53 54 55 56 57 58 59 60 61 62 63 64 65 66 67 68 69 70 71 72 73 74 75 76 77 78 79 80 81 82 83 84 85 86 87 88 89 90 91 92 93 94 95 96 97 98 99 100

ESR-SPECTRUM OF  
AN IRRADIATED  
16 MOLE WATER /MOLE TEOS GEL  
HEAT TREATED AT 900°C

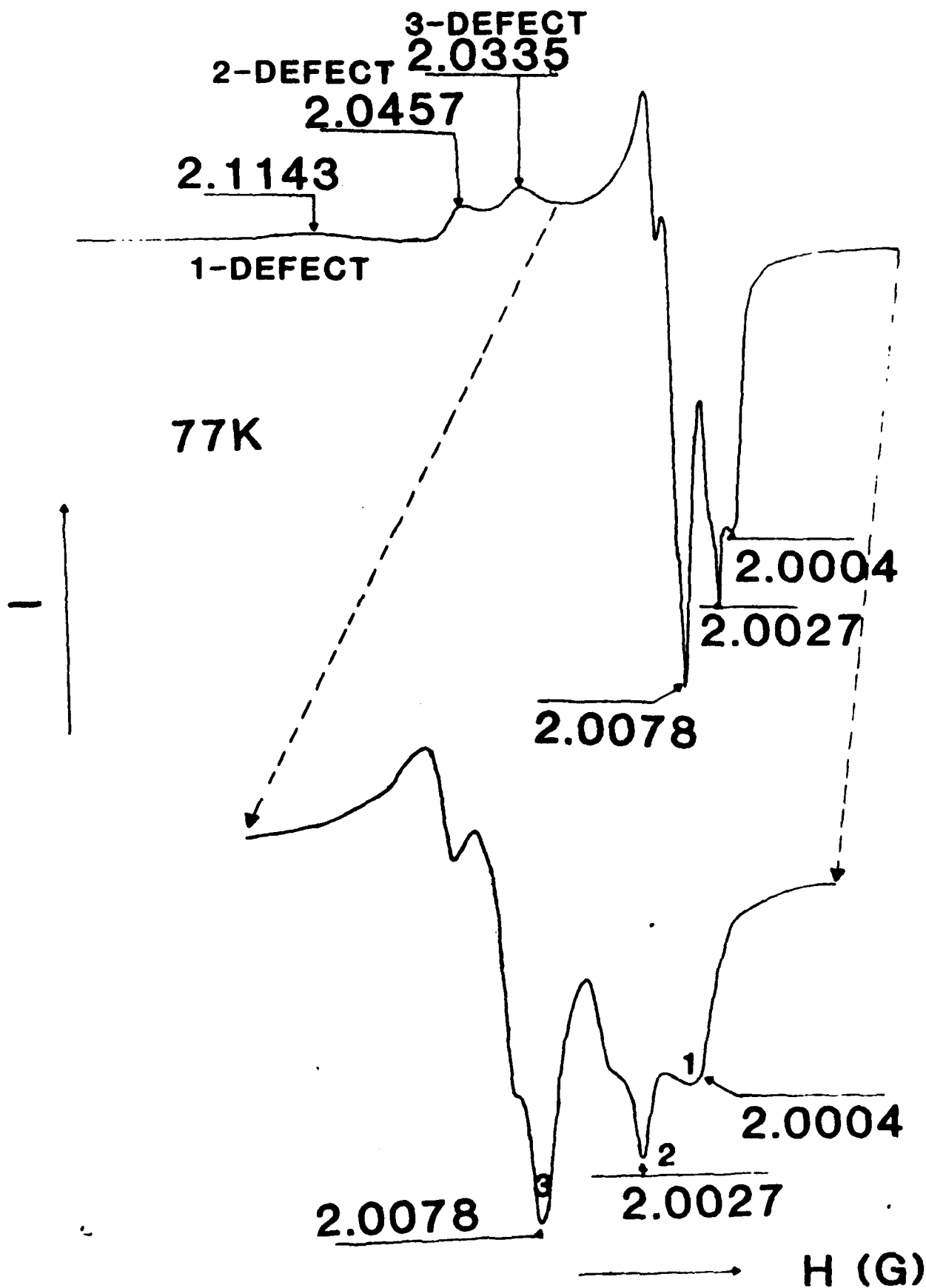
77K, 9GHz



$g_1$  2.0041     $g_2$  2.01     $g_3$  2.0196



# ESR-SPECTRUM OF AN IRRADIATED GEL HEAT TREATED AT 1000°C



	references	9 <sub>1</sub>	9 <sub>2</sub>	9 <sub>3</sub>
CO <sub>2</sub>	12	1.9975	2.0014	2.0032
CO <sub>3</sub>	13	2.0066	2.0086	2.0184
ClO <sub>2</sub>	14	2.0036	2.0088	2.0183
ClO <sub>3</sub>	15	2.007	2.008	2.008
OUR DEFECT		2.004	2.01	2.04

TA

SUMMARY OF G-TENSOR DATA FOR  $O_2^-$  (J.H. LUNSFORD)

	$g_1$	$g_2$	$g_3$	$\Delta$ (eV)
ZrO <sub>2</sub>	2.027	2.008	2.003	1.12
SnO <sub>2</sub>	2.028	2.009	2.002	1.08
GAAS	2.036	2.007	2.007	0.82
ALHYZEOL.	2.038	2.009	2.003	0.78
AL <sub>2</sub> O <sub>3</sub>	2.038	2.006	2.006	0.78
ALSB	2.041	2.005	2.002	0.72
ZNO	2.042-2.052	2.009	2.002	0.70-0.56
LAYZEOL.	2.044	2.009	2.007	0.67
CAYZEOL.	2.046	2.011	2.002	0.64

OUR G-VALUES:

2.04      2.01      2.004

# M O D E L S

	S <sub>1</sub>	S <sub>2</sub>	S <sub>3</sub>	L <sub>1</sub>
1-DEFECT	2.0004	?	2.1143	
O <sub>2</sub> <sup>-</sup> -IN NAYZEOLITE	2.002	2.007	2.113	0.25
NAO <sub>2</sub> (BULK)	2.000	2.000	2.175	0.16
<hr/>				
2-DEFECT	2.0027	?	2.0457	
O <sub>2</sub> <sup>-</sup> -IN CAYZEOLITE	2.002	2.011	2.046	0.64
ZNO	2.002	2.008	2.049	0.60
<hr/>				
3-DEFECT	2.0078	?	2.0335	
O <sub>2</sub> <sup>-</sup> -IN CEO <sub>2</sub> /AL <sub>2</sub> O <sub>2</sub>	2.011	2.014	2.030	1.00
GAAS	2.007	2.007	2.036	0.82
AL <sub>2</sub> O <sub>3</sub>	2.006	2.006	2.038	0.78

1970-1971  
 1972-1973  
 1974-1975  
 1976-1977  
 1978-1979  
 1980-1981  
 1982-1983  
 1984-1985  
 1986-1987  
 1988-1989  
 1990-1991  
 1992-1993  
 1994-1995  
 1996-1997  
 1998-1999  
 2000-2001  
 2002-2003  
 2004-2005  
 2006-2007  
 2008-2009  
 2010-2011  
 2012-2013  
 2014-2015  
 2016-2017  
 2018-2019  
 2020-2021  
 2022-2023  
 2024-2025

APPENDIX II. j.

Fusion Temperature Effects on the Annealing Behavior of  $\text{GeO}_2$  Glasses  
as Measured by the DC Resistivity

R. H. Magruder, D. L. Kinser, and R. A. Weeks

Vanderbilt University

The effect of annealing on the electrical resistance of glasses has been known since the work of Fousserau<sup>(1)</sup>. While most of the earlier works centered around alkali motion in commercial glasses with varying compositions, some were directed at the change in resistivity due to annealing. The earlier studies of Littleton and Wetmore<sup>(2)</sup> and Littleton<sup>(3)</sup> were concerned with commercial glasses used in lamp seals. In the past two decades, substantial research has been directed toward understanding the resistivity of simple glass systems with high alkali content. For the most part, these studies were on as-cooled glasses. A summary of this research is given by Doremus<sup>(4)</sup>, Morey<sup>(5)</sup>, and Owen<sup>(6)</sup>.

A few studies have been directed toward thermal history effects. Ritland<sup>(7)</sup> studied annealing treatment effects on a borosilicate crown glass. He reported differences in resistivity with quench rate from the annealing temperature. Boesch and Moynihan<sup>(8)</sup> reported the effects of thermal history on the conductivity of alkali silicate glasses. In agreement with Ritland, they observed changes in conductivity with the cooling rate. They concluded that, within experimental error, the activation energy was constant and the change in conductivity was caused by changes in the pre-exponential term in the Arrhenius equation for conductivity.

Relatively little research has been reported on high purity simple glass systems. Owen and Douglas<sup>(9)</sup> found a good correlation between resistivity and sodium content. Doremus<sup>(10)</sup> examined the electrical conductivity of high purity fused silica with traces of sodium, lithium and potassium. He concluded that the activation energy for conduction was roughly equal for all three alkalis. Douglas and Isard<sup>(11)</sup> reported that the time required for fused silica to reach an equilibrium density was a function of the temperature from which the glass was quenched and the temperature at which the glass was equilibrated.

Primak<sup>(12)</sup> attributed the results of Douglas and Isard to thermal compaction. Thermal compaction phenomenon can occur according to Primak by annealing and is described as a change in the void volume resulting in a collapse of the SiO<sub>4</sub>- tetrahedra into the void space of the network. Furthermore, Primak points out that this thermal compaction effect can also be annealed such that a statistically equivalent original state but not identical state can be reached. "Thermal compaction begins at a temperature where static rigidity is falling but dynamic rigidity is still rising and indicates that bond change and reconstitution are active."<sup>(12)</sup>

Papodopoulos et al<sup>(13)</sup> studied the resistivity of vitreous silica containing Na<sup>+</sup> ions and reported a minimum in resistivity with the length of heat treatment. They suggested a link between the time required for stabilization of the glass and the behavior of the resistivity.

Bohm<sup>(14)</sup> examined the dc conductivity of low sodium germania glasses and concluded that the conduction mechanism is a thermally activated motion of sodium (Arrhenius behavior) with an activation energy of 1.0 eV. Cordara et al<sup>(15)</sup> confirmed that result and, additionally, reported that the conductivity is also a function of OH content.

We reported results showing the effects of fusion conditions on the DC resistivity of several high purity  $\text{GeO}_2$  glasses<sup>(16)</sup>. In agreement with Bohm<sup>(14)</sup> and Cordara et al<sup>(15)</sup>, we found that the temperature dependence of the conductivity obeyed the Arrhenius equation with an activation energy of 1.0 eV. It was also observed that the resistivity was a function of the temperature of the liquid,  $T_g$ , from which the glass was cooled. We suggested that these changes in resistivity were due to structural changes in the potential wells of the interstitial sites through which the  $\text{Na}^+$  ion moved.

These structural changes bring about a change in the anharmonic term for the vibrational energy levels and as a consequence, a change in the entropy of activation. These changes in structure were then manifested in changes in resistivity of the glasses.

The  $T_g$  is only one parameter among several that can affect the resistivity of glasses. As indicated above, thermal treatments at temperatures below the glass transition temperature,  $T_g$ , also affect the resistivity. In the following, we describe the effects of annealing treatments on glasses used in previously described

experiments<sup>(16)</sup>.

#### EXPERIMENTAL PROCEDURE

GeO<sub>2</sub> glasses were prepared from material and by techniques previously described<sup>(16)</sup>. Melted samples were held at various T<sub>g</sub>'s for the times listed in Table I and then cooled to ~25° at an average rate of 5°C sec from T<sub>g</sub> to 400°C. Gold electrodes were vapor deposited on the samples in a guard ring configuration which were then annealed for 1 hr at 300°C. The DC resistance of the samples was measured in a chamber which permitted measurements in a vacuum of approximately 30 microns of Hg over the temperature range. A computer controlled system discussed in an earlier paper<sup>(16)</sup> was used to control temperature and measure the DC current.

All samples were first measured in the as-quenched state. The gold electrodes were then removed and the samples were annealed at 420°C for 1, 2, 7, and 46 hours and quenched at the same rate. This annealing treatment was conducted 15°C below the measured Littleton softening point of 435°C. After each anneal the electrodes were replaced in the manner described above, and the resistivity measured. Analysis for trace elements are given in Table I.

## RESULTS

In agreement with other work<sup>(14,15)</sup>, the charge carrier in these glasses is the Na<sup>+</sup> ion. The Na<sup>+</sup> mobilities were calculated from the equation:

$$\mu (\text{Na}^+) = 1/nep \quad (1)$$

where  $n$  is the Na concentration as determined by neutron activation analysis,  $e$  the charge of the carrier, and  $p$  the resistivity which was determined from

$$p = p_0 \exp -\Delta S/k \exp \Delta H/kT \quad (2)$$

using the experimental data. A least square fit was used to determine  $\Delta H$  and  $p_0$  from which  $p$  was then calculated.

Figure 1 shows the effect of annealing at 420°C on the Na<sup>+</sup> mobility (or dc resistance) measured at 144°C for various  $T_g$ 's. All glasses show a decrease in mobility with increasing annealing time. The glasses with  $T_g$  of 1450°C and 1350°C show a much larger initial drop in mobility with the first anneal than do the glasses cooled from 1650°C and 1550°C. All glasses, within error limits, appear to approach a stabilized mobility value for the longest anneals. The 1550°C  $T_g$  glasses show an anomalous behavior for the 3 hour anneal.

Figure 2 shows the change in the mobility as a function of  $T_g$  for

the as quenched and the 56 h annealing time. While the mobility drops, the general relation between the mobilities observed for the as quenched glasses as a function of  $T_g$  remains the same. The 1450  $T_g$  glass shows the highest mobility for the as-quenched state and at 56 h annealing time examined.

The activation enthalpy as determined by a least squares fit for the Arrhenius Equation 2. The  $\Delta H$  increases slightly for all the glasses with annealing. The  $\Delta H$  ranged from  $1.01 \pm 0.01$  ev to  $1.03 \pm 0.01$  for all glasses.

#### DISCUSSION

In an earlier paper<sup>(16)</sup>, the mobility was given by

$$\mu = e^2 d^2 / 6h \exp \Delta S / k \exp -\Delta H / kT$$

where  $e$  is the charge of the carrier,  $d$  the jump distance,  $k$  Boltzmann's constant,  $T$  the temperature and  $\Delta S$  and  $\Delta H$  are the entropy and the enthalpy of activation, respectively. The variables affecting the mobility were shown to be  $\Delta S$  and  $\Delta H$ .

We demonstrated that  $\Delta S$  could be related to the anharmonic term in an expansion of the potential of the interstitial site and explained the  $T_g$  dependence of the mobility as a consequence of changes of the anharmonic terms in the vibrational potential energy structure of the average interstitial sites through which the  $\text{Na}^+$  moves. As the activation enthalpy remains constant in the

as-quenched glasses, we concluded that their short range order was similar; however, the melt history controlled the shape of the well as seen in Figure 3 and, hence, the vibration energy states through the anharmonic terms. The potential energy of the site will be determined by the ions surrounding the interstitial site. Slight differences in the configuration of these ions would lead to changes in the well shape. These changes can occur without change of the energy required for the  $\text{Na}^+$  ion to push through the doorway to its next interstitial site. The behavior of the various glasses with annealing time supports our earlier conclusion that the structures are different. We anticipate the effects of annealing to be influenced by the differing initial structures.

In conventional glass theory, the structure as measured by volume would be expected to be the same for the various  $T_g$  for the same cooling rate. This theory is based on the assumption that the melt liquid remains at metastable equilibrium down to  $T_g$  during cooling. Only upon changing the cooling rate would one expect to introduce differences in structure. These differences would be expected to result in changes in the dc resistivity as shown by Boesch and Moynihan<sup>(8)</sup> and Ritland<sup>(7)</sup>. Changing the volume of the glass would result in changes in the potential well structure and hence changes in the energy level structure which we have demonstrated can change the dc resistivity of the glass<sup>(16)</sup>.

With annealing, one would expect that the volume of the glass would approach some equilibrium value characteristic of the

annealing temperature. It might be expected that, as the glass approached this equilibrium volume, the  $\text{Na}^+$  ion mobility through the structure would approach some equilibrium value characteristic of the average well structure.

As seen in Figure 1, this is not the case for annealing times up to 56 hours. Instead, while the mobility of the  $\text{Na}^+$  ions decrease in all glasses, a "memory" of their starting structure is retained and the mobility decreases in a proportional fashion. Figure 2 shows the general shape of the as-quenched curve is maintained with the  $T_g$  of  $1450^\circ\text{C}$  glasses showing the highest mobility for the longest annealing time.

We suggest these changes in mobility are due to a thermal compaction process of the same nature as suggested by Primak for fused silica. Thermal compaction would result in the oxygen ions moving into the interstitial positions changing the distribution of bond angles. Upon quenching from the annealing temperature, these changes are quenched into the structure. The enthalpy of activation  $\Delta H$  values increase only slightly as discussed earlier suggesting the basic short range order of the glass remains constant but the energy required to push apart the Ge-O bond to allow the  $\text{Na}^+$  ion to move has increased slightly. As seen in Table II, the  $\Delta S$  values, the entropy of activation, suggest changes in the energy level structure which would be explained by changes in the bond angle distribution from thermal compaction. The bond angle changes would be expected to affect the anharmonic terms. The increases in  $\Delta H$  are compatible with the redistribution of bond

angles in that they can increase the energy required to push apart the Ge-O bond.

For glasses with differing  $T_g$ 's the differences in reaching equilibrium indicate that stabilization processes in these glasses are different. These differences in stabilization may be in part due to the defect concentration in the glasses. Primak<sup>(12)</sup> has suggested that the E' center may play a role in the compaction of fused silicas. Obviously, more than one defect may play a role in the stabilization processes. Kordas et al<sup>(17)</sup> have reported the E' center concentration in the as-quenched glasses shows a non-Arrhenius behavior such that the  $T_g$  of 1450°C shows a minimum in E' center concentration. Jackson et al<sup>(18)</sup> have reported the defect center concentration associated with 2450 Å absorption peak to be largest in the  $T_g$  of 1650°C and lowest in the  $T_g$  of 1350°C.

The point is that the defect structure of the glass may control the stabilization processes allowing for points of motion for the network to relieve stresses induced from thermal compaction.

It is noteworthy that the maximum time of annealing is insufficient to allow for oxygen diffusion to penetrate sufficiently into the sample to change the redox state of the glass except of a very small surface layer. Using the diffusion coefficient determined by Garina Carnina<sup>(19)</sup>, we calculate the diffusion distance at 420°C to be less than 0.01 mm for 56 hours.

We suggest that the defect structures of the glass is not only important to the electronic structure of the glass but to the overall structure the glass achieves upon cooling from the equilibrated liquid. This is in sharp contrast to crystalline solids where bond angles and bond lengths are predetermined by the crystal structure. For glasses, these bond angles and distances have a distribution of values. This distribution may change slightly with differing defect concentration thereby changing the average interstitial well.

## CONCLUSIONS

Despite relatively long times at a temperature slightly below the softening temperature,  $\text{GeO}_2$  glasses retain a structure that is related to  $T_g$ . The correlation of intrinsic point defects with  $T_g$  and the effects of  $T_g$  on mobility of the Na ions may indicate a causative relation between the two phenomena. The defects may influence the depth of the average well in addition to its shape.

## ACKNOWLEDGEMENTS

The authors wish to gratefully acknowledge the support of the U.S. Army Research Office/Durham under contract #DAAG-29-81-K-0118.

## REFERENCES

1. G. Fousserau, "Influence of Tempering on the Electrical Resistance of Glass," *Compt. Rend.* 96, 785 (1883).
2. J. T. Littleton and W. L. Wetmore, "The Electrical Conductivity of Glass in the Annealing Zone as a Function of Time and Temperature," *Journal of American Ceramic Society*, 19, 243-245 (1936).
3. J. T. Littleton, "Critical Temperature in Silicate Glasses," *Ind. Eng. Chem*, 25, 748-755 (1933).
4. R. H. Doremus, "Ionic Transport in Amorphous Oxides," *Journal of Electrochemical Society*, 115, 181-186 (1968).
5. G. W. Morey, *The Properties of Glass* (Am. Chem. Soc. Monograph), Reinhold, NY (1954).
6. A.E. Owen, *Progress in Ceramic Science*, Vol. 3, J.E. Burke, Ed., Macmillan Company, NY (1969).
7. H. N. Ritland, "Limitation of the Fictive Temperature Concept," *Journal of American Ceramic Society*, 39, 403-407 (1956).
8. L. P. Boesch and C. T. Moynihan, "Effect of Thermal History on Conductivity and Electrical Relaxation in Alkali Silicate Glasses" *Journal of Non-Crystalline Solids*, 17, 44-60 (1975).

9. A. E. Owen and R. W. Douglas, "(title to be furnished)", Journal of Society of Glass Technology, 43, 159 (1959).
10. R. H. Doremus, "Electrical Conductivity and Electrolysis of Alkali Ion in Silica Glass," Physics and Chemistry of Glasses, 10, 28-33 (1969).
11. R. W. Douglas and J. O. Isard, "Density Changes in Fused Silica," Journal of Society of Glass Technology, 35, 206 (1951).
12. W. Primak, The Compacted States of Vitreous Silica, Gordon and Breach, New York (1975).
13. K. Papadopoulos, D. M. Mattox, and T. T. Meek, "The Effect of Heat Treatment on the Na<sup>+</sup> Resistivity in Vitreous Silica," Journal of American Ceramic Society, 66, 120-122 (1983).
14. H. Bohm, "Electrical Conductivity of Vitreous GeO<sub>2</sub>", Journal of Applied Physics, 43, 1103-1107 (1972).
15. J. F. Cordaro, J. E. Kelly, III, and M. Tomozawa, "the Effects of Impurity OH on the Transport Properties of High Purity GeO<sub>2</sub> Glasses," Physics and Chemistry of Glasses, 22, pg. 90 (1981).
16. R.H. Magruder, III, D. L. Kinser, R. A. Weeks, and J. M. Jackson, accepted for publication in Journal of Applied Physics.
17. G. Kordas, R. A. Weeks, and D. L. Kinser, "The Influence of Fusion Temperature on the Defect Center Concentration of GeO<sub>2</sub> Glass,"

Journal of Applied Physics, 54, 5394-5397 (1983).

18. J. M. Jackson, M. E. Wells, D. L. Kinser, and R. A. Weeks, to be submitted for publication, Journal of American Ceramic Society.
19. V. Garino-Canina, "Diffusion of Oxygen in Glassy  $\text{GeO}_2$ , Compter. Rend. de la Academy of Sciences, 24, 1319-1326, (1959).

## FIGURE CAPTIONS

Figure 1. - Na mobility versus log time of annealed at  $435^{\circ}\text{C}$  as a function of  $T_g$ .

Figure 2. - Na mobility versus  $T_g$  for the as-quenched and 56 hour annealed samples.

Figure 3. - Potential Energy  $U(r)$  versus  $r$  distance from equilibrium position for two curves of anharmonic oscillator with different  $\chi_e$ .

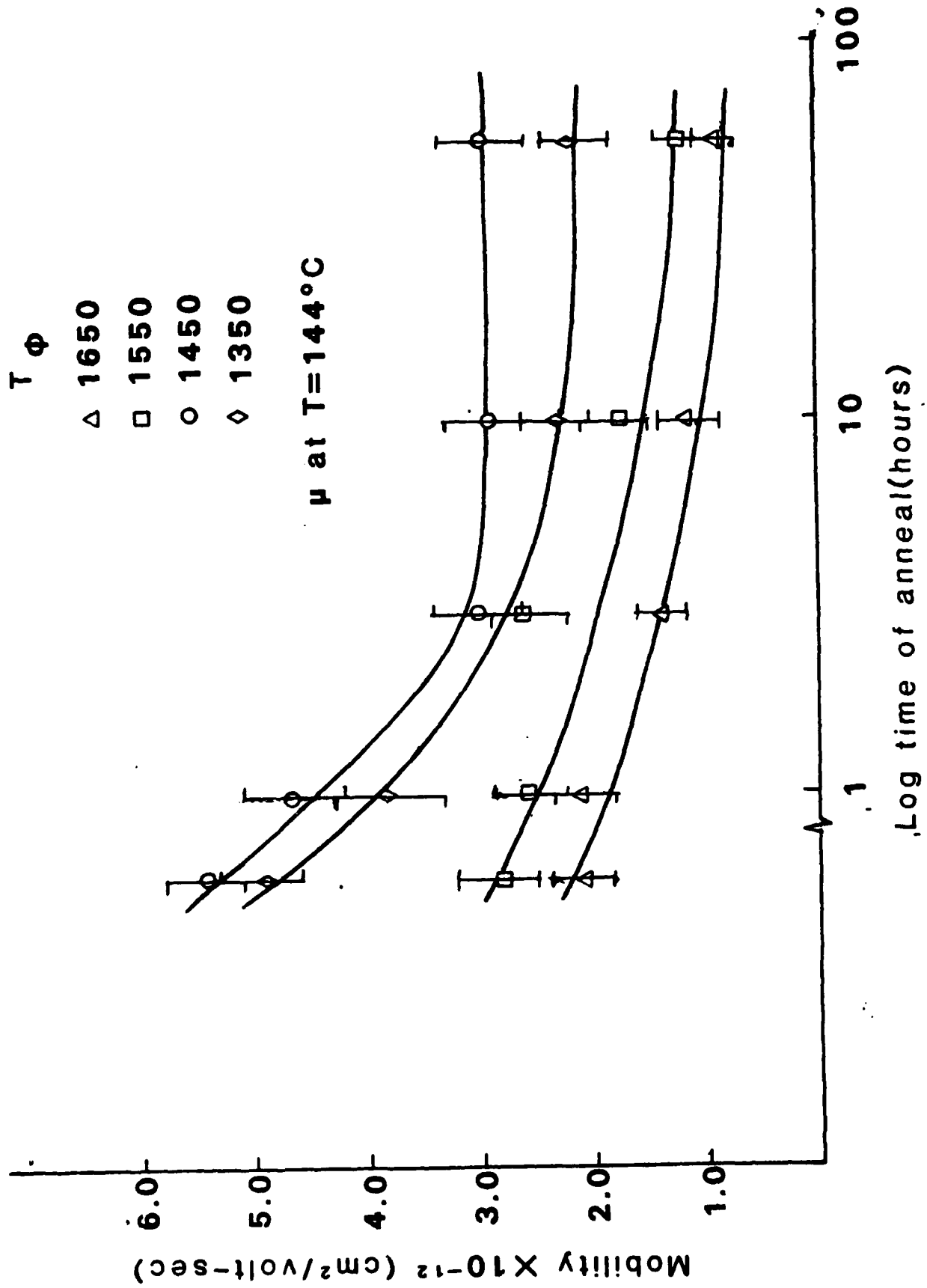


Figure 1. Na mobility vs. log of time annealed at  $435^{\circ}\text{C}$  as a function of  $T\phi$ .

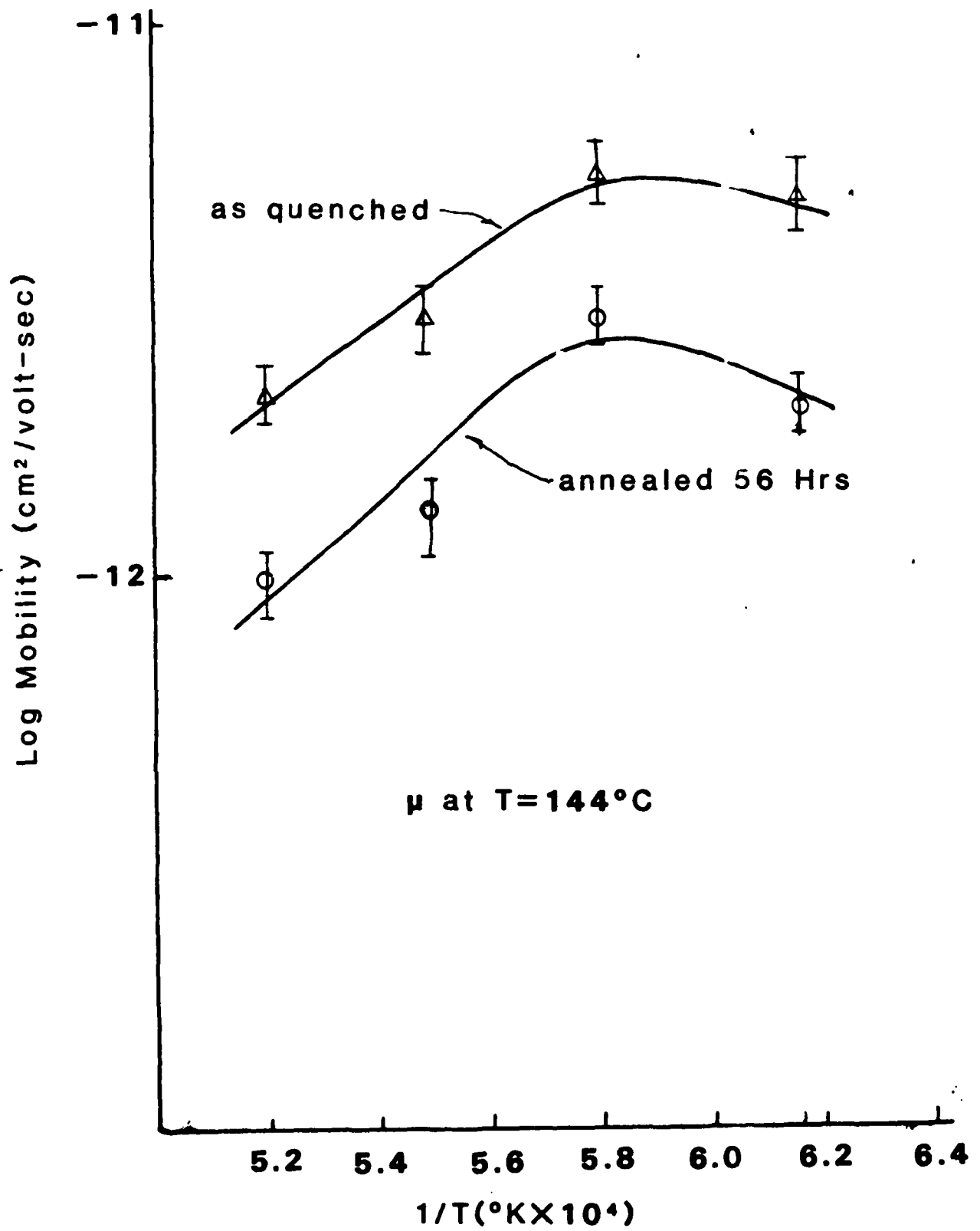


Fig. 2. Na mobility vs.  $T_{\phi}$  for the as-quenched and 56 hours annealed samples.

Figure 3. Potential Energy  $U(r)$  vs.  $r$  distance from equilibrium position for two curves of anharmonic oscillator with different  $\chi_e$ .

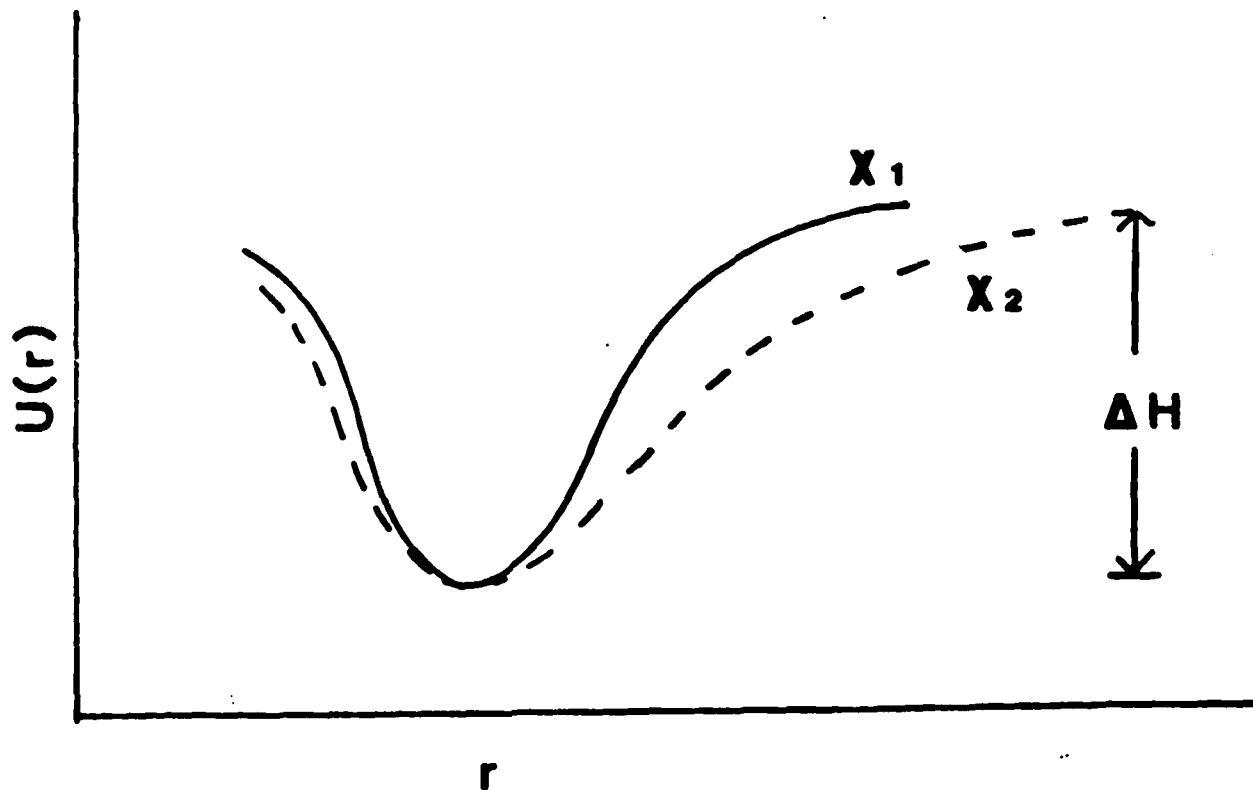


TABLE I

Trace Elements in  $\text{GeO}_2$  Glasses from Neutron Activation Analysis  
and Infrared Analysis in ppm

	Melt Temperature, °C 1650	1550	1450	1350
Melt Time (hrs)	3	3	110	185
Na	12.2	8.7	14.9	13.9
Cl	$1.21 \times 10^3$	$1.60 \times 10^3$	$1.27 \times 10^3$	1.47
Al	4.8	*	4.4	7.9
Li	*	*	*	*
K	*	*	*	*
OH	181	238	206	190

\*less than detectable limit

TABLE II

$$\Delta S \text{ (ev/Bk)} \times 10^{-2*}$$

## Summary of Activation Entropy for Annealed Glasses

$T_g$	1650°C	1550°C	1450°C	1350°C
as quenched	1.2149*	1.2164	1.2191	1.2176
1 hr@420°C	1.2226	1.2232	1.2176	1.2203
3 hr@420	1.2168	1.2231	1.2204	--
10 hrs@420	1.2156	1.2194	1.2202	1.2173
56 hrs@420	1.2085	1.2122	1.2202	1.2174

\*The error as determined by differences between melts is  $\pm 0.0006$ .

APPENDIX II.k.

THE EFFECTS OF THERMAL HISTORY AND IRRADIATION ON THE DC  
CONDUCTIVITY OF HIGH PURITY GeO<sub>2</sub> GLASSES

By

Robert H. Magruder, III

Dissertation

Submitted to the Faculty of the  
Graduate School of Vanderbilt University  
in partial fulfillment of the requirements  
for the degree of

DOCTOR OF PHILOSOPHY

in

Electrical Engineering

December, 1984

Nashville, Tennessee

Approved:

Date:

---

---

---

---

---

---

---

---

---

---

---

---

---

---

## ACKNOWLEDGEMENTS

I would like to thank my adviser, Dr. Donald L. Kinser, for his friendship, guidance and encouragement. I would like to thank the members of my Ph.D. committee, Dr. Ensign Johnson, Dr. Charles Stephenson, Dr. Arthur Brodersen, Dr. Robert Weeks, and Dr. Ernest Jones, for their help and encouragement during my graduate work. All have made significant contributions to this work. I would like to thank John Jackson for his friendship and help with equipment and computer programming. I would like to thank Jim Hightower and Bob McReynolds for their friendship and technical assistance. I would like to thank Mark Wells for his friendship. Special thanks are due to Lorene Morgan for her patience with typing this thesis.

Financial support of Vanderbilt University and the U.S. Army Research Office/Durham Contract # DAAG29-81-k-0118 is gratefully acknowledged.

## TABLE OF CONTENTS

	Page
ACKNOWLEDGEMENTS. . . . .	ii
LIST OF TABLES . . . . .	iv
LIST OF FIGURES . . . . .	v
 Chapter	
I. INTRODUCTION . . . . .	1
Literature Review. . . . .	3
Ionic Conduction Model . . . . .	8
II. THEORY OF IONIC CONDUCTION . . . . .	16
III. $T\phi$ EFFECTS ON THE DC CONDUCTIVITY. . . . .	25
Experimental Procedure . . . . .	25
Results. . . . .	28
Discussion . . . . .	30
IV. ANNEALING EFFECTS ON THE DC CONDUCTIVITY. . . . .	42
Experimental Procedures. . . . .	42
Results. . . . .	42
Discussion . . . . .	44
V. IRRADIATION EFFECTS ON THE DC CONDUCTIVITY. . . . .	52
Experimental . . . . .	52
Results. . . . .	52
Discussion . . . . .	55
VI. CONCLUSIONS . . . . .	66
VII. RECOMMENDATIONS FOR FUTURE RESEARCH . . . . .	67
REFERENCES. . . . .	68

## LIST OF TABLES

Table	Page
1. Trace Elements in GeO <sub>2</sub> Glasses from Neutron Activation Analysis and Infrared Analysis in ppm. . . . .	26
2. Summary of Sodium Concentration and Pre-Exponential Factors for Two Glasses Fused at 1650°C for Three Hours in Air . . . . .	31
3. Summary of Activation Entropy and Enthalpy for Series of Glasses . . . . .	35
4. Summary of Activation Enthalpies for Annealed Glasses $\Delta H(\text{ev})$ . . . . .	46
5. Summary of Activation Entropies for Annealed Glasses $\Delta S$ in $\text{ev}/^\circ\text{k} \times 10^{-2}$ . . . . .	49
6. Summary of Dose Levels (Rads) for Samples with Various $T\phi$ 's Co <sup>60</sup> . . . . .	53
7. Summary of Activation Enthalpy, $\Delta H$ , Values for the Irradiated Glasses (Dose Levels Correspond to Table 6) . . .	56

## LIST OF FIGURES

Figure	Page
1. Energy Plot as a Function of Position for a Glass. . . . .	10
2. Schematic Representation of Diffusion in a Potential Gradient. $\Delta H$ is the Enthalpy of Activation and $d$ is the Distance Between Equilibrium Positions . . . . .	18
3. Temperature Dependence of Resistivity, $\rho$ , for a $T\phi = 1650^\circ\text{C}$ and Varying Na Concentration . . . . .	29
4. Temperature Dependence of Mobility for a Series of Glasses with Varying $T\phi$ . . . . .	32
5. Mobility versus $T\phi$ for a Series of Glasses for Which $T\phi$ Ranged from $1690^\circ\text{C}$ to $1350^\circ\text{C}$ . . . . .	33
6. Potential Energy Versus Distance ( $r$ ) from Equilibrium --- Curve Represents Simple Harmonic Oscillator — Curve Represents Anharmonic Oscillator . . . . .	37
7. Potential Energy $U(r)$ versus $r$ Distance from Equilibrium Position for Two Curves of Anharmonic Oscillator With Difference $\chi_e$ . . . . .	39
8. Mobility Versus Log Time of Annealing as a Function of $T\phi$ . . . . .	43
9. Mobility Versus $T\phi$ for the As-Quenched and 56 Hour Annealed Samples . . . . .	45
10. Resistivity of the $T\phi = 1550^\circ\text{C}$ with Varying Irradiation Doses as a Function of Reciprocal Temperatures . . . . .	54
11. Mobility for a Series of Glasses with Varying $T\phi$ as a Function of Dose (rads). . . . .	57
12. Resistivity of the $T\phi = 1550^\circ\text{C}$ Sample Before Irradiation and the Second Measurement After the Longest Dose as a Function of Reciprocal Temperature . . . . .	58
13. Schematic Representation of Increasing Enthalpy of Activation, $\Delta H$ , on Well Shape. . . . .	60
14. Model of $E'$ Center Formation and Subsequent Relaxation of Lattice After Feigl et al (75). . . . .	62

## CHAPTER I

### INTRODUCTION

The defect structure of glass, and its effects on the physical properties of the glass, has become an area of intensive research in the last decade (1-3). The impetus for this activity stems from two major areas. The first is the use of high purity glasses in fiber optics. With the move toward higher data rates and the need for lower loss fibers, the intrinsic nature of the glasses used has become of central importance. With the ability to manufacture ultra pure glass fibers the intrinsic losses due to the defect structure have become the center of attention to achieve control over this structure to allow preparation of glasses that give absorption losses at the theoretical limits set by Rayleigh scattering. These same intrinsic defects have been related to radiation damage (4) and subsequent loss in optical transparency (4). The understanding of the kinetics of these radiation induced losses and processes of manufacture by which these losses can be controlled are important in developing fibers for use in harsh environments (5).

In addition to use in fiber construction the knowledge of glass structure is important for the development of glass material for use in space where it would be exposed to several types of ionizing irradiation.

The second major driving force has been in electronics. The use of  $\text{SiO}_2$  as an insulating material in electronic devices such as MOS, CMOS,

NMOS and other devices has necessitated the understanding of the physical properties of  $\text{SiO}_2$  for optimum device performance (6). Ionizing irradiation affects device performance in integrated circuits and requires an understanding of how defects arise and how they can be controlled in the glass structure. These defects can lead to device failure (7). Aitken (8) and Sah (9) provide reviews of radiation effects in MOS type devices.

The idea of defects in a glass system must be viewed from the standpoint of a break in the continuous random network. Concepts such as the Bravais lattice and Bloch electrons, which depend on the ordered recurrence of structural units, cannot be used to describe glass systems. A defect in crystalline materials is a break in the perfect translational symmetry of the crystalline structure. This operational description has no meaning in a glass system because it has no translational symmetry. The concepts of vacancies and interstitials, while used to describe glassy systems, must be used with caution because the glass structure is only statistically defined.

It is in this aperiodic structure in which an alkali ion must diffuse through under the influence of an applied electric field. By observing how the ion motion changes with changes in the glass structure one may be able to infer certain properties of the glass itself and what parameters can affect these properties. The philosophy envisioned here is to use the alkali ion motion to develop inferences about the structure of a glass system. The subject of this work, then, is to study the effects of thermal history of a glass on its defect structure.

High purity glasses were required to separate intrinsic effects, i.e. effects due solely to the glass, from the extrinsic effects where

impurities were of such concentration as to make observable changes in the glass structure.  $\text{GeO}_2$  glasses were chosen because of the ability to control the parameters of preparation of the glass.  $\text{SiO}_2$  melts at a temperature of  $1760^\circ\text{C}$  making changes in temperature of equilibration of the melt liquid difficult. However  $\text{GeO}_2$  melts at  $1131^\circ\text{C}$ . This lower melting temperature allows much greater control over the processing parameters. The great bulk of research on glasses to date has been on fused  $\text{SiO}_2$ . Because of the structural similarity (10) between  $\text{GeO}_2$  and  $\text{SiO}_2$  it is reasonable to assume that inferences made on how to control various physical characteristics in  $\text{GeO}_2$  will be transferable to methods for control in  $\text{SiO}_2$ . The ultimate goal is to produce glasses that perform their intended function more near the ideal.

#### Literature Review

The model used to characterize glassy  $\text{SiO}_2$  and  $\text{GeO}_2$  is essentially the structural model developed by Zacharisan (11) and extended by Warren (12) using X-ray diffraction techniques. A summary of their studies is given by Wong and Angell (10). The structure consists of  $\text{SiO}_4$  or  $\text{GeO}_4$  tetrahedra. The short range order, i.e. the Ge-O bond angles and lengths, are found to be almost identical to those for quartz and hexagonal  $\text{GeO}_2$  (10). The random nature of the glassy state is introduced by a distribution of the bond angles found for the Si-O-Si or Ge-O-Ge linkage. The bond angle distribution shows a maximum at  $144^\circ$  for  $\text{SiO}_2$  (10). The distribution of angles destroys the long range order while maintaining the same short-range structural units as the crystalline counterpart.

The influence of fusion conditions upon the physical properties of  $\text{GeO}_2$  glasses has been a subject of continuing interest. Garina-Canina (13) has examined the effect of fusion conditions and subsequent thermal treatments on an optical absorption band at 245 nm in  $\text{GeO}_2$  glasses. He observed that the intensity of this band increased with fusion temperature and suggested that it was due to an oxygen vacancy. Cohn and Smith (14) examined the effect of fusion temperature as well as ultraviolet bleaching upon this peak and corroborated the results of Garina-Canino. Vergano and Uhlmann (15) reported on the crystallization kinetics of  $\text{GeO}_2$  glasses and concluded that reduced glasses, i.e., higher fusion temperatures, have higher crystallization rates. Purcell and Weeks (16) have described some of the intrinsic paramagnetic defects in  $\text{GeO}_2$  crystals and glasses and characterized their concentrations as a function of thermal history. They concluded that one of the defects observed is due to singly-charged oxygen vacancies. Bohm (17) measured the dc conductivity of low sodium germania glasses and concluded that the conduction mechanism is a thermally activated motion of sodium, with an Arrhenius behavior and activation energy of 1.0 eV. Cordaro et al (18) have confirmed that result and, additionally, reported that the influence of increasing OH content is to decrease the conductivity.

There are numerous reports in the literature which can be interpreted to argue that the structure of a glass is dependent upon the structure of the melt from which it was cooled. The local environment of the sodium ion does not totally relax to a structure characteristic of a glass transition temperature but, instead, retains a structure determined by fusion temperature. This argument is, of course, contrary

to the conventional view that the structure of a glass is in metastable equilibrium at temperatures above the glass transition temperature. This is supported by the work of Galeener et al (19) who reported Raman measurements of  $\text{GeO}_2$  glasses fused at different temperatures but quenched through the glass transition regime at the same rate. They concluded that the Raman results indicate differences in structure among glasses quenched in such a fashion. Bohm (20,21) reported differences in photoconductivity and thermoluminescence in  $\text{GeO}_2$  glasses fused at different temperatures. These observations can be interpreted as indicating that the electronic structure associated with these processes is influenced by the melting temperature and that the electronic structure differences necessarily require that atomic structural differences also exist.

Kordas et al (22) measured the electron paramagnetic resonance spectra of a series of  $\text{GeO}_2$  glasses melted at different temperatures and quenched at a constant rate. Several paramagnetic defects are reported whose functional dependence upon fusion temperature are not Arrhenius. They suggested that this result indicates that the defect concentrations are not controlled by oxidation/reduction equilibria exclusively but are also influenced by structural differences in the liquid which are a function of fusion temperature.

Primak (23) reviewed the Douglas and Isard (24) density measurements upon  $\text{SiO}_2$  glasses with differing glass transition temperatures and concluded that remnants of the high temperature structure are responsible for the observed density differences. Douglas and Isard (24) stated that "the high temperature phases are readily quenched," and Primak

added the observation that clearly these configurational differences are quite stable at lower temperatures.

Hetherington et al (25) reported a survey of the viscosity of  $\text{SiO}_2$  in which they defined the term equilibrium viscosity. The viscosity of a glass held for a long period of time at a particular temperature is said to be the equilibrium value, but after a change in temperature the equilibrium viscosity is reached only after times of from 2 to 50,000 hours, depending upon the new temperature. These equilibration times affect the time dependent structural rearrangement when the "melt temperature" is changed; and, thus, the structure characteristic of a given melting temperature can be expected to persist during cooling to room temperature.

The further importance of structure for the physical properties of fused silica and other oxide glasses is evidenced by atomic structural variation arguments. These arguments were advanced by several researchers of the Si-O-Si bond to explain some of the anomalous properties of oxide glasses such as acoustic and dielectric losses, temperature dependences of compressibility and negative thermal expansion below room temperature. Vukceovich (26) proposed a model based on two preferred angles of the Si-O-Si bond angles to explain the above mentioned properties. Anderson and Bommel (27) proposed a model based on two equilibrium positions of the bridging oxygen that are perpendicular to the Si-O-Si bond. Strakner (28) suggested a model of two equilibrium positions that lie parallel to the Si-O-Si bond and represent an elongation of the Si-O-Si bond.

The effect of ionizing radiation on the physical properties of glass has been known since the observation of the cracking of glass

vials containing radium by Mme. Curie (29). Reviews of the more recent work are given by Primak (30), Bichmay (31), Friebele and Griscom (4) and Kreidl (32).

Shelby (33) reported the densification of borosilicate glasses with gamma irradiation. He noted the compositional dependence caused a difference of a factor of 30 in the change of densification of these glasses.

Primak (30) in his review of the compaction of vitreous silica with ionizing radiation attributes this compaction to structural changes. He suggests that ionizing radiation causes fragmentation of the network resulting in "slight twisting of network segments relative to each other ...", and that "... the rate controlling factor for ionization compaction was the process of locking it in."

Numerous studies (4,7,16,22) have documented the formation of stable defects in fused silica and glassy  $\text{GeO}_2$ . Weeks and Purcell (16) studied the radiation induced paramagnetic states in  $\text{GeO}_2$  glasses. They suggested that the paramagnetic state induced is due to a single charged oxygen vacancy. Kordas et al (22) found  $\gamma$  irradiation effects on the paramagnetic states of high purity  $\text{GeO}_2$  glasses to depend in a non-Arrhenius fashion on the temperature at which the melt liquid was equilibrated,  $T_\phi$ , before being cooled.

Fontanella et al (34) reported increases in low temperature dielectric losses in high purity fused silica with  $\gamma$  irradiation. They attributed these losses to structural changes with irradiation.

Cullen and Rexford (35) found decreases in resistivity of silicate glasses with gamma irradiation. Wahim et al (36) reported the resistivity of iron phosphate glasses to decrease with gamma irradiation. They

also found that the induced effects decayed with time at room temperature. Mike et al (37) examined the effects of electron irradiation on the dc resistivity of sodium silicate glasses. They found no statistically significant irreversible effects. Magruder et al (38) reported effects on  $\gamma$  irradiation on the dc properties of high purity  $\text{GeO}_2$  glasses. They found, "... the dc resistivity to increase with irradiation in a stable and reproducible fashion." They attribute this effect to the interaction of radiation induced defects on the potential well through which the sodium ion moves.

While no model has been shown to describe all the experimental phenomena, the important aspect of the above discussion is the importance of the structure of oxide glasses on the physical properties exhibited. From the foregoing discussion it would be plausible to expect the structure of glass to affect the dc conduction mechanism in the glass, and, conversely, a study on the dc behavior for a glass would be expected to give insight into the structure of the glass.

#### Ionic Conduction Model

Historically the study of the dc electrical properties of oxide glasses goes back to the late 1880's. Fousereau (39) studied the effect of heat treatment on the electrical resistivity of glasses. At the turn of the century Gray and Dobbie (40) studied the electrical resistivity of various glasses. The charge carriers have been considered to be the alkali ion. Warburg (41) in 1884 demonstrated that the charge carrier in Thuringian glass was the Na ion. Kraus and Darby (42) using silver ions to replace sodium ions, confirmed earlier work that the Na

ion was the charge carrier. Owen and Douglas (43) showed that Na was the charge carrier for fused silica when the Na concentration was as small as .04 ppm by weight. As Owen (44) comments, "It is now generally accepted that in glasses containing appreciable amounts of alkali oxide (especially sodium) the current is carried virtually completely by alkali ion. Even in fused silica where there are only trace impurities of the alkali metals present it is believed that the mechanism is unchanged ...."

While it has been demonstrated that the Na ions are the current carriers in these oxide glasses, the actual mechanisms by which they move through the glass structure are not well established. Obviously the structure of the glass will play a dominant role in the possible ways their motion can occur. The concentration of the Na ions will also play a role through electrostatic interaction with other alkali ions.

There is no universally accepted model for ionic conduction in glasses. The development of a model is an on-going research problem and indirectly is a subject of this work. The lack of symmetry, constant bond angles and bond lengths cause differences in local environments in the glass structure. These local environments lead to a model of energy versus position as seen in Figure 1. For the Na ion Kircheim (45) points out: "Contrary to the crystalline state, however, interstices of different structural neighborhoods are provided in the disordered materials. These atoms dissolved within interstice of the glass will have a distribution of potential energies ... At temperatures above zero Fermi Dirac statistics have to be used to calculate the distribution of the dissolved atom among the different interstitial sites ... According to the considerations above the mobile atom or

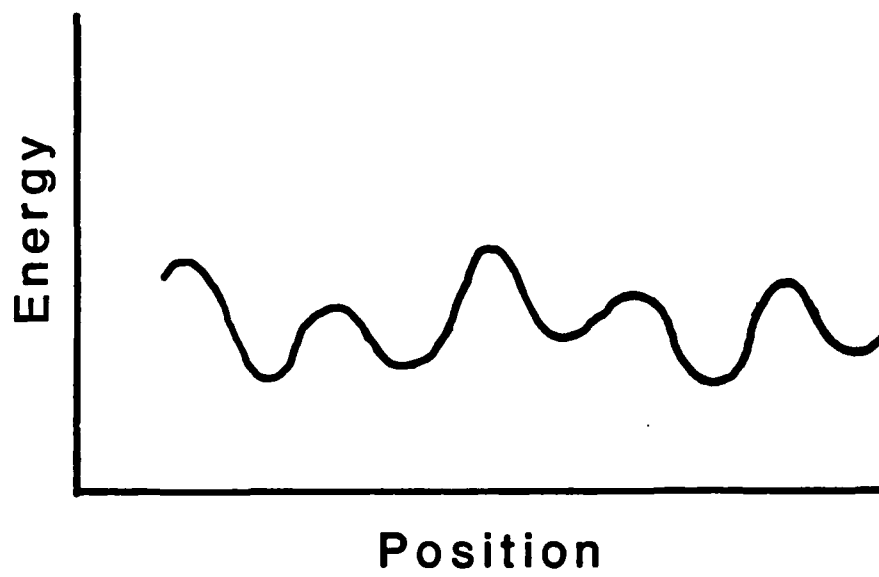


Figure 1. Energy Plot as a Function of Position for a Glass.

ions will face an irregular potential trace ...." The difference in potential wells is due to the fluctuations of the local structure. This conventional model suggests that these potential wells may result from interstitial and vacancy sites, with vacancy and interstitial defined essentially the same as for crystalline materials even though the crystalline structure does not exist.

Haven and Verlick (46) suggested that the Na ion has a preferred site which they refer to as a sodium site of lowest energy with other sites higher in energy. "The sites corresponding to energy levels of sodium ions higher than the levels of the bulk of the sodium sites will be called interstitial sites." This type of energy configuration would give rise to that configuration as pictured in Figure 1.

Lim and Day (47) measured the Na diffusion and electrical conductivity in high silica glasses containing less than 1 mole percent alkali. They conclude that for low alkali glasses the alkali diffuses by an uncorrelated vacancy or interstitial mechanism through the glass structure. They further point out a  $\text{Na}_2\text{O}$  concentration of less than 0.4 mole percent results in an approximate separation of  $22\text{\AA}$  for the Na ion, resulting in several "quasi-interstitial" jumps before the Na ion can reach another "lattice" site or state of lowest energy.

Doi and Day (48) in studying conduction polarization in sodium germanate glasses suggested that the Na ions occupy sites that are the same in principle as Haven and Verlick (46) lowest energy sites. This model proposes that the Na ion can then jump to nearby interstitial sites under the influence of an electric field. They use their conduction process to explain the thermally stimulated conduction peak

they see in sodium germanate glasses.

Hence the idea of interstitial sites is important to explain not only conduction but also the polarization processes.

Kelly et al (49), in studying correlation effects of alkali ions in high purity  $\text{GeO}_2$  glasses, suggested a mechanism of ion motion similar to that of Lim and Day (47). "A mechanism similar to an interstitial mechanism with random jumps between Na sites via intermediate site is indicated by correlation factor near unity for low alkali glasses". The existence of interstitial sites has been inferred from the dissolving of molecular gases into the glass structure as shown by Shelby (50).

The work of Shackelford et al (51) has documented the existence of these interstitial wells and suggests that their size obeys a log normal distribution function.

The motion of the ion through the network under the influence of a dc field has been found experimentally to obey an Arrhenius equation (42,43,44,46,49).

Anderson and Stuart (52) were the first to attempt a theoretical calculation for the activation energy for ionic conduction in silica glasses where the conducting species is an alkali ion residing in an interstitial position. They arrived at the expression for the activation energy:

$$F = \frac{\beta z z_0 e^2}{\gamma(r+r_0)} + 4\pi G r_0 (r-r_0)^2$$

where

F = activation energy

$z, z_0$  = valence of ion pair

- $r_o$  = radius of oxygen ion
- $r$  = radius of diffusion ion
- $r_D$  = radius of doorway for ion passage
- $\gamma$  = experimental determined constant of material
- $G$  = shear modulus
- $\beta$  = finite displacement factor

The first term represents the electrostatic interaction between the alkali and the ion field of the interstitial site. The second term represents the strain energy involved in separating the structure enough to allow the diffusion ion to pass through. They note that "... according to this treatment ions smaller than Na have high activation energy because they have excessive binding energies, whereas ions larger than Na have high activation energies because they induce excessive network strain energies."

Comparing the experimental data they reviewed, Anderson and Stuart (52) concluded, "... It is possible to compute the activation energy of ionic conductivity, provided the chemical composition, the shear modulus and the dielectric constant are known."

Doremus (53) concluded that the ionic conduction mechanism was the interstitial movement of a monovalent alkali that displays an Arrhenius type behavior. However, while molecular diffusion is a strong function of the sizes of the diffusion molecule, Doremus found that for the diffusing species he examined there was no "... effect of ion size on activation energy of ionic transport in fused silica." Doremus suggested, as did Anderson and Stuart (52), that there are two competing processes involved in the alkali ion movement. The first is an elastic squeezing process which involves the movement of the ion between its

neighbors as it migrates. The second factor is an electrostatic process in which electrostatic attraction between the alkali and the non-bridging oxygen must be broken. He further suggested that the ion size would affect the above two processes oppositely.

Hahim and Uhlmann (54), in studying the compositional dependence of the activation energy for conduction in alkali silicate glasses, found the data to fit a modified version of the Anderson and Stuart (52) equation. They concluded that the strain energy term becomes dominant as the ion size increases with the electrostatic term being dominant for smaller ion size.

Rothman et al (55), in examining the diffusion of alkali ion in vitreous silica found an increase in activation energy for diffusion with ion size. They assumed a model of an interstitial alkali near a non-bridging oxygen jumping to an adjacent interstitial site. Using a method for calculating the activation energy developed by Anderson and Stuart (52) they found reasonable agreement between experiment and theory.

Because of the structural similarities of fused silica and fused  $\text{GeO}_2$ , the same considerations are expected to apply to fused  $\text{GeO}_2$ . While the  $\text{GeO}_2$  system has not been studied as extensively as fused silica, some work has been done. A. V. Ivanon et al (56) demonstrated that the alkali ion is the charge carrier in a wide range of sodium and potassium germanate glasses. Bohm (17) found the dc conductivity in high purity  $\text{GeO}_2$  glasses to be a thermally activated process. He concluded that conductivity was ionic, and the charge carriers were the alkali ions.

Kelly et al (49) studied Na conductivity in high purity  $\text{GeO}_2$  glasses. They concluded, as Lim and Day (47), "A mechanism similar

to an interstitial mechanism with random jump between Na sites via intermediate site is indicated by correlation factor near unity for low alkali glasses." The intermediate site is suggested on the basis that the Na-Na separation distance is the order of  $100\text{\AA}$  for high purity glasses which is too great for single jump distances. Cordaro et al (18), in studying the effects of OH on the transport properties of high purity  $\text{GeO}_2$  glasses, suggested that there is an increase in activation energy for transport with increasing OH content.

To the present author's knowledge, there has been no systematic study of the effects of fusion conditions on the dc electrical properties of high purity glasses. Most research to date has involved the effects of concentration, ion sizes, mixed alkali, OH content and impurities on the conductivity in glasses. This literature has been reviewed by Doremus (57), Morey (58), Hughes and Isard (59) and Owen (44).

## CHAPTER II

### THEORY OF IONIC CONDUCTION

Dc conduction in ionic conducting materials is generally explained in terms of diffusion of charged cations in the gradient of a potential field in glasses (52-59).

Diffusion, first formulated by Fick, was assumed to be proportional to the concentration gradient as:

$$j = - D \left( \frac{\partial c}{\partial x} \right) \quad (1)$$

where  $j$  is the particle flux,  $c$  the concentration, and  $D$  the diffusion coefficient. The above expression allows for the definition of the diffusion coefficient  $D$ . Equation 1 can be written in a more general form where the driving force for the diffusion is more explicit. It is given by Kofstad (60) as

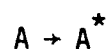
$$j = \frac{-c}{kT} D \nabla \mu_c \quad (2)$$

where  $c$ ,  $D$ , and  $j$  are defined as before,  $k$  is Boltzmann constant,  $T$  is the absolute temperature, and  $\nabla \mu_c$  is the gradient of chemical potential. This equation shows  $\nabla \mu_c$  as the driving force for the diffusion.

Experimental results have established that in general the diffusion is an activated process that obeys an Arrhenius type equation (52-59).

$$D = D_0 \exp(-Q/kT) \quad (3)$$

where  $D_0$  is a pre-exponential that depends on the material,  $Q$  the activation energy,  $k$  Boltzmann's constant and  $T$  the absolute temperature. Equation 3 is derived below, following the derivation given by Kingery, Bowen, and Uhlmann (61) using reaction rate theory. The process involves the formation of an activated complex in surmounting a potential energy barrier as seen in Figure 2.



where  $A^*$  represents the activated complex and  $A$  the equilibrium state.

The equilibrium constant  $K$  for this process can be written as

$$K = \frac{C_A^*}{C_A} \quad (4)$$

where  $C_A^*$  is the concentration of activated species and  $C_A$  is the concentration of  $A$ . The reaction rate constant  $\bar{k}$  can then be written as:

$$\bar{k} = vC_A^* = vKC_A \quad (5)$$

where  $v$  is the jump frequency of the diffusing species.

The equilibrium constant  $K$  can also be expressed in terms of the free energy change  $\Delta G$  as

$$K = \exp \frac{-\Delta G}{kT} = \exp \left( \frac{-\Delta H}{kT} \right) \exp \left( \frac{\Delta S}{k} \right) \quad (6)$$

where  $\Delta H$  is the change in enthalpy and  $\Delta S$  the change in entropy.

Then  $\bar{k}$  can be written in this notation from Equation (5) as:

$$\bar{k} = vC_A \exp \left( \frac{-\Delta H}{kT} \right) \exp \left( \frac{\Delta S}{k} \right) \quad (7)$$

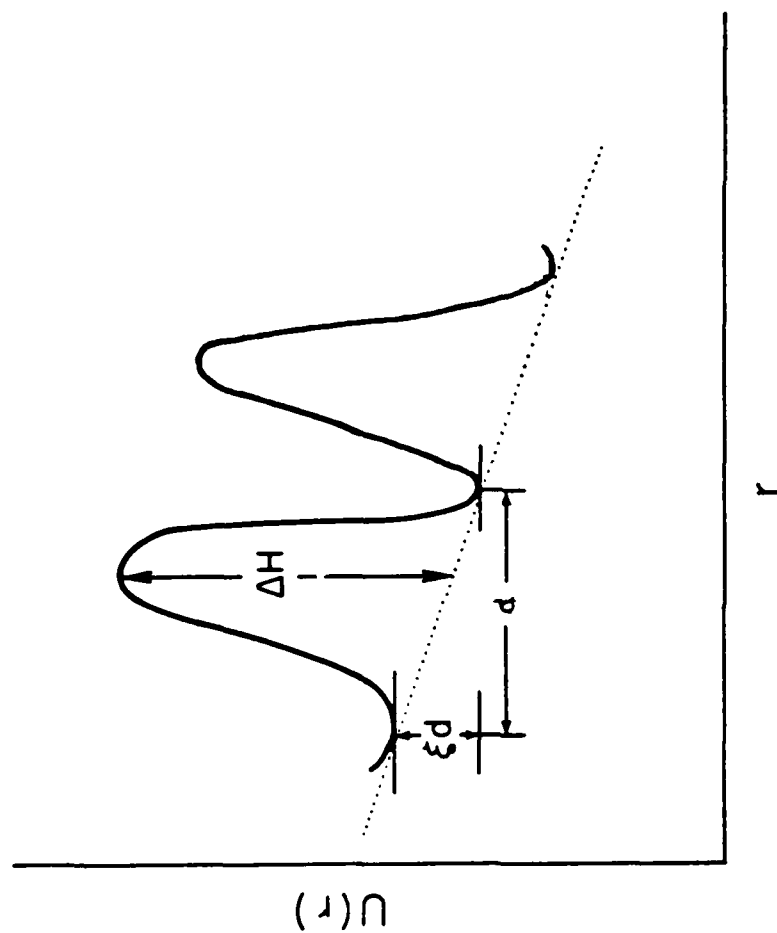


Figure 2. Schematic Representation of Diffusion in a Potential Gradient.  $\Delta H$  is the Enthalpy of Activation and  $d$  is the Distance between Equilibrium Positions.

For diffusion under a concentration gradient or electric potential gradient the barrier is shifted as seen in Figure 2 resulting in a net flow of the diffusing species. Defining the chemical potential gradient as

$$\xi = \frac{-d\mu_C}{dx} \quad (8)$$

the change in  $\mu_C$ ,  $\Delta\mu_C$ , becomes

$$\Delta\mu_C = -\xi d \quad (9)$$

where  $d$  is distance between minima as seen in Figure 2.

Using Equation (7),  $\bar{k}$  in the forward direction is given by:

$$\bar{k}_{\text{forward}} = vC_A \exp - \frac{(\Delta G - 1/2 \xi d)}{kT} \quad (10)$$

where the barrier height has been lowered by  $1/2 \xi d$ . In the reverse direction the barrier height has been increased by  $1/2 \xi d$  resulting in  $\bar{k}$  in the reverse direction to be given by

$$\bar{k}_{\text{reverse}} = vC_A \exp - \left( \frac{\Delta G + 1/2 \xi d}{kT} \right) \quad (11)$$

The factor  $1/2$  arises in both equation (10) and (11) because the activated complex is considered at midpoint of the jump. The net  $\bar{k}$ ,  $\bar{k}_{\text{net}}$ , then becomes the difference of  $\bar{k}_{\text{forward}}$  and  $\bar{k}_{\text{reverse}}$ .

$$\bar{k}_{\text{net}} = \bar{k}_{\text{forward}} - \bar{k}_{\text{reverse}} \quad (12)$$

$$\begin{aligned}\bar{k}_{\text{net}} &= vC_A \exp\left(\frac{-\Delta G}{kT}\right) \left[ \exp\left(\frac{\xi d}{kT}\right) - \exp\left(-\frac{\xi d}{kT}\right) \right] \\ &= 2vC_A \exp\left[\frac{-\Delta G}{kT}\right] \sinh\left(\frac{\xi d}{2kT}\right)\end{aligned}\quad (13)$$

If  $\frac{\xi d}{2kT} \ll 1$  the approximation for the sinh term can be made and results in

$$\bar{k}_{\text{net}} = vC_A \frac{\xi d}{kT} \exp\left[\frac{-\Delta G}{kT}\right] \quad (14)$$

Recalling that  $\xi = \frac{-d\mu_c}{dx}$  equation 14 can be written as

$$\bar{k}_{\text{net}} = -RC_A \frac{v}{kT} \frac{d\mu_c}{dx} \exp\left(\frac{-\Delta G}{kT}\right) \quad (15)$$

The distance  $d$  times the reaction rate will give the flux  $j$

$$j = d \bar{k}_{\text{net}} \quad (16)$$

$$j = \frac{-vR^2}{kT} C_A \frac{d\mu_c}{dx} \exp\left(\frac{-\Delta G}{kT}\right) \quad (17)$$

Comparing Equation (2) with Equation (17) one finds

$$D = d^2 v \exp\left(\frac{-\Delta G}{kT}\right) \quad (18)$$

Equation (18) makes no assumption about availability of neighboring sites for the diffusing species, hence a geometrical factor dependent upon symmetry must be included (60,61). For cubic symmetry this factor is 1/6 resulting in an equation for  $D$  of

$$D = \frac{vd^2}{6} \exp\left(\frac{-\Delta G}{kT}\right) \quad (19)$$

The derivation given above assumes a concentration gradient driving force of  $\nabla\mu_c$ . However, for charged particles in an electric field the derivation is the same with a driving force of  $\nabla\psi$ , where  $\psi$  is the potential field. The relation between  $D$  and the conductivity  $\sigma$  is developed as follows.

For ionic charge carriers under the influence of a potential field the current density  $j$  is given by:

$$j = czev \quad (20)$$

where  $c$  is the concentration,  $z$  the valence,  $v$  the velocity and  $e$  the electronic charge. The current density may also be expressed as:

$$j = \sigma E \quad (21)$$

where  $E$  is the electric field yielding

$$\sigma = \frac{czev}{E} \quad (22)$$

If  $z=1$ , the case for current carried by monovalent ions, the conductivity becomes

$$\sigma = \frac{cev}{E} \quad (23)$$

Velocity divided by the electric field  $E$ ,  $v/E$ , is defined as the mobility,  $\mu$ , giving for

$$\sigma = ce\mu \quad (24)$$

and

$$j = ce\mu E \quad (25)$$

For diffusion due to a concentration gradient and a potential field

gradient (recalling  $E = -\nabla\psi$ ) the total current can be written as the sum

$$J = ce\mu E - \frac{eD}{kT} c \nabla\mu_c. \quad (26)$$

using  $\mu = v/E$  and  $V = \nabla\psi$  yields

$$J = -ce\mu \nabla\psi - \frac{eD}{kT} c \nabla\mu_c \quad (27)$$

$\nabla\mu_c$  can be expressed as

$$\nabla\mu_c = kT \frac{d \ln c}{dx}$$

If the concentration  $c$  obeys Boltzmann statistics (61), i.e.

$$c = c_0 \exp\left(\frac{-e\psi}{kT}\right) \quad (28)$$

where  $\psi$  is again the potential field

$$\begin{aligned} \nabla\mu_c &= \frac{-ekt}{kT} c_0 \exp\left(\frac{-e}{kT}\right) \frac{d\psi}{dx} \\ &= -e \frac{d\psi}{dx} \end{aligned} \quad (29)$$

Substituting this result into equation 26 gives  $J$

$$J = -ce\mu \frac{d\psi}{dx} + \frac{e^2 Dc}{kT} \frac{d\psi}{dx} \quad (30)$$

For equilibrium conditions the current density  $J$  is zero and equation (30) becomes

$$ce\mu \frac{d\psi}{dx} = \frac{e^2 Dc}{kT} \frac{d\psi}{dx} \quad (31)$$

Solving for  $\mu$ , one finds

$$\mu = \frac{eD}{kT} \quad (32)$$

Substituting this value of  $\mu$  into equation (24) and solving for  $\sigma$  one finds

$$\sigma = \frac{ce^2D}{kT}, \quad (33)$$

the Nernst Einstein equation. This equation relates the diffusion coefficient  $D$  to the conductivity  $\sigma$ . Then  $\sigma$  can be written using Equation (19) for  $D$  as

$$\sigma = \frac{ce^2vd^2}{6kT} \exp\left(\frac{-\Delta G}{kT}\right) \quad (34)$$

The above expression is more generally seen as

$$\sigma = \sigma_0 \exp\left(\frac{-\Delta G}{kT}\right) \quad (35)$$

where  $\sigma_0$  is given by

$$\sigma_0 = \frac{ce^2vd^2}{6kT} \quad (36)$$

Using Equation (24), the mobility of the Na ion in the presence of an electric field may be written as

$$\mu = \frac{evd^2}{6kT} \exp\left(\frac{-\Delta G}{kT}\right) \quad (37a)$$

or

$$\mu = \frac{evd^2}{6kT} \exp\left(\frac{\Delta S}{k}\right) \exp\left(\frac{-\Delta H}{kT}\right) \quad (37b)$$

where  $\Delta S$  and  $\Delta H$  are the entropy and enthalpy of activation respectively. Syed et al (62) have suggested that for ionic conducting glasses  $v$  represents a full vibrational degree of freedom such that  $v = kT/h$  to best interpret the experimental data they examined. Substitution into Equation (37b) results in

$$\mu = \frac{ed^2}{6h} \exp\left(\frac{\Delta S}{k}\right) \exp\left(\frac{-\Delta H}{kT}\right) \quad (38)$$

## CHAPTER III

### $T\phi$ EFFECTS ON THE DC CONDUCTIVITY\*

#### Experimental Procedure

A series of  $\text{GeO}_2$  glasses was prepared by melting high purity  $\text{GeO}_2$  powder (electronic grade from Eagle Pitcher Corporation) in a platinum crucible in an electrically heated furnace with air atmosphere for various times which were dependent upon the fusion temperature. The melt equilibration times are tabulated in Table 1. The melt times were chosen to allow equilibration of the melt. The temperature of the equilibrated melt is designated  $T\phi$ . Equilibration was determined by observation of the  $2450 \text{ \AA}$  UV band. This band is assumed to be that of an oxygen vacancy (13). By measuring the absorption coefficient on samples from top to bottom of the crucible, equilibrium at temperature with atmospheric conditions is assumed when the absorption coefficient is constant (63). The crucible with glass was removed from the furnace and cooled to room temperature at an average rate of  $5^\circ\text{C}/\text{sec}$  from  $T\phi$  to  $400^\circ\text{C}$ . The cooling rate below  $400^\circ\text{C}$  was less than  $5^\circ\text{C}/\text{sec}$ . Samples were removed from the crucibles by core drilling a cylinder approximately 17 mm in diameter from the center. This cylinder was then cut into discs approximately 1 mm thick. Wafers were polished with petroleum lubricants through 400 grit abrasive, then washed with

---

\*This chapter will appear as part of a paper in the Journal of Applied Physics.

TABLE 1

TRACE ELEMENTS IN GeO<sub>2</sub> GLASSES FROM NEUTRON ACTIVATION  
ANALYSIS<sup>†</sup> AND INFRARED ANALYSIS IN ppm

T <sub>0</sub>	1690	1650	1550	1450	1350
Equilibration Time (hrs)	1	3	3	110	185
Na	20.3	12.2	8.7	14.9	13.9
Cl	1.41x10 <sup>3</sup>	1.21x10 <sup>3</sup>	1.60x10 <sup>3</sup>	1.27x10 <sup>3</sup>	1.47
Al	*	4.8	*	4.4	7.9
Li	*	*	*	*	*
K	*	*	*	*	*
OH	214	181	238	206	190

\*Less than detectable limit.

<sup>†</sup>Neutron activation analyses conducted by L. Bate, Oak Ridge  
National Laboratory.

ethanol. Samples were then placed in a vacuum evaporator and heated at 230°C for approximately 30 minutes after which gold electrodes were vapor deposited. The guarded configuration gold electrodes were annealed for one hour at 300°C. Measurements were made with the samples in a chamber which permitted measurements under a vacuum of approximately 30 microns over the temperature range from room temperature to 300°C. Computer control of the dc measurements was employed. Predetermined target temperatures were chosen so that they were equally spaced in  $1/T$  between the extremes of the measurement temperatures. The present experiment used 30 target temperatures. A three modes proportional control algorithm was used to calculate the percent duty cycle of the heating element with the design characteristics of minimum overshoot with reasonable convergence time. Temperatures were scanned from lowest to highest to minimize annealing processes during measurement.

The sample temperature is measured every 10 seconds. When the rms deviation from the target temperature of the last 50 of these measurements is less than 1°K, the convergence criterion is met. With this criterion the sample temperature is stable over a period of 500 seconds which is consistent with the relatively long thermal time constant of the system.

After the sample temperature has converged to the target temperature, the applied sample voltage is switched on for 30 seconds to allow for polarization processes. Immediately following this, the electrometer is activated and auto ranges to the appropriate scale.

To enhance accuracy, 10 current measurements are taken at each measurement temperature. The recorded current value is the computed

root mean square average of these values, and the rms error is stored for subsequent statistical calculations.

At the completion of the run, the data is converted to resistivity and the rms errors in current are similarly transferred. To effect the statistical analysis and determine the pre-exponential and exponent for the Arrhenius fit, Equation (39) is linearized, and the data plotted as  $1/T$  vs.  $\log$  resistivity. For the statistical analysis, the measurement error in  $T$  is assumed to be negligible ( $< \pm 0.5^\circ\text{C}$ ). The parameters are determined by a Chi square fit to the linearizing function with the individual resistivity uncertainties propagated through the calculations to give the uncertainties in pre-exponential and exponent (64).

Analysis for trace elements was made by neutron activation analysis at ORNL\*. The OH content was determined by measurements of the intensity of the 2.7 micron IR absorption band (65). Results of the analysis are given in Table 1.

### Results

The DC resistivity of two samples with differing Na concentrations with  $T_0$  equal to  $1650^\circ\text{C}$  are shown in Figure 3. The data show a proportional decrease in resistivity with increase in Na concentration. The activation enthalpy was calculated for both samples using a least square fit to the Arrhenius equation:

$$\rho = \rho_0 \exp^{-\Delta S/k} \exp^{\Delta H/kT} \quad (39)$$

---

\*The analyses were made by Lamont Bate, Oak Ridge National Laboratory.

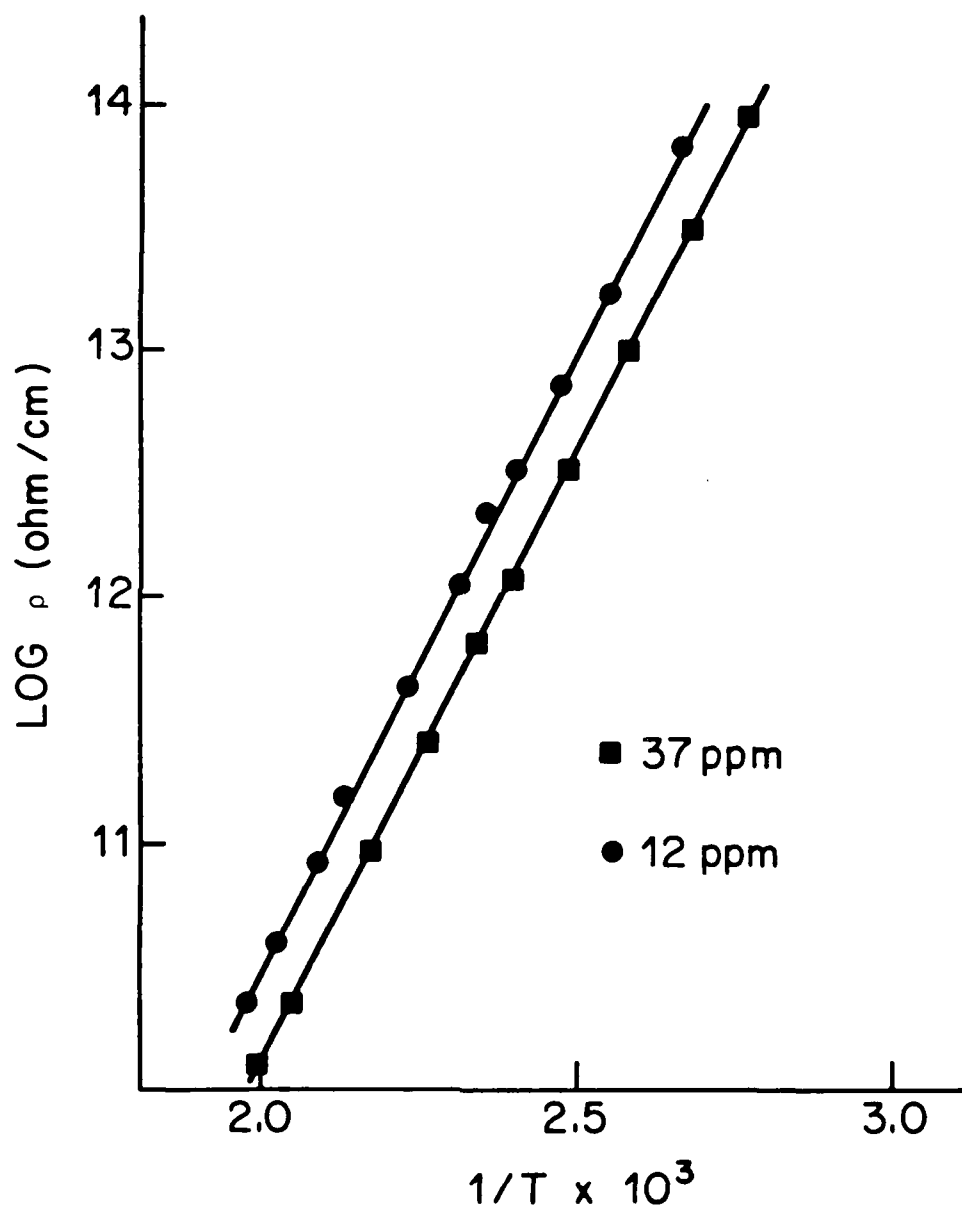


Figure 3. Temperature Dependence of Resistivity,  $\rho$ , for a  $T_{\phi} = 1650^{\circ}\text{C}$  and Varying Na Concentration.

$\Delta H$  is given in Table 2 with the Na concentration, pre-exponential factor  $\rho_0$  and OH concentration.

The mobility of the Na ion, calculated from the equation

$$\mu = 1/nep, \quad (40)$$

is plotted in Figure 4 as a function of temperature for glasses with  $T\phi$  equal to 1450°C, 1550°C, and 1690°C. Measurements made on glasses with  $T\phi$  at other temperatures are omitted for clarity. The mobility of the sodium as measured at 144°C on samples with  $T\phi$  equal to a series of temperatures is plotted as a function of  $T\phi$  in Figure 5.

The sodium ion mobility exhibits a maximum at approximately 1450°C.

#### Discussion

The equation for mobility as derived from reaction rate theory is Equation (38):

$$\mu = e^2 d^2 / 6h \exp \Delta S/k \exp - \Delta H/kT \quad (38)$$

where  $e$  is the charge of the carrier,  $d$  the jump distance,  $k$  Boltzmann's constant, and  $T$  the temperature.  $\Delta S$  and  $\Delta H$  are the entropy of activation and enthalpy of activation respectively. The variables in the expression above are  $\Delta S$  and  $\Delta H$  and  $d$ .

It is assumed that the jump distance is of the order of the distance between interstitial sites, i.e. approximately 5 Å. If the variation in mobility is attributed to a variation in jump distance, then the jump distance  $d$  must range over a factor of 2, i.e. up to 10 Å. Such a large jump distance would require a great deformation of

TABLE 2

SUMMARY OF SODIUM CONCENTRATION AND PRE-EXPONENTIAL  
FACTORS FOR TWO GLASSES FUSED AT 1650°C FOR  
THREE HOURS IN AIR

Na (ppm)	$\rho_0$ (ohm/cm)	OH (ppm)	$\Delta H$ (ev)
12.3	1.18	181 ppm	1.02
37.3	0.370	204	1.02

AD-A147 216

THE RELATIONSHIP BETWEEN RADIATION SENSITIVITY AND  
REDOX EQUILIBRIA(U) VANDERBILT UNIV NASHVILLE TN DEPT  
OF MECHANICAL AND MATERIALS. D L KINSER SEP 84

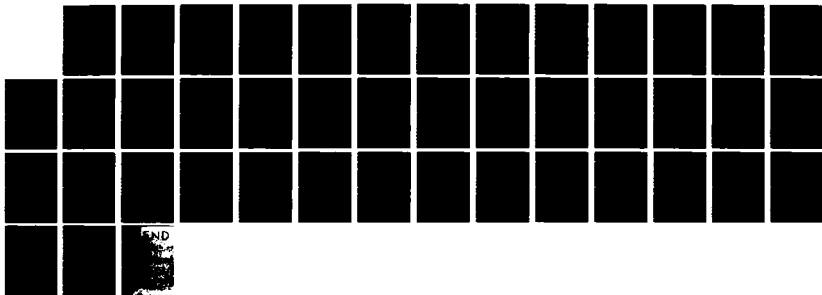
3/3

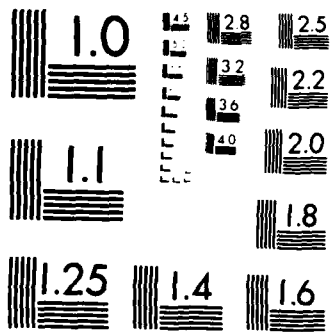
UNCLASSIFIED

ARO-17942.8-MS DAAG29-81-K-0118

F/G 11/2

NL





MICROCOPY RESOLUTION TEST CHART  
NATIONAL BUREAU OF STANDARDS-1963-A

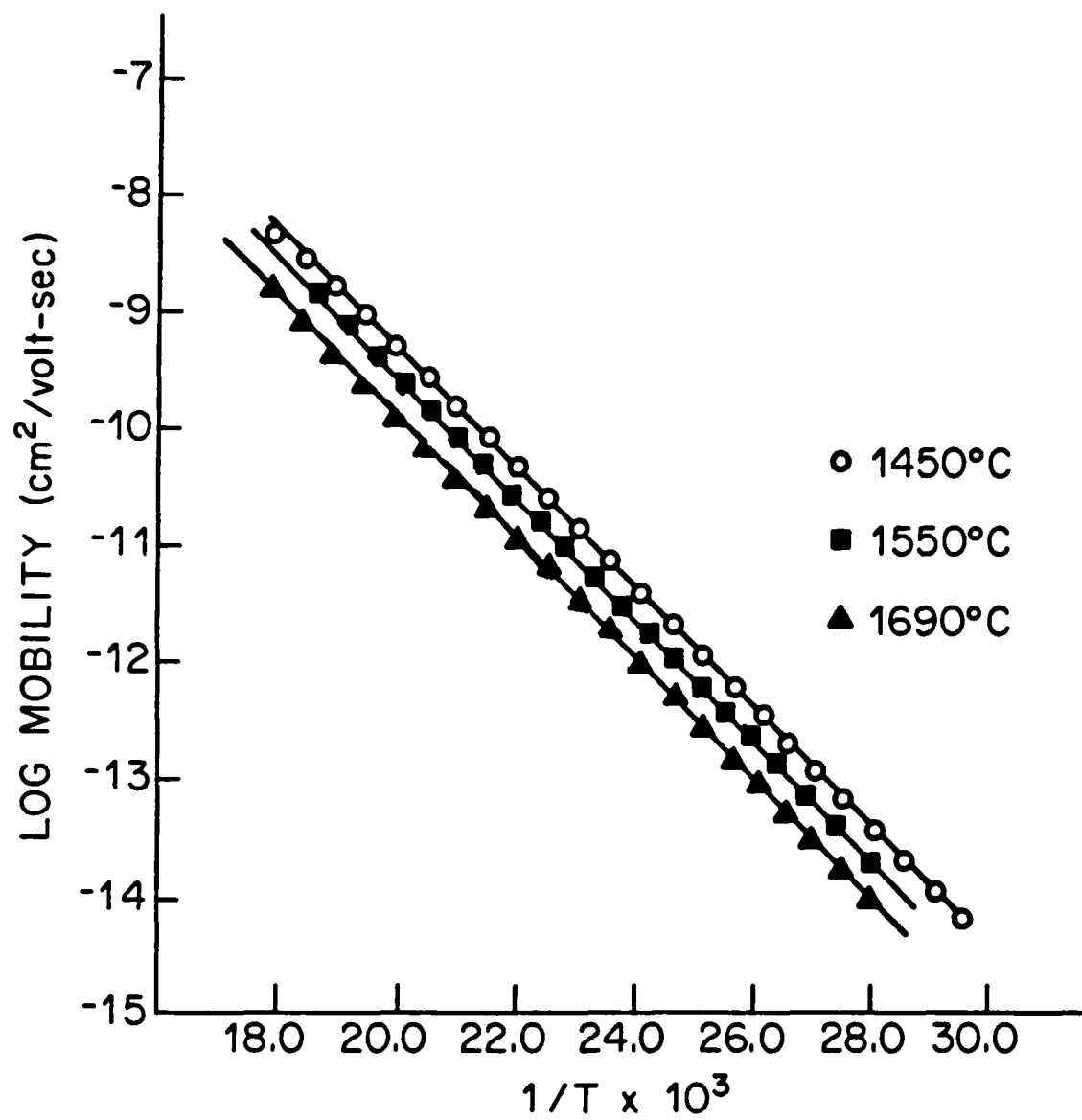


Figure 4. Temperature Dependence of Mobility for a Series of Glasses With Varying  $T_{\phi}$ .

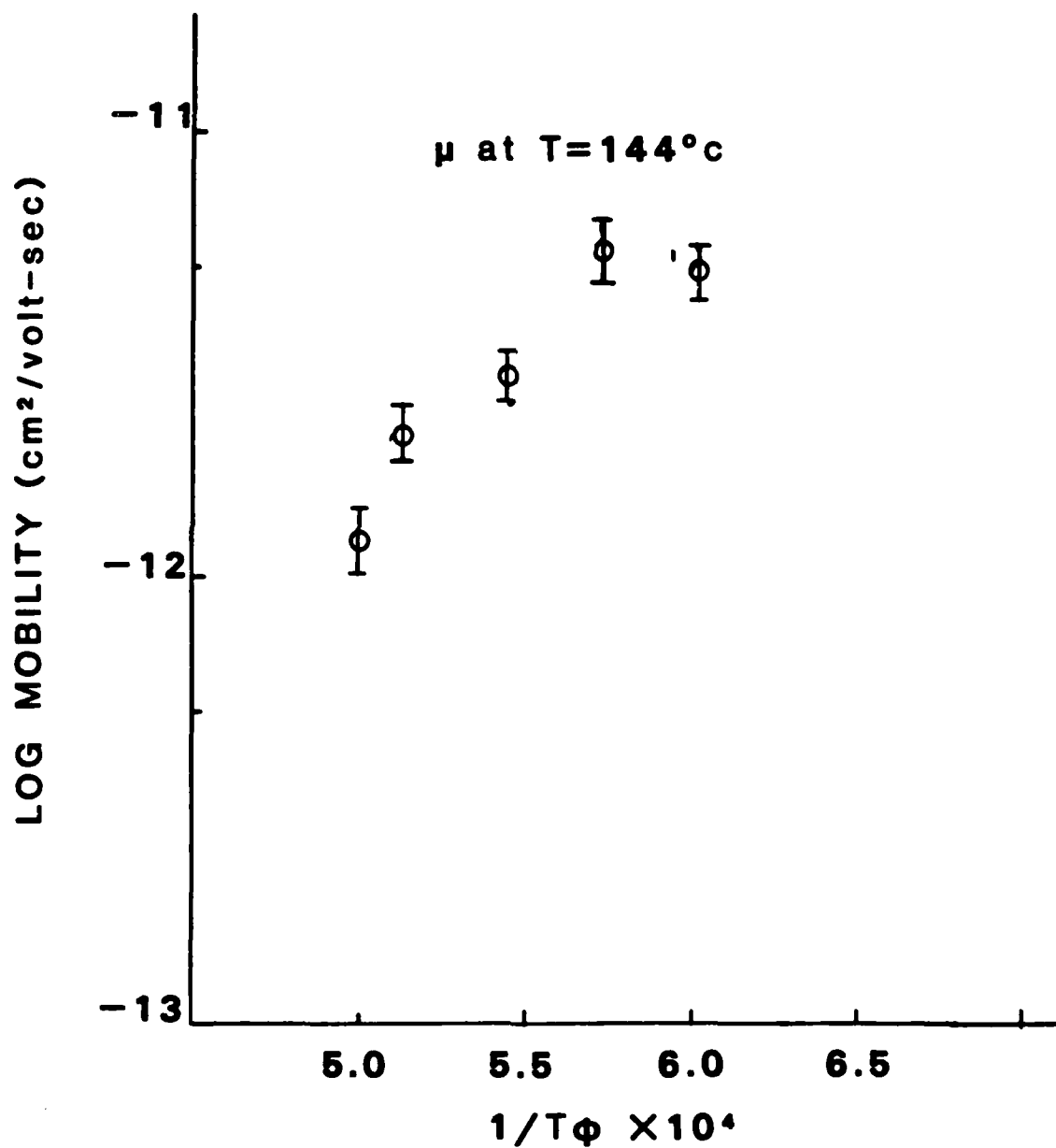


Figure 5. Mobility versus  $T\phi$  for a Series of Glasses for Which  $T\phi$  Ranged From  $1690^{\circ}\text{C}$  to  $1350^{\circ}\text{C}$ .

the structure involving a jump over several interstitial sites. It is physically unreasonable to expect the jump distance sites to be larger because of the large lattice deformation required in pushing through more than one interstitial site. The activation enthalpy,  $\Delta H$ , is invariant with  $T\phi$  as shown in Table 3. Hence, the assumption is made that the short range order is the same in these glasses. A consequence of this assumption is that the "doorway" through which the ion must pass from one site to another is invariant with  $T\phi$ . The changes seen in mobility of the glasses with  $T\phi$  between 1690°C and 1350°C are then due to changes in the entropy of activation  $\Delta S$ . Table 3 lists the values calculated for  $\Delta S$ .

Entropy can be expressed as (66):

$$S = k \ln \omega \quad (41)$$

where  $\omega$  represents the thermodynamic probability of a given state. In accord with this definition of entropy, the entropy of activation,  $\Delta S$ , represents the probability that an activated state will be reached, i.e.

$$\Delta S \propto k \ln \omega^A \quad (42)$$

where  $\omega^A$  represents change in the thermodynamic probability of the activated state. The probability of the transition to an activated state is dependent upon the density of energy levels available. This density is not independent of the energy (66) and is the origin of the  $\Delta S$  term (66). Table 3 shows that  $\Delta S$  increases with a decrease in  $T\phi$ . It is suggested that these observations indicate the probability of reaching an activated state increases with decreasing fusion temperature.

TABLE 3

SUMMARY OF ACTIVATION ENTROPY AND ENTHALPY  
FOR SERIES OF GLASSES

$T_{\phi}$	$\Delta S$ (ev/°K) <sup>+</sup>	$\Delta H$ (ev) <sup>*</sup>
1690	$1.2082 \times 10^{-2}$	1.01
1650	$1.2149 \times 10^{-2}$	1.02
1550	$1.2164 \times 10^{-2}$	1.01
1450	$1.2191 \times 10^{-2}$	1.00
1350	$1.2176 \times 10^{-2}$	1.00

<sup>+</sup>The error in these values as determined by differences between two melts is  $\pm 0.0006 \times 10^{-2}$ .

<sup>\*</sup>The rms error as determined by least square fit calculations to Arrhenius equation is  $\pm 0.0003$ .

To reach an activated state, an ion must gain sufficient energy from the vibrational modes of the atoms surrounding Na ion. Thus, the change in  $\Delta S$  implies a change in the local structure around the Na ion. A model for this change is discussed in the following.

The sodium ions are seen as occupying a series of "interstitial" wells in the glass structure. The existence of the interstitial wells has been documented by the studies of Shackleford et al (51,68). While there is a statistical distribution of well depths, the following discussion is restricted to a statistically average well.

These wells represent minima in the potential energy curve for the Na ion. They are caused by the ion fields of the oxygen surrounding the interstitial sites in the glass. These ion fields cause a potential,  $U(r)$ , where  $r$  is a configurational coordinate as seen in Figure 6.

$U(r)$  is an aperiodic potential function in that the oxygen ion configuration around each site is variable as are the dimensions of each site resulting in no translational symmetry. However, depth of the wells is determined by the energy required to dilate the structure and to overcome the electrostatic field of the surrounding ions. This energy, from measurements of dc conductivity, is found to be constant.

A Taylor series expansion of  $U$  for a particular potential well yields:

$$U(x) = U_{x=0} + (dU/dx)_{x=0}x + 1/2!(d^2U/dx^2)_{x=0}x^2 + 1/3!(d^3U/dx^3)_{x=0}x^3 + \dots \quad (43)$$

Following the treatment of Barrow (69)  $U_{x=0}$  and  $(dU/dx)_{x=0}$  are 0. The resulting expression for  $U(x)$  becomes

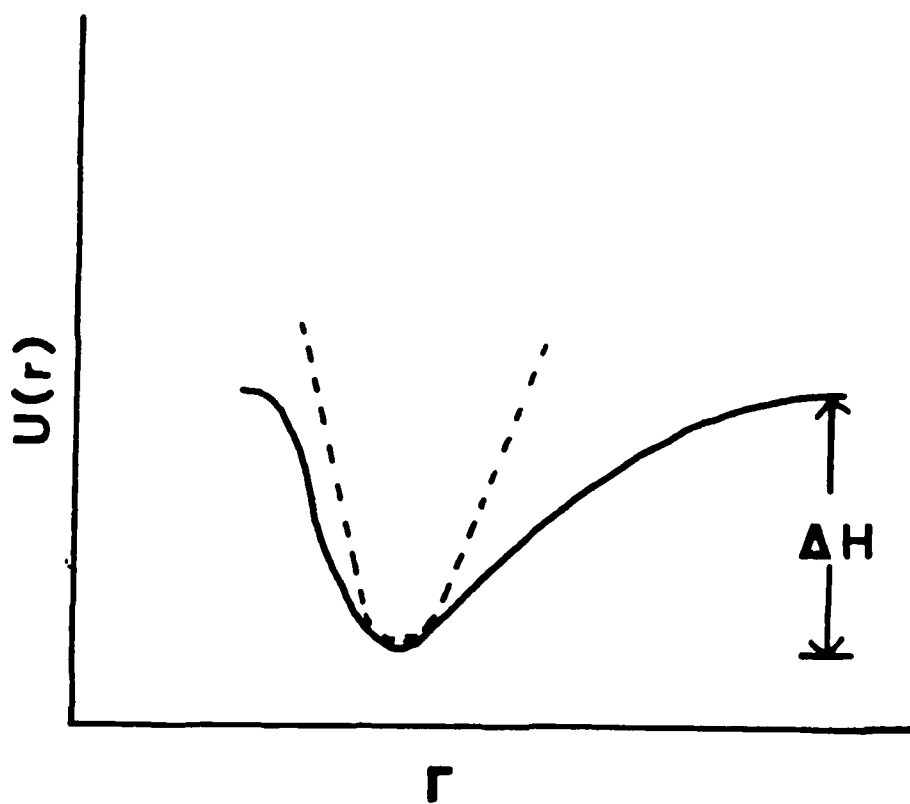


Figure 6. Potential Energy Versus Distance ( $r$ ) From Equilibrium.  
---Curve Represents Simple Harmonic Oscillator.  
—Curve Represents Anharmonic Oscillator.

$$U(x) = 1/2! \left( \frac{d^2U}{dx^2} \right)_{x=0} x^2 + 1/3! \left( \frac{d^3U}{dx^3} \right)_{x=0} x^3 + \dots \quad (44)$$

The first term on the right is the same term obtained for Hooke's law where  $K$  the force constant is given by

$$\left( \frac{d^2U}{dx^2} \right)_{x=0}$$

The second term on the right will then determine the anharmonicity induced in the system.

Using a power series expansion, Schrödinger's equation can be solved for the energy levels

$$\epsilon_n = h\omega(n+1/2) - h\omega X_e(n+1/2)^2 + \dots \quad (45)$$

where  $\omega = 1/2\pi\sqrt{K/m}$  and  $K = \left( \frac{d^2U}{dx^2} \right)_{x=0}$ .

$X_e$  is the anharmonicity constant and is related to  $\left( \frac{d^3U}{dx^3} \right)_{x=0}$ . In contrast to a simple harmonic oscillator whose energy levels are equidistant in energy, the anharmonic term causes the spacing of the levels to decrease with increasing  $n$  as seen from equation (45).

The  $X_e$  term then determines the variation in the spacing of the energy levels and affects the symmetry of the function as seen in Figure 7.

The  $\left( \frac{d^2U}{dx^2} \right)$  term would determine the well shape in the absence of the anharmonic term. The change from the parabolic structure is then determined by the  $\frac{d^3U}{dx^3}$  term and as a consequence affects the energy level density of the well. Barrow (68) comments that as the well structure is broadened, "... (it) confines the vibrating particle less

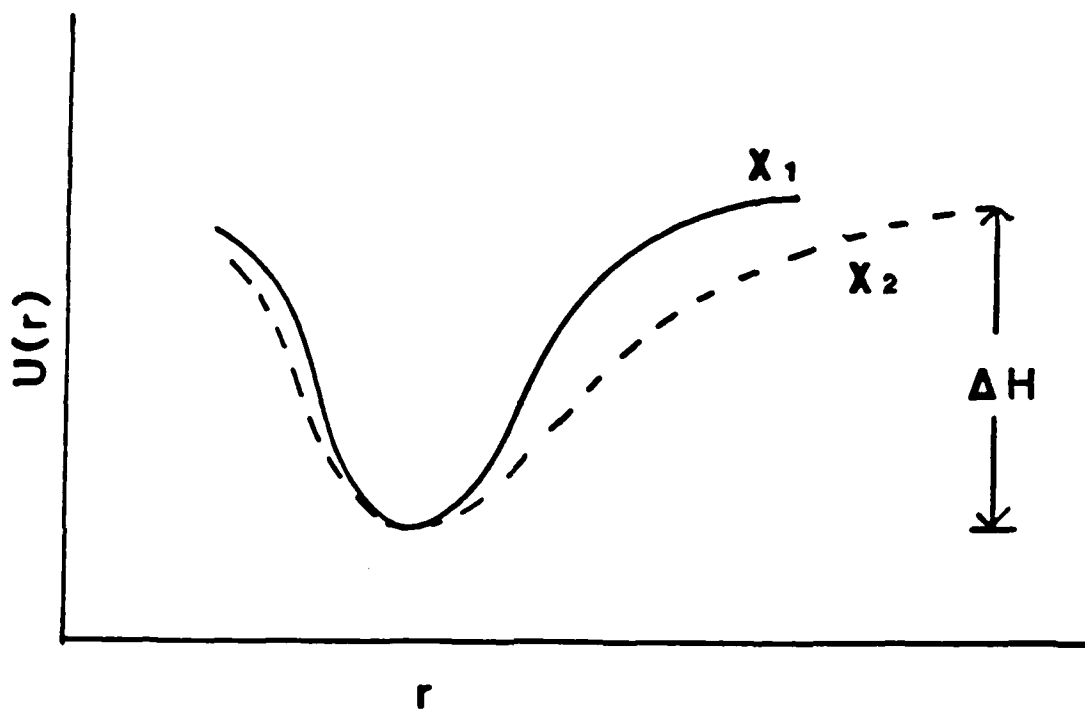


Figure 7. Potential Energy  $U(r)$  Versus  $r$  Distance From Equilibrium Position for Two Curves of Anharmonic Oscillator With Different  $\chi_e$ .

closely than would a parabolic curve. Such loosening of the restriction on the motion of particles always leads to more closely spaced allowed energy levels."

The average well seen by the sodium ion is characterized by the force constant that determines the depth of the well and by the anharmonic term that determines its departure from a true harmonic oscillator.

A change in the glass structure is then manifested in the anharmonic term. This change in the anharmonic term results in a difference in the energy level spectrum of the well in which the Na ions reside. These differences change the statistical average value of the vibrational modes of the well. As the Na ion moves through the glass structure, it encounters wells characteristic of the melt temperature. As  $T\phi$  is shifted, the vibrational states of the wells change. These changes appear in the anharmonic term.

From Boltzmann statistics (66), it is known that the fractional occupancy of a particle between energy states is given by

$$f_a = \frac{\exp(-\epsilon_a/kT)}{\sum_n \exp(-\epsilon_n/kT)} \quad (46)$$

where  $\epsilon_a$  is the level of interest,  $\epsilon_n$  is the nth energy level. The denominator in Equation (49) is the partition function L.

$$L = \sum_n \exp(-\epsilon_n/kT) \quad (47)$$

As n increases, i.e. the density of states increase, the partition function must increase causing the fractional occupancy at a particular

temperature to decrease. Hence, the structure of wells is broadened as shown schematically in Figure 7.

Changes in  $T\phi$  change the density of energy levels in the Na sites. These changes produce a change in the partition function. This change in the partition function causes a change in the average fractional occupancy of the activated states in the glass. With  $f_a$  decreasing the probability of reaching the activated state decreases, then  $\Delta S$  decreases in accordance with Equation (42) resulting in a mobility decrease.

As the  $\Delta H$  values given in Table 3 are constant, the argument is advanced that the short range order in the glasses with  $T\phi$  from 1690°C to 1350°C is essentially the same. This short range order in the configuration of the ions determines the height of the potential barrier. If, however, as the fusion temperature is changed, slight changes in the bond angles, as suggested by Primak (39) to explain density changes with fictive temperature as seen by Douglas and Isard (24) in fused silica occur, then one can reasonably expect the configurational coordinates of the well to change. Geissberger and Galeener (69) have recently reported evidence of Si-O-Si bond angle changes in fused silica with changes in fictive temperature.

The fundamental change produced by changes in  $T\phi$  are in the configurational coordinates of the interstitial sites. These differences in well shape are manifested in the entropy of activation and result in the differences of mobility with  $T\phi$ .

## CHAPTER IV

### ANNEALING EFFECTS ON THE DC CONDUCTIVITY\*

#### Experimental Procedure

A series of  $\text{GeO}_2$  glasses was prepared from material and by techniques previously described in Chapter III. All samples were first measured in the as-quenched state. The electrodes were removed and the samples were annealed at  $420^\circ\text{C}$  for 1, 2, 7, and 46 hours and quenched at the same rate from the annealing temperature. This annealing treatment was conducted at  $15^\circ\text{C}$  below the observed Littleton softening point of  $435^\circ\text{C}$ . After each annealing the electrodes were replaced in the manner previously described, and the resistivity measured. Analysis for trace elements are given in Table 1.

#### Results

The mobilities are calculated using the same method as in the previous chapter. Figure 8 shows the effect of annealing at  $420^\circ\text{C}$  on the mobility measured at  $144^\circ\text{C}$  for various  $T_\phi$ 's. All samples show a decrease in mobility with increasing annealing time. The samples with  $T_\phi$  of  $1450^\circ\text{C}$  and  $1350^\circ\text{C}$  show a much larger initial drop in mobility with the first annealing than do those with  $T_\phi$  of  $1650^\circ\text{C}$  and  $1550^\circ\text{C}$ . All mobility values within error limits, approach a stabilized value for

---

\*The contents of this chapter were presented in a paper at the conference on the Effects of Modes of Formation of the Structure of Glass, Vanderbilt University, Nashville, TN, 1984. Conference proceedings are to be published in the Journal of Non-Crystalline Solids.

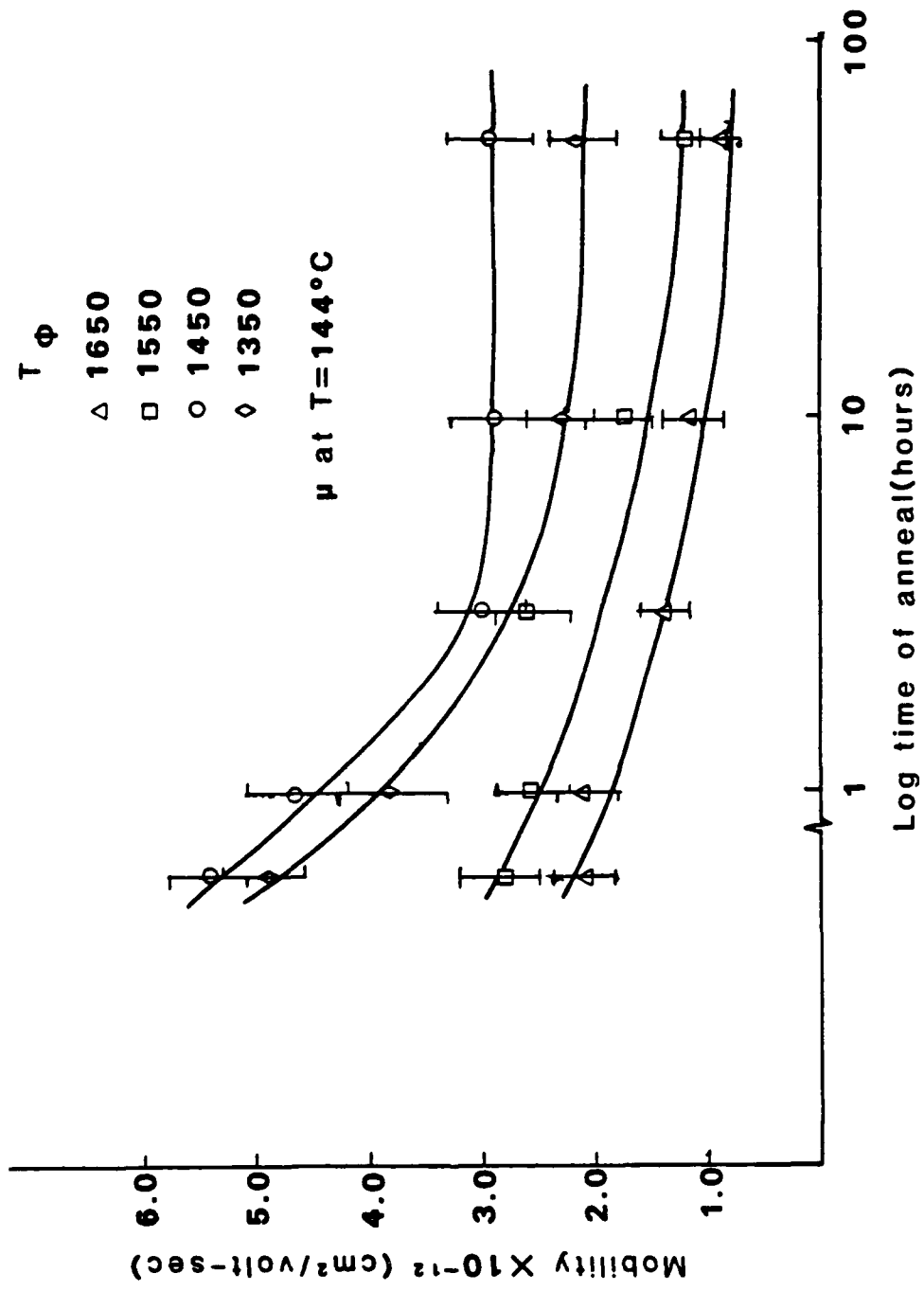


Figure 8. Mobility Versus Log Time of Annealing as a function of  $T_{\phi}$ .

the longest annealings. The 1550°C  $T\phi$  sample shows an anomalous behavior for the three hour annealing.

Figure 9 shows the behavior of the mobility as a function of  $T\phi$  for the as-quenched and the longest annealing time. The mobilities decrease while maintaining the relation between the mobilities observed for the as-quenched samples. The mobility of the sample with  $T\phi$  of 1450°C is highest for the as-quenched state and for the longest annealing time.

Table 4 lists the activation enthalpy as determined by a least squares fit for the Arrhenius Equation 39. The  $\Delta H$  terms show a small increase for all samples with annealing.

#### Discussion

In Chapter 3, the mobility was given by

$$\mu = \frac{e^2 d^2}{6h} \exp \frac{\Delta S}{k} \exp - \frac{\Delta H}{kT} \quad (38)$$

where  $e$  is the charge of the carrier,  $d$  the jump distance,  $k$  Boltzmann's constant and  $T$  the temperature.  $\Delta S$  and  $\Delta H$  are the entropy of activation and the enthalpy of activation respectively. The variables affecting the mobility are then  $\Delta S$  and  $\Delta H$  as seen in Chapter III.

$\Delta S$  was shown to be related to the anharmonicity term in an expansion of the potential of the interstitial site. The dependence of mobility on  $T\phi$  was attributed to changes of the anharmonic terms in the vibrational potential energy structure of the average interstitial sites through which the Na moves. As the activation enthalpy remains constant in the as-quenched samples, however, the melt history controlled the shape of the well as seen in Figure 7. Hence, the alteration in the

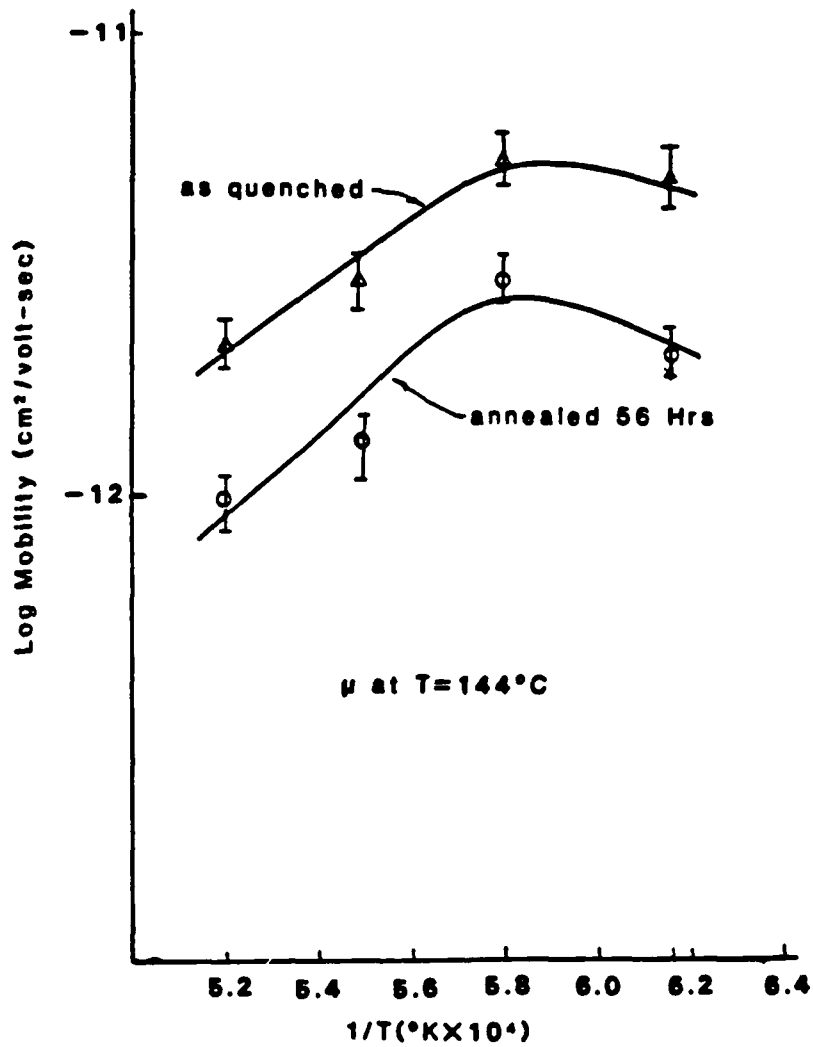


Figure 9. Mobility Versus  $T_0$  for the As-Quenched and 56 Hour Annealed Samples.

TABLE 4

SUMMARY OF ACTIVATION ENTHALPIES FOR ANNEALED GLASSES  
 $\Delta H(\text{ev})^*$ 

$T\phi$	1650°C	1550°C	1450°C	1350°C
as-quenched	1.02	1.01	1.00	1.00
1 Hr @ 420	1.05	1.04	1.01	1.02
3 Hr @ 420	1.04	1.04	1.03	-
10 Hr @ 420	1.04	1.04	1.03	1.03
56 Hr @ 420	1.02	1.03	1.03	1.03

\*The rms error as determined by least square fit calculation to the Arrhenius Equation is  $\pm 0.0003$ .

vibration energy states was attributed to the anharmonic terms. The potential energy of the site will be determined by the ions surrounding the interstitial site. Slight differences in configuration of these ions would lead to changes in the well shape. These changes can occur without change of the energy required for the Na ion to push through the doorway to its next interstitial site. The behavior of the various samples with annealing time supports the earlier conclusion that the structures are different. The effects of annealing are then expected to be influenced by the differing initial structures.

In conventional glass theory, the structure as measured by volume would be expected to be the same for the various  $T\phi$ 's for the same cooling rate. This theory is based on the assumption that the melt liquid remains at metastable equilibria down to  $T_g$  upon cooling. Only upon changing the cooling rate would one expect to introduce differences in structure. These differences would be expected to result in changes in the dc resistivity as seen by Boesch and Moynihan (70) and Ritland (71). Changing the volume of the glass would result in changes in the potential well structure and hence changes in the energy level structure. These changes will then result in changes in the dc resistivity as seen in Chapter III.

With annealing, one would expect that the volume of the glass would approach some equilibrium value characteristic of the time and temperature of annealing (72). It then might be expected that as the glass approached this equilibrium volume that the mobility of the Na ion through the structure would approach some common equilibrium value characteristic of the average well structure.

As seen in Figure 8, this is not the case for annealing times up to 56 hours for these samples. Instead, while the mobility of the Na ions decreases in all samples a "memory" of their starting structure is retained and the decreases are in a proportional fashion. Figure 9 shows that the general relation between the as-quenched mobilities is retained for all  $T\phi$ 's.

These changes in mobility are suggested to be due to a thermal compaction process of the same nature as suggested by Primak (23) for fused silica. Thermal compaction would result in the oxygen ions moving into the interstitial positions changing the distributions of bond angles. Upon quenching from the annealing temperature, these changes become frozen into the structure. The values for the enthalpy of activation,  $\Delta H$ , increase only slightly as seen in Table 4. It is suggested the basic short range order of the glass remains constant. However, the energy required to dilate the Ge-O structure and to overcome electrostatic fields of the surrounding atoms increases slightly. As seen in Table 5, the values of the entropy of activation,  $\Delta S$ , are changing, which is attributed to changes in the energy level structure. These changes in the energy level structure are tentatively attributed to changes in bond angle distributions which result from thermal compaction. The bond angle changes would be expected to affect the anharmonic terms. The increases in  $\Delta H$  are compatible with the redistribution of bond angles in that they can increase the energy required by the Na ion to move from one interstitial site to the next.

The differences of the various  $T\phi$ 's in reaching equilibrium for samples which differing  $T\phi$ 's indicate that stabilization processes in

TABLE 5

SUMMARY OF ACTIVATION ENTROPIES FOR ANNEALED GLASSES  
 $\Delta S$  in  $\text{ev}/^\circ\text{k} \times 10^{-2\dagger}$

$T\phi$	1650°C	1550°C	1450°C	1350°C
as-quenched	1.2149	1.2164	1.2191	1.2176
1 Hr @ 420°C	1.2226	1.2232	1.2176	1.2203
3 Hr @ 420°C	1.2168	1.2231	1.2204	-
10 Hr @ 420°C	1.2156	1.2194	1.2202	1.2173
56 Hr @ 420°C	1.2085	1.2122	1.2202	1.2174

<sup>†</sup>The error in these values as determined by difference between melts is  $0.0006 \times 10^{-2}$ .

these glasses are different. These differences in stabilization may be in part due to defect concentration in the glasses. Primak (30) has suggested that the E' center may play a role in compaction phenomena observed in fused silicas. Obviously, more than one defect may play a role in the stabilization processes. Kordas et al (22) have reported the E' center concentration in the as-quenched samples shows a non-Arrhenius behavior such that a minimum in E' center concentration occurs in glasses with  $T_{\phi} = 1450^{\circ}\text{C}$ . Jackson et al (73) have reported the defect center concentration associated with  $2450\text{\AA}$  absorption peak to be largest in samples with  $T_{\phi} = 1650^{\circ}\text{C}$  and the lowest with  $T_{\phi} = 1350^{\circ}\text{C}$ .

The defect structure of the glass may control the stabilization processes in the glasses by allowing motion of the network to relieve stresses induced from thermal compaction.

Using the diffusion coefficient determined by Garina-Carrina (74), we calculate the diffusion distance at  $420^{\circ}\text{C}$  to be less than 0.01 mm for time of 56 hours. Hence, it is noteworthy that the oxygen penetration from the surface for the maximum time of annealing is insufficient to change the redox state of the glass except for a thin surface layer.

The above argument suggests that the defect structure of the glass is not only important for the electronic states of the glass but also for the overall structure that the glass reaches upon cooling from the equilibrated liquid. This is in sharp contrast to a crystalline structure in which bond angles and bond lengths are determined by the crystal structure. For glasses, these bond angles and distances are distributed about a mean value and may change slightly with differing

defect concentration. Such modifications of structure may result in change of the average interstitial well through which the Na ion moves.

The initial structure appears set by  $T\phi$ . Subsequent annealing treatments at 420°C for the times used in these experiments do not change the general behavior of the mobility with  $T\phi$  even though there is a decrease. This retention of structure determined by  $T\phi$  indicates that point defects may influence the intrinsic structure of the glass and hence the average interstitial well the Na ion moves through.

## CHAPTER V

### IRRADIATION EFFECTS ON THE DC CONDUCTIVITY

#### Experimental

The samples used in these experiments correspond to those used in Chapter III. The chemistry for these samples is given in Table 1. All samples were first measured in the as-quenched state. Each sample was subsequently irradiated for a series of irradiations tabulated in Table 6. The samples were irradiated in a  $\text{Co}^{60}$  source ( $3.1 \times 10^6$  rads/hr). After each irradiation the resistivity was measured from room temperature to  $300^\circ\text{C}$  using the apparatus described in Chapter III. No additional treatments were given to the samples between irradiations.

#### Results

The mobility of the Na ion was calculated using the methods of the previous two chapters. The resistivity for all samples was measured over the temperature range from  $80^\circ\text{C}$  to  $300^\circ\text{C}$  after each irradiation. Figure 10 shows resistivity for  $T\phi = 1550^\circ\text{C}$  sample after irradiation dose from  $7.1 \times 10^6$  rads to  $3.6 \times 10^8$  rads. Other  $T\phi$  samples behave in an analogous fashion. The unirradiated samples shows Arrhenius behavior over the full temperature range. With increasing dose level all samples show two regions of behavior. The resistivity in the low temperature region displays an Arrhenius behavior from approximately  $80^\circ\text{C}$  to  $200^\circ\text{C}$ . Above  $200^\circ\text{C}$  the system undergoes changes during the measurements.

TABLE 6

SUMMARY OF DOSE LEVELS (RADS)  
FOR SAMPLES WITH THE VARIOUS  $T\phi$ 's  
 $Co^{60}$

$T\phi$	1st dose (rads)	2nd dose (rads)	3rd dose (rads)
1690°C	$1.24 \times 10^7$	$7.44 \times 10^7$	$7.5 \times 10^8$
1650°C	$9.1 \times 10^6$	$6.7 \times 10^7$	$7.3 \times 10^8$
1550°C	$7.1 \times 10^6$	$6.3 \times 10^7$	$3.6 \times 10^8$
1450°C	$7.2 \times 10^6$	$7.2 \times 10^7$	$7.4 \times 10^8$
1350°C	$7.2 \times 10^6$	$6.9 \times 10^7$	$7.4 \times 10^8$

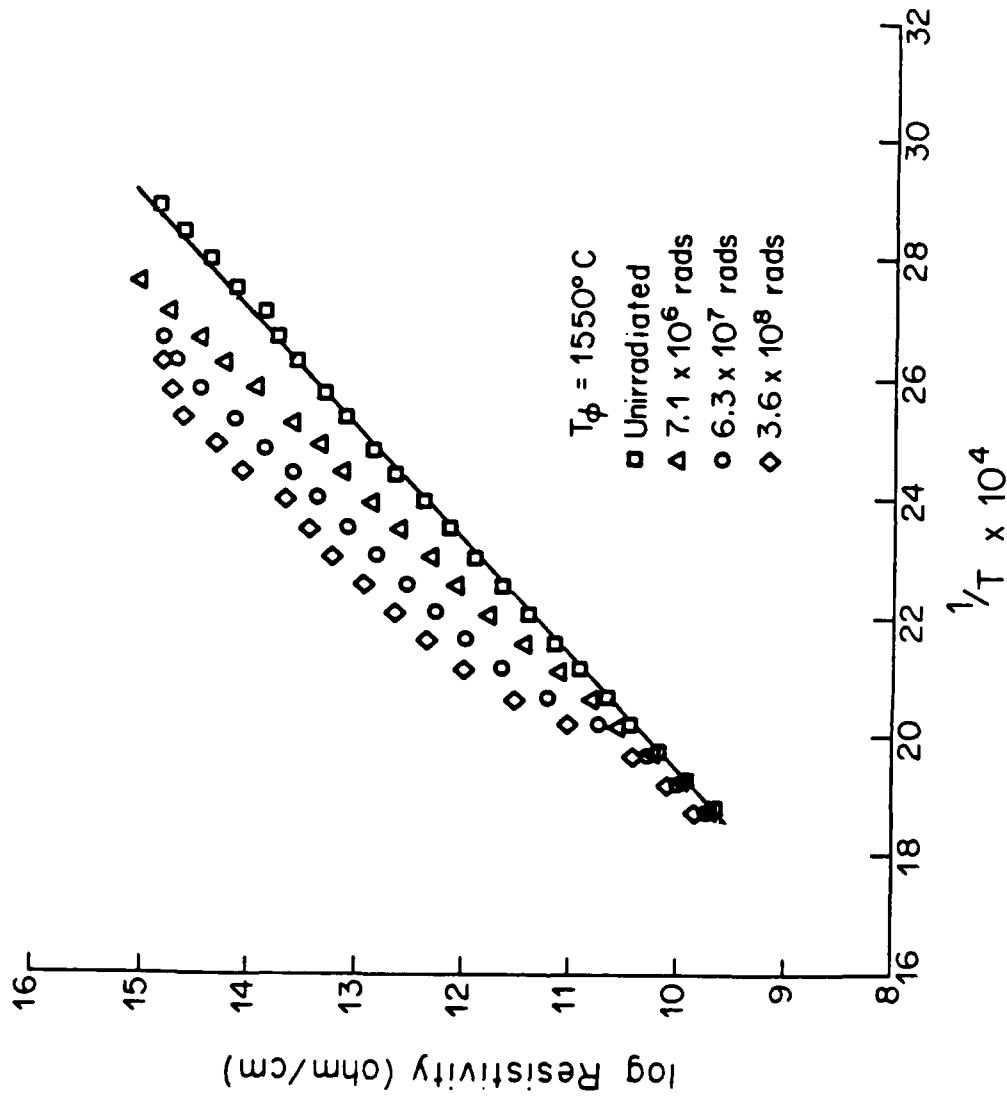


Figure 10. Resistivity of the  $T_\phi = 1550^\circ\text{C}$  with Varying Irradiation Doses as a Function of Reciprocal Temperatures.

Consequently, values for the mobility and  $\Delta H$  were not calculated. The mobilities for all samples were calculated at 144°C using Equation (40). Figure 11 shows these values versus dose (rads). As seen in Figure 11 the mobilities of all samples decrease with increasing dose level. Concurrent with the increase in resistivity, an increase in activation energy with dose is also observed (Table 7).

At temperatures greater than 200°C the irradiation effects anneal during measurements. Thus samples were measured for a second time for the highest dose level to ascertain what effects the temperature of measurement had on the samples. Figure 12 shows the resistivity of samples with  $T\phi = 1550^\circ\text{C}$  in the unirradiated state and the resistivity for the second measurement. The resistivity has returned to approximately its original temperature dependence.

#### Discussion

The mobility for the Na ion in irradiated samples is discussed using Equation (38).

$$\mu = \frac{e^2 d^2}{6h} \exp\left(\frac{\Delta S}{k}\right) \exp\left(-\frac{\Delta H}{kT}\right) \quad (38)$$

where the terms are defined as in Chapter III. The jump distance  $d$  is assumed to be constant in these samples. For  $d$  to change would require changes in the short range order of the glass, i.e. the distance between interstitial sites. For these dose levels the basic short range order remains essentially unchanged. Wong and Angell (10) in their review of the literature for fused silica concluded that for  $\gamma$  irradiation,

TABLE 7

SUMMARY OF ACTIVATION ENTHALPY,  $\Delta H$ , VALUES FOR THE  
IRRADIATED GLASSES (DOSE LEVELS CORRESPOND TO TABLE 6)

$T_{\phi}$	unirradiated (ev)	1st Irradiation (ev)	2nd irradiation (ev)	3rd irradiation (ev)
1690°C	1.01	1.01	1.08	1.29
1650°C	1.02	1.06	1.12	1.39
1550°C	1.01	1.14	1.17	1.20*
1450°C	1.00	1.07	1.11	1.31
1350°C	1.00	1.05	1.14	1.32

\*Lower Dose

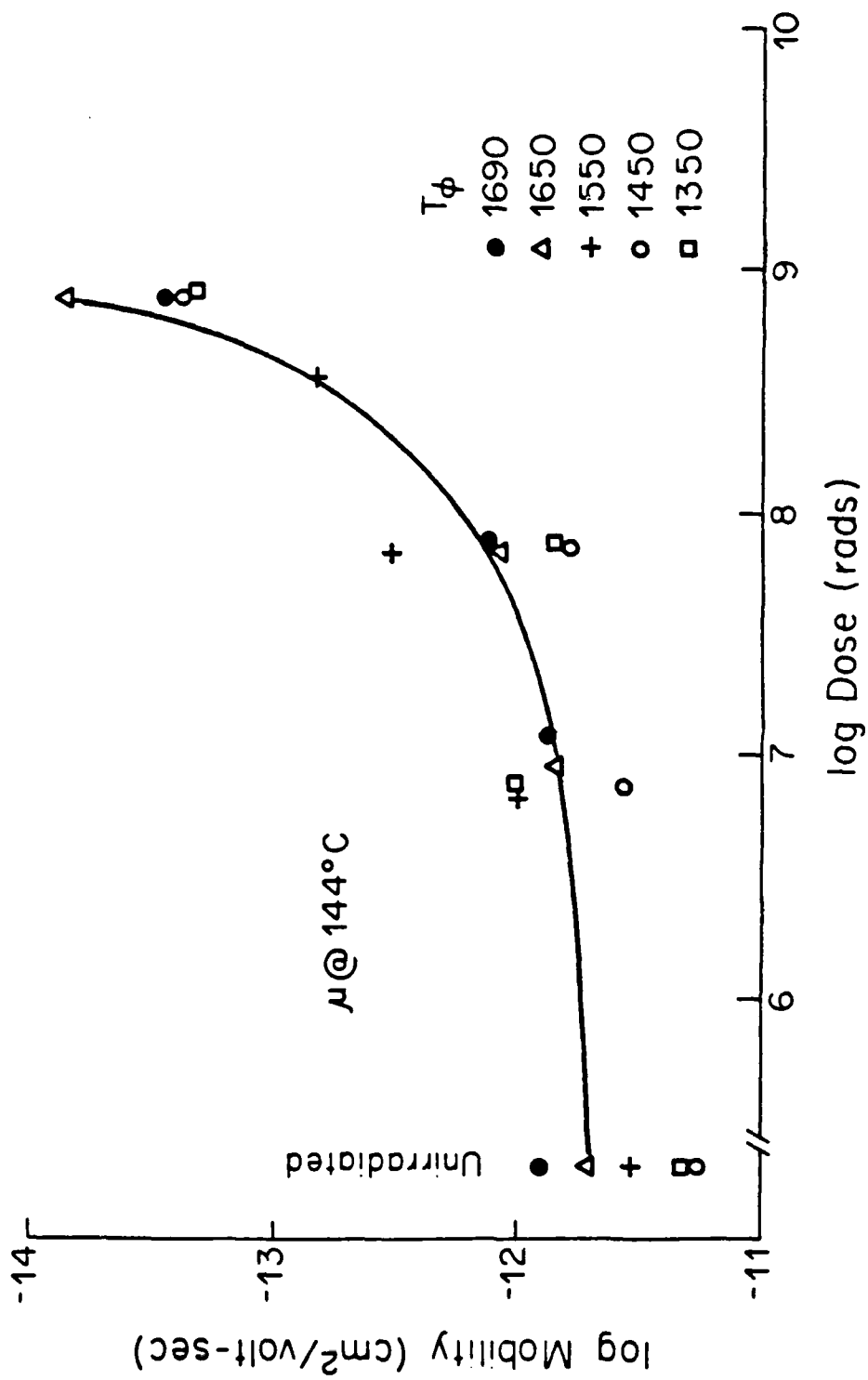


Figure 11. Mobility for a Series of Glasses with Varying T $\phi$  as a Function of Dose (rads).

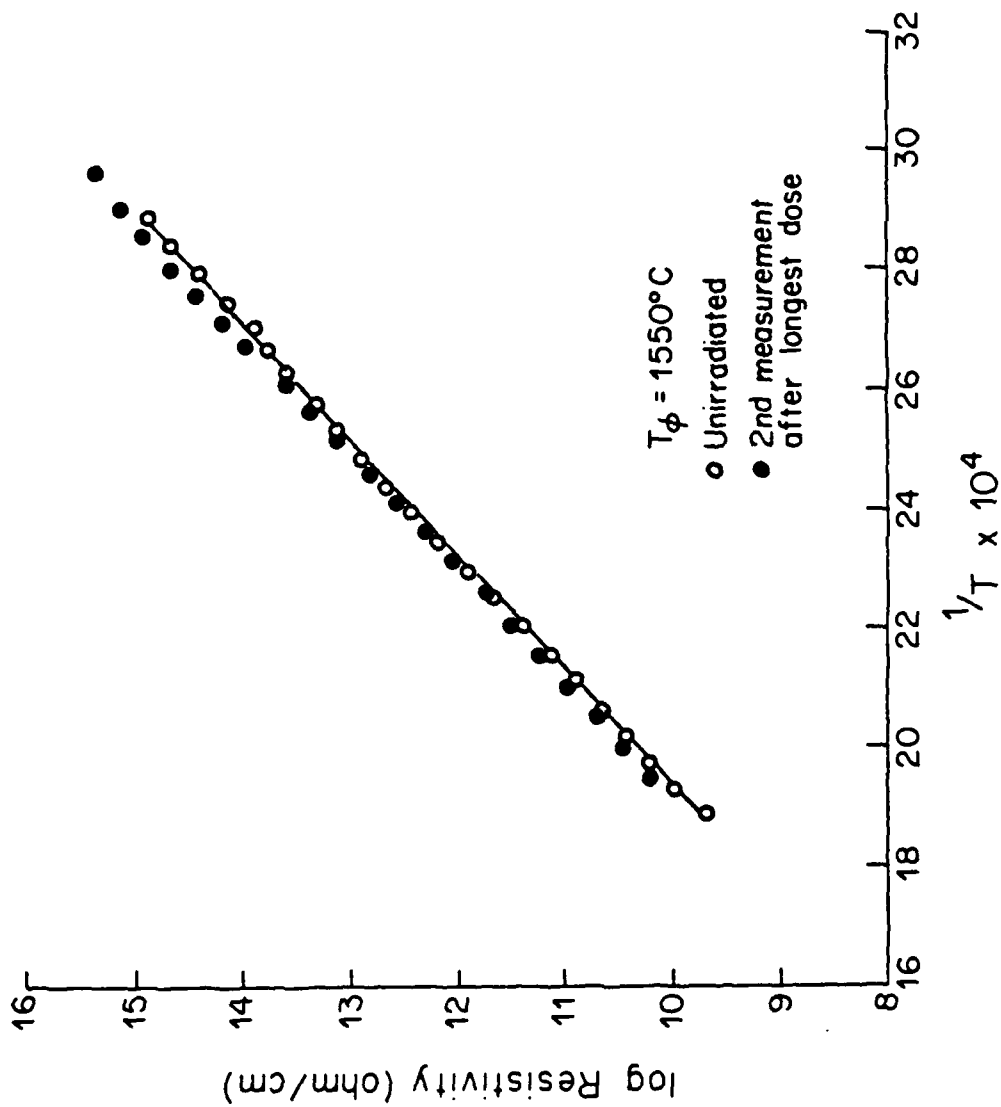


Figure 12. Resistivity of the  $T_\phi = 1550^\circ\text{C}$  Sample Before Irradiation and the Second Measurement After the Longest Dose as a Function of Reciprocal Temperature.

"... the Si-O bond distances are unchanged but the Si-Si distances are somewhat decreased, implying a decrease in the Si-O-Si bond angle. ... the radial distances between the O-O and Si-2nd O exhibit a wider distribution than in irradiated silica glass." Hence the distance between interstitials is expected to remain essential constant. An indication of the increase in energy required to dilate the structure and overcome the electrostatic field is found in the increase in  $\Delta H$ .

In accord with the model discussed above, the behavior of these samples with ionizing radiation is attributed to changes induced in the structure by the  $\gamma$  irradiation. These changes result in an increased depth of the average potential well for the Na ion (Figure 13). These changes are reflected in increased  $\Delta H$  values with dose level in Table 7. and decreasing mobilities (Figure 11).

The energy level structure of the average interstitial well may be altered in two related ways with ionizing radiation. The first is compaction and the second is change in the charge state of defect centers.

According to Primak (30) the compaction phenomena occurs in vitreous silica when the oxygen moving into an interstitial void volume is frozen into the excited state. This position of the oxygen leads to microscopic stress in the structure in the immediate environment (30). These induced stresses in the structure would then make it more difficult for the Na ions to dilate the Ge-O structure and to overcome electrostatic fields of the surrounding atoms. These changes in strain energy would produce changes in the well structure that increase the  $\Delta H$  values in accordance with the Anderson and Stuarts (52) strain component of the activation enthalpy.

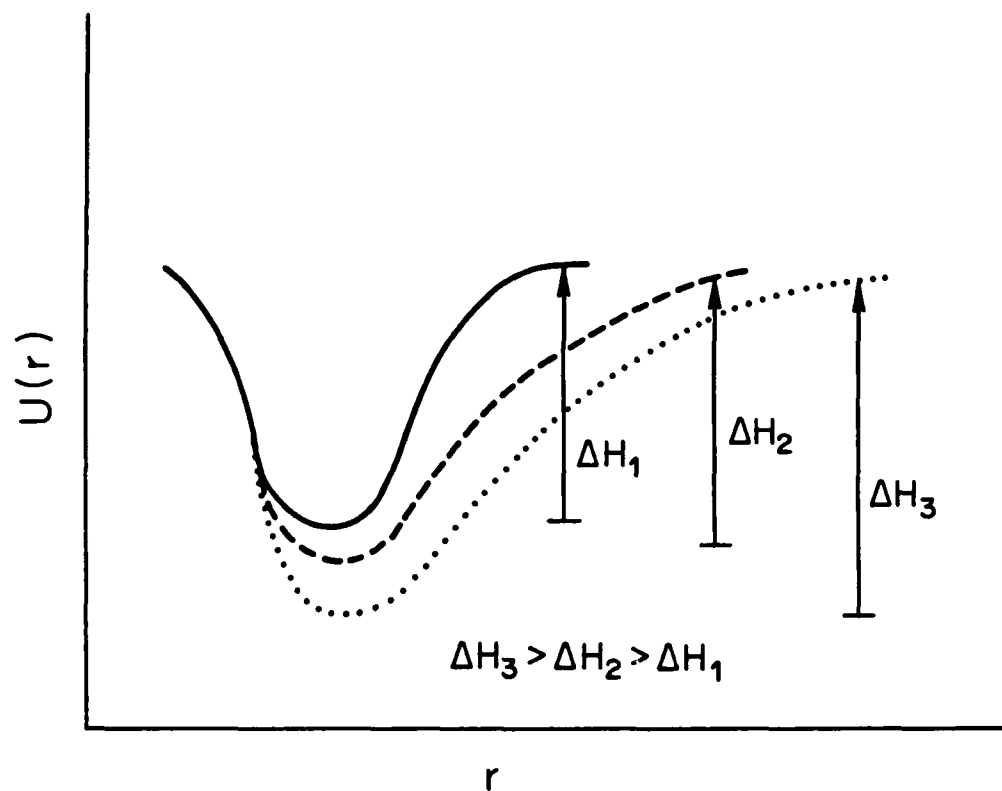


Figure 13. Schematic Representation of Increasing Enthalpy of Activation,  $\Delta H$ , on Well Shape.

The second mechanism by which the interstitial wells can be changed is through the change in the charge state of defect centers with ionizing irradiation. With the release of electrons and holes with irradiation, defects in the glass serve as traps (4). Once the defect has trapped a hole or electron it can induce structural changes through the relaxation of the ions surrounding the defect. These relaxations are a consequence of the long range nature of coulombic forces of the charged center. An example of these effects is seen in Figure 14. The E'' center (a doubly charged oxygen vacancy) traps a hole to give a E' center (a singly charged oxygen vacancy) with concurrent relaxation of the oxygen ions (4). These relaxations of the oxygen ions as well as the charge of the defect can affect the energy level structure of the neighboring interstitial site through the coulombic forces.

These two processes are closely related. Compaction can result in bond cleavage yielding defect centers (30) while charged defects have been suggested by Primak (30) to be involved in compaction phenomena.

The unirradiated samples show an activation enthalpy of  $1.01 \pm .01$  ev for all samples measured as seen in Table 7. However with irradiation enthalpy is seen to increase with increasing dose. The present writer suggests that the reason for these increases is due to compaction and the creation of charged defect centers. Weeks et al (26) have demonstrated that in these glasses the defect concentration does not obey an Arrhenius behavior with  $T\phi$ ; however, the defect concentration does increase with increasing dose. While compaction in fused  $\text{GeO}_2$  has not to this author's knowledge been investigated, it is reasonable to expect,

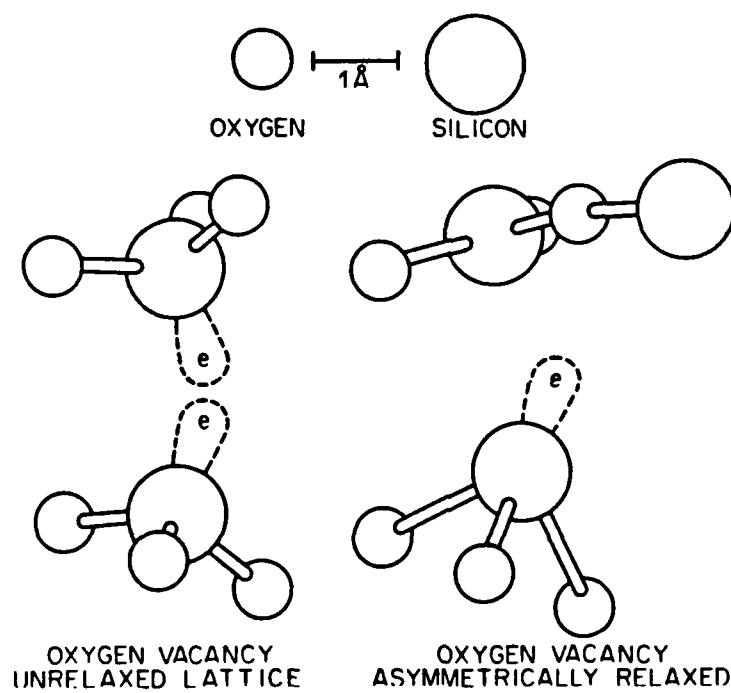


Figure 14. Model of E' Center Formation and Subsequent Relaxation of Lattice After Feigl et al (75).

because of the similarity of the structure of fused  $\text{SiO}_2$  and fused  $\text{GeO}_2$  (10), that this process would occur in fused  $\text{GeO}_2$ . Both of these related processes could then explain the increase of  $\Delta H$  with irradiation. With the increase of defects with dose (76) and the increase of compaction with dose causing additional strain in the structure, greater changes in the interstitial wells through which the Na ion moves would be anticipated (38).

The increasing  $\Delta H$  values account for the increase in resistivity in these glasses as in the  $T_\phi$  of  $1550^\circ\text{C}$  sample shown in Figure 10. From Equation (38) it can be seen that increasing  $\Delta H$  will cause a decrease in the mobility as shown in Figure 11.

All samples show, with the higher dose levels, a decrease in resistivity at temperatures greater than  $200^\circ\text{C}$ . This change occurs during the time of measurement. I suggest these changes in resistivity and hence mobility behavior are due to thermal annealing of the charged defects caused by the ionizing irradiation and the concurrent release of compaction. Primak (30) has discussed the release of irradiation compaction with thermal energy in fused silica and concluded that fused silica can return to a statistical state similar to the unirradiated state. The thermal energy of measurement can also cause the release of the trapped charges on the defects. These free charges can be recaptured by either the same centers or centers equivalent to those from which they were released by irradiation. This release would be concurrent with the release of compaction in the samples.

Griscom (77) has reported results on the thermal bleaching of  $E'$  centers in fused silica and has suggested a mechanism for their

irradiation and annealing behavior that are consistent with the above hypothesis. These results are also supported by the work of Devine (78).

That these samples undergo dynamic change with measurements above 200°C and return to a statistical similar state as the unirradiated samples can be seen in Figure 12. Upon a second measurement after the longest dose, the  $T\phi$  of 1550°C sample displays a behavior of the resistivity similar for that of the unirradiated sample. The samples with other  $T\phi$ 's behave in an analogous fashion.

The  $\gamma$  irradiation of these high purity  $\text{GeO}_2$  glasses causes an increase in the resistivity of all samples and an increase in  $\Delta H$  the enthalpy of activation. The increase in  $\Delta H$  results in the increases seen in the resistivity or the drop in mobility. The creation of additional defect centers and compaction with  $\gamma$  irradiation are suggested to be the cause of the increased  $\Delta H$  values. The return of the resistivity to its unirradiated behavior with heating supports this hypothesis.

## CHAPTER VI

### CONCLUSIONS

The dc conductivity of high purity  $\text{GeO}_2$  glasses depends upon the temperature,  $T_\phi$  at which the liquid is equilibrated before cooling. This dependence occurs because the average well structure occupied by the Na ion depends upon  $T_\phi$ . The fundamental change produced by changes in  $T_\phi$  are in the configurational coordinates of the interstitial sites. These differences are found in the anharmonicity of the well structure and are manifested by the changes in  $\Delta S$ , the entropy of activation.

The initial structure that is set by  $T_\phi$  is retained by the glass after annealing treatments at a temperature slightly below the softening temperature. The correlation of intrinsic point defects with  $T_\phi$  and the effects of  $T_\phi$  on the mobility may indicate a causative relation between the two phenomena.

With  $\gamma$  irradiation, stable and reproducible increases in resistivity are encountered for all  $T_\phi$ 's. The increase of  $\Delta H$  and the known increase of point defects with  $\gamma$  irradiation suggest a causative relation. Defects interact not as traps but as modifiers to the average potential well by coulombic interaction and relaxation. These effects anneal and the glass returns to a statistical similar state.

The overall conclusion that may be drawn is the importance of  $T_\phi$  in determining the properties of these high purity  $\text{GeO}_2$  glasses. This conclusion is contrary to conventional glass theory which suggests that

the liquid above the glass transition state equilibrates with each successively lower temperature as the melt is cooled. A consequence of this theory is that the interstitial wells are independent of  $T\phi$ . However, the measurements obtained by varying  $T\phi$  and by subsequent annealing treatments show that  $T\phi$  is important in determining the structure as revealed by mobility measurements. The effects of irradiation suggest point defects are also important in determining well properties.

The implication of these  $T\phi$  dependencies is that point defects through coulombic interaction and relaxation have an effect on the overall structure frozen into the glass upon cooling.

## CHAPTER VII

### RECOMMENDATIONS FOR FUTURE RESEARCH

#### 1. Low Temperature Specific Heat Measurements

As these measurements are determined by the vibrational modes of the structure (66), they would be useful in studying the differences induced in the structure by changing  $T\phi$ .

#### 2. $T\phi$ Dependence of Mobility in Glasses with Increasing Na Concentration

Measurement of the mobilities with increasing sodium concentration would clarify the role of intrinsic defects in the  $T\phi$  dependence of mobility.

#### 3. Study of the Kinetics of the Annealing of Irradiation Effects on the Mobility as a Function of $T\phi$ .

The kinetic study would allow determination of the activation energy of the process. This activation energy would provide information for determining the process involved that results in the increased  $\Delta H$  values seen in the mobility measurements with irradiation.

#### 4. Thermal Stimulated Polarization Current Measurements on Irradiated Samples

These measurements would allow the determination of the activation energy required for the release of charges trapped at defect centers after irradiation. This activation energy would help in the characterization of the defect centers involved in the process.

## REFERENCES

1. D. L. Griscom, E. J. Friebele, K. J. Long and J. W. Freeman, "Fundamental Defect Centers in Glass; Electron Spin Resonance and Optical Absorption Studies of Irradiated Phosphorus-doped Silica Glass and Optical Fibers," Journal of Applied Physics, 54, 3743-3762 (1983).
2. A. Paul, Chemistry of Glasses, Chapman and Hall, London, 1982.
3. N. F. Mott, The Structure of Non-Crystalline Materials, P. H. Gaskell, editor, Taylor and Francis LTD, London, 1977, 101-107.
4. E. J. Friebele and D. L. Griscom, Treatise on Material Science and Technology, Volume 17, edited by M. Tomozawa and R. H. Doremus, Academic Press, New York, 1979, 257-351.
5. G. A. Taylor and J. C. Thacker, Fibre Optics System for Space Applications, Optics and Laser Technology, 14, 93-97, 1982.
6. R. C. Hughes, "Charge Transport and Storage in  $\text{SiO}_2$ ," International Symposium on Electrets and Dielectrics, Ed. by Academia Brasileira de Ciencias, Rio de Janeiro, 1977, 255-271.
7. D. B. Brown, D. I. Ma, C. M. Dozier and M. C. Peckerar, Thermal Annealing of Radiation Induced Defects: A Diffusion-Limited Process, IEEE Transactions on Nuclear Science, 30, 4059-63 (1983).
8. J. M. Atkin, "Radiation-induced Trapping Centers in Thin Silicon Dioxide Films," Journal of Non-Crystalline Solids 40, 31-47 (1980).
9. C. T. Sah, "Origin of Interface States and Oxide Charges Generated by Ionizing Radiation," IEEE Transactions on Nuclear Science, NS-23, 1563-1568 (1976).
10. J. Wong and C. A. Angell, Glass Structure by Spectroscopy, Marcel Dekker, Inc., New York, 1976.
11. W. H. Zachariasen, "The Atomic Arrangement in Glass," Journal of the American Ceramic Society, 54, 3841-3851 (1932).
12. B. E. Warren, "The Diffraction of X-Rays in Glass," The Physical Review, 45, 657-661 (1934).

13. V. Garina-Canina, "Several Optical Properties of Pure Germanium Oxide Glasses in the Ultraviolet," Comptes Rendus de la Academy of Sciences, 247, 593-96 (1958).
14. A. J. Cohen and H. L. Smith, "Ultraviolet and Infrared Absorption of Fused Germania," Journal of Physics and Chemistry of Solids, 7, 301-306 (1958).
15. P. J. Vergano and D. R. Uhlmann, "Crystallization Kinetics of Germanium Dioxide: The Effect of Stoichiometry on Kinetics," Physics and Chemistry of Glasses 11, 30-38 (1970).
16. T. Purcell and R. A. Weeks, "Radiation Induced Paramagnetic States of Some Intrinsic Defects in GeO<sub>2</sub> Glasses and Crystals," Physics and Chemistry of Glasses, 10, 198-208 (1969).
17. H. Bohm, "Electrical Conductivity of Vitreous GeO<sub>2</sub>," Journal of Applied Physics, 43, 1103-1107 (1972).
18. J. F. Cordaro, J. E. Kelly, III, and M. Tomozawa, "The Effects of Impurity OH on the Transport Properties of High Purity GeO<sub>2</sub> Glasses," Physics and Chemistry of Glasses, 22, 90-93 (1981).
19. F. L. Galeener and R. H. Geils, The Structure of Non-Crystalline Materials, P. H. Gaskell, Editor, Taylor and Francis, LTD, London 223-226 (1977).
20. H. Bohm, "On the Photoconductivity of Vitreous GeO<sub>2</sub>," Journal of Non-Crystalline Solids, 7, 192-202 (1972).
21. H. Bohm, "On the Thermoluminescence of Vitreous GeO<sub>2</sub>," Physics and Chemistry of Glasses, 11, 177-185 (1970).
22. G. Kordas, R. A. Weeks and D. L. Kinser, "The Influence of Fusion Temperature on the Defect Center Concentration of GeO<sub>2</sub> Glasses," Journal of Applied Physics, 54, 5394-5399 (1983).
23. W. Primak, "The Annealing of Vitreous Silica," Physics and Chemistry of Glasses, 24, pp. 8-18 (1983).
24. R. W. Douglas and J. D. Isard, "Density Changes in Fused Silica," Journal of Society of Glass Technology, 35, 206-225 (1951).
25. G. H. Hetherington, K. H. Jack and J. C. Kennedy, "The Viscosity of Vitreous Silica," Physics and Chemistry of Glasses, 5, 130-136 (1964).
26. M. R. Vukceovich, "A New Interpretation of the Anomalous Properties of Vitreous Silica," Journal of Non-Crystalline Solids, 11, 25-63 (1972).

27. D. L. Anderson and H. E. Bommel, "Ultrasonic Absorption in Fused Silica at Low Temperatures and High Frequencies," Journal of American Ceramic Society, 38, 115-131 (1955).
28. R. E. Strakna, "Investigation of Low Temperature Ultrasonic Absorption in Fast Neutron Irradiated  $\text{SiO}_2$  Glasses," The Physical Review, 123, 2020-2026 (1961).
29. Mme. Curie, Le Radium 4, 349 (1907) as quoted in E. Rutherford, Radioactive Substances and their Radiations, Cambridge Press, Cambridge, 315 (1913).
30. W. Primak, The Compacted States of Vitreous Silica, Gordon and Breach, New York (1975).
31. A. Bishmay, "Radiation Induced Color Centers in Multicomponent Glasses," Journal of Non-Crystalline Solids, 3, 54-114 (1970).
32. N. J. Kreidl, Ceramics in Severe Environments, Kriedl and Palmer, eds., Plenum Press, New York, 1971.
33. J. E. Shelby, "Effect of Radiation on the Physical Properties of Borosilicate Glasses," Journal of Applied Physics, 51, 2561-2565 (1980).
34. J. Fontanella, R. L. Johnston and G. H. Sigel, "The Dielectric Properties of as Received and Gamma Irradiated Fused Silica," Journal of Non-Crystalline Solids, 31, 401-414 (1979).
35. V. E. Cullen and H. E. Rexford, "Gamma Radiation Induced Conductivity in Glasses," Proceedings of the IEEE Conference on Dielectric and Insulating Materials, London, 1964.
36. F. Wakim, J. M. Lee and D. L. Kinser, "The Effect of High Energy Gamma Radiation on the Electrical Properties of Iron Phosphate Glasses," Journal of Non-Crystalline Solids, 29, 423-426 (1978).
37. T. M. Mike, B. L. Steierman, and E. F. Degering, "Effects of Electron Bombardment on Properties of Various Glasses," Journal of American Ceramic Society, 13, 405-407 (1960).
38. R. H. Magruder, III, D. L. Kinser, and R. A. Weeks, "Effects of Gamma Radiation on the Direct Current Resistivity of  $\text{GeO}_2$ ," Journal of American Ceramic Society, C62-63 (1983).
39. G. Fousserau, "Influence of Tempering on the Electrical Resistance of Glass," Comptes Rendus de la Academy of Sciences, 96, 785 (1883).

40. Gray and Dobbie, Proceedings Royal Society of London, 67, 200 (1900) as discussed by J. W. Rebbeck, M. J. Mulligan, and J. B. Ferguson, "The Electrolysis of Soda-Lime Glass--Part II," Journal of American Ceramic Society, 8, 329-338 (1925).
41. Warburg, Wied. Ann. 21, 622 (1884) as discussed by J. W. Rebbeck M. J. Mulligan, and J. B. Ferguson, "The Electrolysis of Soda-Lime Glass--Part II," Journal of American Ceramic Society, 8, 329-338 (1925).
42. C. A. Kraus and E. H. Darby, "A Study of the Conduction Process in Ordinary Soda-Lime Glass," Journal of American Ceramic Society 44, 2783 (1922).
43. A. E. Owen and R. W. Douglas, "The Electrical Properties of Vitreous Silica," Journal of Society of Glass Technology, 43, 159T-178T (1959).
44. A. E. Owen, Progress in Ceramic Science, Vol. 3, J. E. Burke, ed., Macmillan Co., New York, 77-196 (1963).
45. R. Kirchheim, "Influence of Disorder on the Diffusion of Alkali Ions in  $\text{SiO}_2$  and  $\text{GeO}_2$  Glasses," Journal of Non-Crystalline Solids, 55, 243-255 (1983).
46. Y. Haven and B. Verlick, "Diffusion and Electrical Conductivity of Sodium Ions in Sodium Silicate Glasses," Physics and Chemistry of Glasses, 6, 38-45 (1965).
47. C. Lim and D. E. Day, "Sodium Diffusion in High Silica Glasses," Journal of the American Ceramic Society, 61, 329-332 (1978).
48. A. Doi and D. E. Day, "Conduction Polarization in Sodium Germanate Glasses," Journal of Applied Physics, 52, 3433-3438 (1981).
49. J. E. Kelly, J. F. Cordaro and M. Tomozawa, "Correlation Effects on Alkali Ion Diffusion in Binary Alkali Oxide Glasses," Journal of Non-Crystalline Solids, 41, 47-55 (1980).
50. J. E. Shelby, "Pressure Dependence of Helium and Neon Solubility in Vitreous Silica," Journal of Applied Physics, 47, 135-139 (1976).
51. J. F. Shackelford and J. S. Masaryk, "The Interstitial Structure of Vitreous Silica," Journal of Non-Crystalline Solids, 30, 127-139 (1978).
52. D. L. Anderson and D. A. Stuart, "Calculation of Activation Energy of Ionic Conductivity in Silica Glasses by Classical Methods," Journal of the American Ceramic Society, 37, 573-580 (1954).

53. R. H. Doremus, "Electrical Conductivity and Electrolysis of Alkali Ion in Silica Glass," Physics and Chemistry of Glasses, 10, 28-33 (1969).
54. R. M. Hakim and D. R. Uhlmann, "Electrical Conductivity of Alkali Silicate Glasses," Physics and Chemistry of Glasses, 12, 132-138 (1971).
55. S. J. Rothman, T. L. M. Marcuso, L. J. Nowicki, P. M. Baldo, A. W. McCormick, "Diffusion of Alkali Ions in Vitreous Silica," Journal of the American Ceramics Society, 65, 578-582 (1982).
56. A. V. Ivanov, "Electrical Conductivity of Mixed Alkali Glasses of the  $\text{Na}_2\text{O}-\text{K}_2\text{O}-\text{GeO}_2$  Systems," Soviet Physics-Solid State, 5, 1933-1937 (1964).
57. R. H. Doremus, Glass Science, John Wiley and Sons, New York, 1973.
58. G. W. Morey, The Properties of Glass. Reinhold Publishing Company, New York, 1954.
59. K. Hughes and J. O. Isard, Physics of Electrolytes, J. Hladik, ed., Academic Press, London, 351-400 (1972).
60. P. Kofstad, Nonstoichiometry Diffusion and Electrical Conductivity in Binary Metal Oxides, John Wiley and Sons, New York (1972).
61. W. D. Kingery, H. K. Bowen, D. R. Uhlmann, Introduction to Ceramics, 2nd edition, John Wiley and Sons, New York (1976).
62. R. Syed, D. L. Gavin and C. T. Maynihan, "Functional Form of the Arrhenius Equation for Electrical Conductivity in Glass," Journal of the American Ceramics Society, 65, C129-130 (1982).
63. M. E. Wells, "Correlation Between Processing Variables and the Optical Properties of  $\text{GeO}_2$  Glasses," Masters Thesis, Vanderbilt University.
64. P. R. Bevington, Data Reduction and Error Analysis for the Physical Sciences, McGraw-Hill, New York (1969).
65. G. H. A. M. Van der Steen and E. Papanikalan, "Introduction and Removal of Hydroxyl Groups in Vitreous Silica: Part II," Philips Research Report, 30, 192-205 (1975).
66. R. A. Swalin, Thermodynamics of Solids, 2nd Edition, John Wiley and Sons, New York (1972).

67. J. F. Shackelford and B. D. Brown, "The Lognormal Distribution in the Random Network Structure," Journal of Non-Crystalline Solids, 44, 379-382 (1981).
68. G. M. Barrow, Introduction to Molecular Spectroscopy, McGraw-Hill, Kogakusha Ltd., Tokyo (1962).
69. A. E. Geissberger and F. L. Galeener, "Raman Studies of Vitreous SiO<sub>2</sub> Versus Fictive Temperature," Physical Review B 28, 3266-3271 (1983).
70. L. P. Boesch and C. J. Moynihan, "Effect of Thermal History on Conductivity and Electrical Relaxation in Alkali Silicate Glasses," Journal of Non-Crystalline Solids, 44-60 (1975).
71. H. N. Ritland, "Limitations of the Fictive Temperature Concept," Journal of the American Ceramics Society, 39, 403-406 (1956).
72. A. E. Owen, Electronic and Structural Properties of Amorphous Semiconductors, edited by P. G. LeComber and J. Mort, 161-190. Academic Press, London (1973).
73. J. M. Jackson, M. Wells, D. L. Kinser and R. A. Weeks, to be submitted to the Journal of the American Ceramics Society.
74. V. Garino Canina, "Diffusion of Oxygen in Glassy GeO<sub>2</sub>," Comptes Rendus de la Academy of Sciences 248, 1319-1322 (1959).
75. F. J. Feigl, W. B. Fowler and K. L. Yip, "Oxygen Vacancy Model for the E' Center in SiO<sub>2</sub>," Solid State Communications, 14, 225-229 (1974).
76. R. A. Weeks, D. L. Kinser, G. Kordas, R. Magruder and M. Wells, "The Influence of Melting Condition on the Radiation Sensitivity of GeO<sub>2</sub> Glass," Journal de Physique, 43, C9-149-153 (1982).
77. D. L. Griscom, "Characterization of Three E'-Center Variants in X and  $\gamma$ -Irradiated High Purity  $\alpha$ -SiO<sub>2</sub>," Nuclear Instruments and Methods in Physics Research, B1, 481-488 (1984).
78. R. A. B. Devine, "Isothermal Annealing of E' Defects in Ion Implanted SiO<sub>2</sub>," Nuclear Instruments and Methods in Physics Research, B1, 378-382 (1984).

END

FILMED

12-84

DTIC